



AFRL-RX-WP-TR-2008-4170

DURABLE HYBRID COATINGS

Annual Performance Report

**Bret J. Chisholm, Douglas L. Schulz, Gregory J. McCarthy, Dante Battocchi,
and Gordon P. Bierwagen**

North Dakota State University

OCTOBER 2007

Interim Report

Approved for public release; distribution unlimited.

See additional restrictions described on inside pages

STINFO COPY

**AIR FORCE RESEARCH LABORATORY
MATERIALS AND MANUFACTURING DIRECTORATE
WRIGHT-PATTERSON AIR FORCE BASE, OH 45433-7750
AIR FORCE MATERIEL COMMAND
UNITED STATES AIR FORCE**

NOTICE AND SIGNATURE PAGE

Using Government drawings, specifications, or other data included in this document for any purpose other than Government procurement does not in any way obligate the U.S. Government. The fact that the Government formulated or supplied the drawings, specifications, or other data does not license the holder or any other person or corporation; or convey any rights or permission to manufacture, use, or sell any patented invention that may relate to them.

This report was cleared for public release by the Air Force Research Laboratory Wright-Patterson Air Force Base (AFRL/WPAFB) Public Affairs Office (PAO) and is available to the general public, including foreign nationals. Copies may be obtained from the Defense Technical Information Center (DTIC) (<http://www.dtic.mil>).

AFRL-RX-WP-TR-2008-4170 HAS BEEN REVIEWED AND IS APPROVED FOR PUBLICATION IN ACCORDANCE WITH ASSIGNED DISTRIBUTION STATEMENT.

**//Signature//*

STEPHEN L. SZARUGA, Project Manager
Thermal Sciences and Materials Branch
Nonmetallic Materials Division

//Signature//

SHASHI K. SHARMA, Acting Deputy Chief
Nonmetallic Materials Division
Materials and Manufacturing Directorate

This report is published in the interest of scientific and technical information exchange and its publication does not constitute the Government's approval or disapproval of its ideas or findings.

*Disseminated copies will show “//Signature//” stamped or typed above the signature blocks.

REPORT DOCUMENTATION PAGE				<i>Form Approved</i> OMB No. 0704-0188	
<p>The public reporting burden for this collection of information is estimated to average 1 hour per response, including the time for reviewing instructions, searching existing data sources, gathering and maintaining the data needed, and completing and reviewing the collection of information. Send comments regarding this burden estimate or any other aspect of this collection of information, including suggestions for reducing this burden, to Department of Defense, Washington Headquarters Services, Directorate for Information Operations and Reports (0704-0188), 1215 Jefferson Davis Highway, Suite 1204, Arlington, VA 22202-4302. Respondents should be aware that notwithstanding any other provision of law, no person shall be subject to any penalty for failing to comply with a collection of information if it does not display a currently valid OMB control number. PLEASE DO NOT RETURN YOUR FORM TO THE ABOVE ADDRESS.</p>					
1. REPORT DATE (DD-MM-YY) October 2007		2. REPORT TYPE Interim		3. DATES COVERED (From - To) 19 July 2004 – 17 October 2007	
4. TITLE AND SUBTITLE DURABLE HYBRID COATINGS Annual Performance Report				5a. CONTRACT NUMBER FA8650-04-1-5045	
				5b. GRANT NUMBER	
				5c. PROGRAM ELEMENT NUMBER 62102F	
6. AUTHOR(S) Bret J. Chisholm, Douglas L. Schulz, and Gregory J. McCarthy (Center for Nanoscale Science and Engineering, North Dakota State University) Dante Battocchi and Gordon P. Bierwagen (Department of Coatings and Polymeric Materials, North Dakota State University)				5d. PROJECT NUMBER 4347	
				5e. TASK NUMBER 60	
				5f. WORK UNIT NUMBER 65100002	
7. PERFORMING ORGANIZATION NAME(S) AND ADDRESS(ES) North Dakota State University Center for Nanoscale Science and Engineering 1805 NDSU Research Park Drive N. Fargo, ND 58102				North Dakota State University Department of Coatings and Polymeric Materials 1735 NDSU Research Park Drive N. Fargo, ND 58105	
9. SPONSORING/MONITORING AGENCY NAME(S) AND ADDRESS(ES) Air Force Research Laboratory Materials and Manufacturing Directorate Wright-Patterson Air Force Base, OH 45433-7750 Air Force Materiel Command United States Air Force				8. PERFORMING ORGANIZATION REPORT NUMBER	
				10. SPONSORING/MONITORING AGENCY ACRONYM(S) AFRL/RXBT	
				11. SPONSORING/MONITORING AGENCY REPORT NUMBER(S) AFRL-RX-WP-TR-2008-4170	
12. DISTRIBUTION/AVAILABILITY STATEMENT Approved for public release; distribution unlimited.					
13. SUPPLEMENTARY NOTES PAO Case Number: WPAFB 08-0434, 21 Feb 2008. Report contains color.					
14. ABSTRACT The goal of this program is to contribute to the development of the next-generation anti-corrosion and other protective coating systems for USAF aircraft. The initial emphasis of the program was on improvements in NDSU's promising Mg-based primer, which NDSU recently licensed to the major international aircraft coatings manufacturer. Work continued over the last year on improvements in primer binder, additions to NDSU's world-class high-throughput (HT) research and development capabilities that are necessary to work with this class of coatings, and meeting additional Air Force protective coatings needs such as hard surface pretreatments to work with the binder, and development of a methodology for depot-based repair indium tin oxide aircraft canopy coatings. A new effort was initiated late in the year on prognostic measurement techniques to monitor the effectiveness of the magnesium-based primers previously developed. Accomplishments included successful research on a new two component binder system, hybrid organic-inorganic binders, and UV-curable low-VOC binders for Mg-rich primers. The HT approach was instrumental for efficient and effective binder research. Studies of a range of Mg-alloys in the primer have shown that, similar to pure Mg primer, all Mg alloy primers provide cathodic protection to the Al alloy substrate. The composition of the Mg alloy, such as the content of Al and the composition of the third element, can greatly influence performance. Work was largely completed on HT tools needed for development of aerospace coatings: robotic viscous liquid handling, high shear mixing for pigment dispersion, screening methods for characterizing corrosion protection, and HT screening methods for characterizing weatherability.					
15. SUBJECT TERMS Hybrid organic-inorganic binders, UV-curable low-VOC binders, high-throughput (HT), weatherability					
16. SECURITY CLASSIFICATION OF:			17. LIMITATION OF ABSTRACT: SAR	18. NUMBER OF PAGES 138	19a. NAME OF RESPONSIBLE PERSON (Monitor) Stephen L. Szaruga 19b. TELEPHONE NUMBER (Include Area Code) N/A
a. REPORT Unclassified	b. ABSTRACT Unclassified	c. THIS PAGE Unclassified			

Table of Contents

Summary	1
1.0 Introduction	1
2.0 Mg-Rich Primer Development	3
2.1 Background	3
2.2 Polymer Binder Developments	4
2.2.1 Two Component Epoxy Binder Development	4
2.2.2 Hybrid Organic-Inorganic Binder Development	4
2.2.3 UV-Curable Mg-Rich Primer	4
2.2.4 Flexible Binders for Mg-rich Coatings	7
2.3 Magnesium Alloys	
3.0 Development of New Combinatorial Capabilities	12
3.1 Viscous Liquid Handling Workflow	13
3.2 Coating Deposition Workflow	13
3.3 Tribology Workflow	13
3.4 High-Throughput Measurements of Corrosion Protection	14
3.5 Equipment for Automated Color and Gloss Measurements	16
4.0 Plasma Deposition of Inorganic Coatings	18
4.1 Trimethylsilane-based Permanent Pretreatments in a Mg-rich Primer Corrosion Prevention System	18
4.1.1 Experimental methodology	18
4.1.1.1 SiC-based Film Growth by PECVD	18
4.1.1.2 Mg-rich Primer Applied to Coated Substrates	18
4.1.1.3 Electrochemical Impedance Spectroscopy (EIS) Testing	19
4.1.2 Results and Discussion	19
4.1.2.1 Temperature screening study	19
4.1.2.2 Pressure screening study	20
4.1.3 Conclusions	22
4.2 Deposition of Transparent Conductive Indium and Tin Oxides by Atmospheric Pressure Plasma Jet – Toward In-field Aircraft Canopy Repair	22
5.0 Remote Sensing for Coating Prognostics	25
6.0 References	29
7.0 Program Management	31
Technical Appendix: Positron Annihilation Studies	32
Appendices: Manuscripts and Published Papers (indexed to report sections)	

Acknowledgements

This material is based on research sponsored by Air Force Research Laboratory under agreement number FA8650-04-1-5045.

The views and conclusions contained herein are those of the authors and should not be interpreted as necessarily representing the official policies or endorsements, either expressed or implied, of Air Force Research Laboratory or the U.S. Government.

Distribution List

Air Force Research Laboratory

AFRL/MLBT: Dr. Stephen L. Szaruga 1 e-mail copy; Steve.Szaruga@wpafb.af.mil
2941 P. Street, Rm 136
Wright-Patterson Air Force Base, Ohio 45433-7750

AFRL: Michael A. Cramer 1 e-mail copy; Michael.Cramer@wpafb.af.mil

Copy to:
AFRL/PKMM: Pam S. Strader 1 e-mail copy; Pam.Strader@WPAFB.AF.MIL

Office of Naval Research – Administrative Grants Officer

Sandra Thomson 1 e-mail copy; Sandra_Thomson@onr.navy.mil
ONR Seattle Regional Office
1107 NE45th Street, Suite 350
Seattle WA 98105-4631

North Dakota State University

Dr. Gordon Bierwagen 1 e-mail copy: Gordon.Bierwagen@ndsu.edu
Dr. Bret Chisholm 1 e-mail copy: Bret.Chisholm@ndsu.edu
DrEng. Dante Battocchi 1 e-mail copy: Dante.Battocchi@ndsu.edu
Dr. Douglas Schulz 1 e-mail copy: Doug.Schulz@ndsu.edu
Dr. Philip Boudjouk 1 e-mail copy: Philip.Boudjouk@ndsu.edu

Contact information for inquiries

Programmatic:

Gregory McCarthy, Director CNSE
1805 NDSU Research Park Dr. N.
Fargo, ND 58102
(701) 231-7193 (voice)
(701) 231-7916 (fax)
Greg.McCarthy@ndsu.edu

Technical:

Gordon Bierwagen, Professor
Department of Coatings & Polymeric
Materials
1735 NDSU Research Park Dr. N.
Fargo, ND 58102
(701) 231-8294 (voice)
(701) 231-8439 (fax)
Gordon.Bierwagen@ndsu.edu

Financial:

Mark Lande, Asst. Dir. CNSE
Admin. and Financial Services
1805 NDSU Research Park Dr.
Fargo, ND 58102
(701) 231-5882 (voice)
(701) 231-7916 (fax)
Mark.Lande@ndsu.edu

Summary

The goal of this program is to contribute to the development of the next-generation anti-corrosion and other protective coating systems for USAF aircraft. The initial emphasis of the program was on improvements in NDSU's promising Mg-based primer, which NDSU recently licensed to the major international aircraft coatings manufacturer. Work continued over the last year on improvements in primer binder, additions to NDSU's world-class high-throughput (HT) research and development capabilities that are necessary to work with this class of coatings, and meeting additional Air Force protective coatings needs such as hard surface pretreatments to work with the binder, and development of a methodology for depot-based repair indium tin oxide aircraft canopy coatings. A new effort was initiated late in the year on prognostic measurement techniques to monitor the effectiveness of the magnesium-based primers previously developed. Accomplishments included successful research on a new two component binder system, hybrid organic-inorganic binders, and UV-curable low-VOC binders for Mg-rich primers. The HT approach was instrumental for efficient and effective binder research. Studies of a range of Mg-alloys in the primer have shown that, similar to pure Mg primer, all Mg alloy primers provide cathodic protection to the Al alloy substrate. The composition of the Mg alloy, such as the content of Al and the composition of the third element, can greatly influence performance. Work was largely completed on HT tools needed for development of aerospace coatings: robotic viscous liquid handling, high shear mixing for pigment dispersion, screening methods for characterizing corrosion protection, and HT screening methods for characterizing weatherability. A trimethylsilane-precursor-based coating was investigated as a pretreatment with SiC-based thin films deposited onto Al-2024 substrates by plasma-enhanced chemical vapor deposition (PECVD). Promising results were obtained on the deposition of transparent conductive indium and tin oxides by an atmospheric pressure plasma jet technique. The as-deposited films met the stated targets for transparency, but not yet for conductivity. Research on *in situ* monitoring of a coating with *ac* involves the application of an embedded electrode or sensor within the coating (not the Al substrate).

1.0 Introduction

The *goal* of this North Dakota State University (NDSU) program is to contribute to the development of the next-generation anti-corrosion and other protective coating systems for USAF aircraft. The initial emphasis of the program was on improvements in NDSU's promising Mg-based primer, which NDSU recently licensed to the major international aircraft coatings manufacturer. Work continued over the last year on improvements in primer binder improvements, additions to NDSU's world-class high-throughput (HT) research and development capabilities that are necessary to work with this class of coatings, and meeting additional Air Force protective coatings needs such as hard surface pretreatments to work with the binder, and development of a methodology for depot-based repair indium tin oxide aircraft canopy coatings. A new effort was initiated late in the year on prognostic measurement techniques to monitor the effectiveness of the magnesium-based primers previously developed.

This report is organized around the Durable Hybrid Coatings program tasks:

- **Task 1.** Mg-based primer research focusing on the primer itself and its electrochemical behavior in the coating. Research coordinated by Dr. Dante Battocchi, with Prof. Gordon Bierwagen as senior scientific advisor, and performed in the Department of Coatings and Polymeric Materials (CPM). Initiated in 2004. Progress described in **Section 2.3**.
- **Task 2.** Hard pretreatment research that would permit depot repainting without damaging the airframe. Work led by Dr. Douglas Schulz, and performed in the NDSU Center for Nanoscale Science and Engineering (CNSE). Initiated in 2004. Progress described in **Section 4.1**.
- **Task 3.** Primer formulation optimization research, and research and development on high-throughput coatings design, development and evaluation of these primers. Work led by Dr. Bret Chisholm, and performed in the NDSU Center for Nanoscale Science and Engineering (CNSE). Initiated in 2005. Progress described in **Sections 2.2 and 3.0 and Technical Appendix**.

- **Task 4.** Develop indium tin oxide coatings for in-field canopy repair. The Task 4 supplement also added research to Tasks 1 and 3. Initiated in 2006. Progress described in *Section 4.2*.
- **Task 5.** Initiating new work on prognostic measurement techniques to monitor the effectiveness of the magnesium-based primers previously developed. Follow-on work would include design and development of low-cost, potentially wireless, electronics that utilize these techniques. In addition, NDSU will continue to develop combinatorial laboratory techniques to reduce the time and resources required to formulate aerospace coatings. Task 5 was initiated in July 2007 under this program. It builds on previous work by Drs. Bierwagen and Allahar in an AFOSR program. Progress described in *Section 5.0*.

In cases where a significant portion of a study has been completed, and a manuscript has been prepared or paper published, the work will only be summarized, with reference to the manuscript for details. A series of such manuscripts is appended to this report. Each is indexed to the section of the main report that it supports.

2.0 Mg-Rich Primer Development

2.1. Background

Durable hybrid coatings for aluminum aircraft systems are comprised of three layers: a topcoat that maintains barrier and appearance properties; a primer layer with anticorrosion properties; and, a surface pretreatment that serves as an adhesion-promoting layer between the aluminum substrate and the primer (Figure 2.1-1).

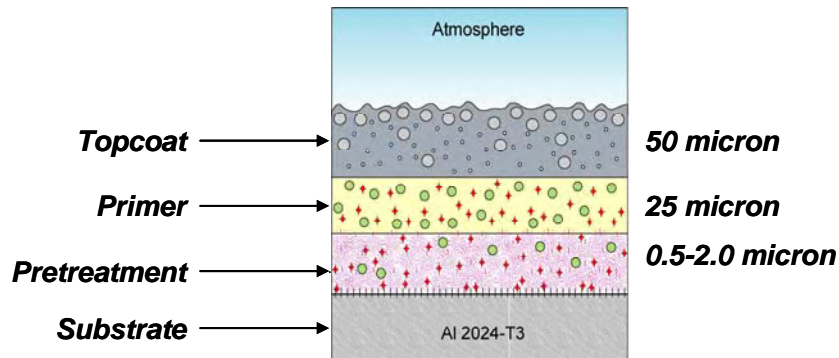


Figure 2.1-1. Schematic diagram of the cross section of a durable hybrid coating for aircraft systems. (AFRL diagram)

NDSU is a leader in the field of galvanic primer systems as evidenced by the particulate Mg-rich pigmentation that has been designed as an alternative to chromate pigments and pretreatments for corrosion control of Al alloys, with particular attention to the alloy 2024 T-3. This system was designed by analogy to pigmented Zn-rich primer coatings used for the protection of steel. The Mg pigments are incorporated in an organic binder system. The use of Mg as a pigment was possible after addressing two features specific to the properties of Mg particulate. Mg can be a fire hazard, and this concern was alleviated by the manner in which Mg pigment was delivered by Eckart GmbH. This particulate Mg has a thin oxide layer that stabilizes it against further oxidation. The second concern was connected to the products generated after exposing Mg in aqueous solutions. It was thought that the oxidation products of Mg, MgO and its various hydroxides in hydrated form, would create such basic conditions that Al would undergo basic corrosion. Studies conducted by Perrault and Krammer, produced such results that could alleviate this concern [Perrault, 1978; Krammer, 2001].

The anti-corrosive properties of the Mg-rich primer are based on two different mechanisms: firstly, the coating acts as a barrier; secondly, the coating acts as a cathodic protector with the pigment undergoing corrosion preferentially versus the Al substrate. Characterization studies via electrochemical measurements as well as SVET investigation have been conducted on different primer formulations. In addition, several Mg-rich primers with different binder polymer systems were exposed to severe weathering in accelerated weathering chambers. Some of the formulation have exceeded 7,000 hours of accelerated weathering exposure and are still currently under test.

2.2. Polymer Binder Development

In addition to the active corrosion inhibition derived from the presence of Mg particles, corrosion protection is also affected by the composition of the coating binder. Over the course of the Durable Hybrid Coatings program, several tasks have been associated with the development of new binder

systems for Mg-rich primers. The next few subsections of this document provide an overview of the results obtained with different binder systems for the development of new Mg-rich primers.

2.2.1. Two Component Epoxy Binder Development

The Mg-rich primer initially developed that showed outstanding corrosion protection was based on a three-component polymer binder system [Nanna, 2004]. Almost all conventional coatings are either one component or two component systems, with a one component system being the most desirable due to its simplicity. Primers used for corrosion protection are typically two component, solvent-based systems comprised of an epoxy functional oligomer and an amine functional curing agent. Experimentation was conducted in order to develop a two component, epoxy-based binder system for Mg. The results obtained were summarized in a conference proceeding which is provided as Appendix 2.2.1.

2.2.2. Hybrid Organic-Inorganic Binder Development

Hybrid organic-inorganic binders for Mg-rich primers were investigated using the combinatorial approach. The results obtained were summarized in two conference proceedings manuscripts, which are provided as Appendices 2.2.2-1 and 2.2.2-2.

2.2.3. UV-curable Mg-rich Primer

The objective of this task is to investigate the feasibility of developing a UV curable Mg-rich primer. This technology, if successful, will provide a primer with no or very low VOC and much faster curing response than other primer systems. Since Mg-rich primers require a heavy loading of Mg powder in order to provide cathodic protection, our initial concern was that the high loading of Mg would block or scatter the incident UV light preventing the bottom layer of resin curing. An initial trial using a phosphine oxide based photoinitiator (Irgacure 819), a commercially-available hyperbranched acrylate CN2300 and 10% to 50% wt. Mg powder (ECKART PK31) gave a tack-free film after UV exposure. The measurement of open circuit potential (OCP) revealed that the samples containing greater than wt30 wt. % Mg displayed an OCP below -1.0 V indicating good electrical conductivity between Mg particles and the substrate. However, after 30 minutes of EIS testing, all the sample films blistered or delaminated at the spot contact with the electrolyte solution. This was attributed to the poor wet adhesion of the coatings or the insufficient curing of the bottom layer of the coating. Raman spectroscopy was identified as a powerful tool to examine the extent of cure of the coating near the coating-substrate interface. A new confocal Raman microscope is being acquired to assist in the measurement of “through-cure” for these primer compositions.

In order to improve the wet adhesion, we have been investigating hyperbranched acrylate-based free radical UV curable binders for Mg-rich primer development. Hyperbranched acrylates have the characteristics of multi-functionality, low photopolymerization shrinkage (thus better adhesion), good mechanical properties (such as flexibility, toughness etc.) and low viscosity, which make them suitable for UV curable systems containing high pigment levels. In addition, it was proposed that the incorporation of silanol functionalized colloidal silica nanoparticles, alkoxy silanes and/or acrylates with hydroxyl functionality into the hyperbranched acrylates would further increase adhesion since the silanol or hydroxyl groups will form some covalent or secondary hydrogen bonding between the Al surface and the primer. Thus, experiments were focused on using the combinatorial pull-off adhesion station to screen binder compositions in a high-throughput manner.

The first combinatorial pull-off adhesion experiment was designed to determine the most appropriate photoinitiator level and hyperbranched acrylate composition. Also, formulations with and without 5 wt.% of a silanol functionalized colloidal silica nanoparticle (MEK-ST) were included to determine the effect

on adhesion. The categorical analysis and ranking of the results concluded that two hyperbranched acrylates, CN2300 and CN2301, and 4 wt.% photoinitiator provide the best adhesion. Also, samples with 5% MEK-ST gave better adhesion than the samples without MEK-ST.

In a follow-up experiment, four commercially available colloidal silica nanoparticles with various particle sizes (10-15 nm or 40-50 nm) and one acrylate functionalized trimethoxy silane were combined with CN2300 and CN2301, respectively, at three loading levels (2.5, 5 and 7.5 wt.%). The results of pull-off adhesion testing showed that all CN2301-based samples gave lower adhesion strength than the CN2300-based samples. For the CN2300-based samples, the addition of MEK-ST and MA-ST (10-15 nm colloidal nanoparticles) at 5 wt.%, and the addition of acrylated trimethoxy silane at 5 wt.% showed a little higher adhesion strength than the control sample (UV curing of CN2300 only). From this set of experiments, it was determined that CN2300 + 5% MEK-ST or 5% acrylated trimethoxy silane were the best formulations for further experimentation.

An experiment was conducted which involved the synthesis of acrylated hyperbranched polyols. Acryloyl chloride was reacted with two hyperbranched polyols at different acrylate:polyol ratios (5:1, 10:1 and 1:1) as shown in Figure 2.2.3-1.

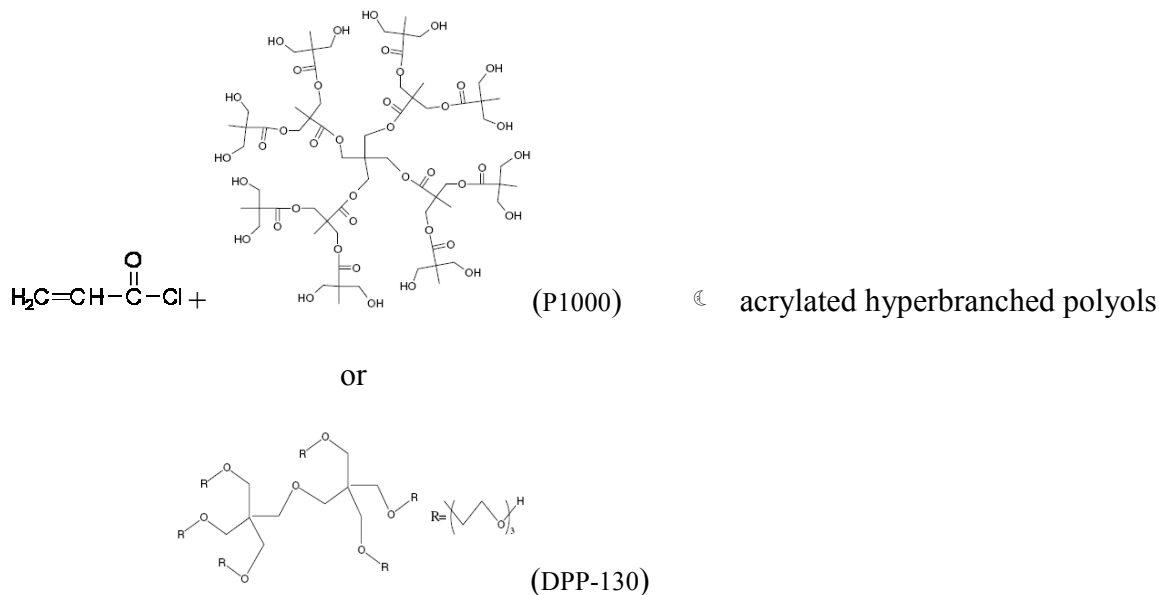


Figure 2.2.3-1. Schematic for the synthesis of acrylated hyperbranched polyols.

The acrylated polyols synthesized were then combined with CN2300 at various loading levels (10 - 50% wt.) adhesion tested. It was found that 10-30% 1:1 acrylated DPP-130 polyol and 10% 10:1 acrylated P1000 polyol gave higher adhesion strength than the control (CN2300 only, adhesion force ~ 10 lb).

Samples were prepared that contained CN2300, 4% photoinitiator, 30% wt. Mg, 10% 10:1 acrylated P1000 polyol or 5% MEK-ST. The samples can now withstand overnight constant immersion in the electrolyte as shown in Figure 2.2.3-2.

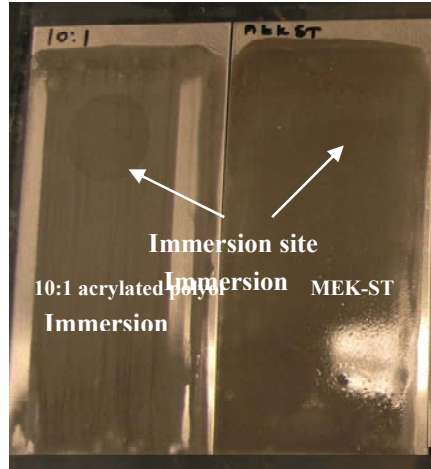


Figure 2.2.3-2. Samples after conducting EIS measurements.

Follow-up experiments will be conducted in which acrylated polyols and MEK-ST or acrylated trimethoxy silane will be formulated together and tested for adhesion. The most promising compositions will be further developed using different loading levels of Mg.

2.2.4. Flexible Binders for Mg-rich Coatings

Epoxy polymers have been widely used in coatings and adhesives even though they tend to be brittle and crack when flexed at low temperatures. For aircraft coatings, superior flexibility even at very low temperatures is a necessary to provide long-term corrosion protection and adhesion.

Polysulfides are known to possess exceptionally good flexibility due to the relatively low energy of rotation of –S-S- bonds (0.95 – 1.05 Kcal/mol) as compared to the energy of rotation of –C-C- bonds (3.9 – 4.4 Kcal/mol). Additionally, the following characteristics of this class of polymers make them very attractive for application as a flexible anti-corrosion coating:

1. Polysulfides are known to have low gas permeability, and it is well known that one of the most important factors contributing to corrosion is the access of oxygen to metal substrate;
2. They have outstanding chemical resistance. One of the most demanding and critical polymer applications, the seals in integral aircraft fuel tanks, are made almost exclusively from polysulfides.
3. They have high UV resistance and inhibit all the radical-based chemical reactions that greatly contribute to the destruction and deterioration of polymeric materials. Among polymers, only silicones have better UV resistance than polysulfides.

The candidate coating, TZ 904, was obtained from Chevron Philips Company. It is a two-component epoxy coating with an amino terminated polysulfide curing agent. The carboxyl and hydroxyl group terminated structures revealed are shown in Figures 2.2.4-1 and 2.2.4-2, respectively.

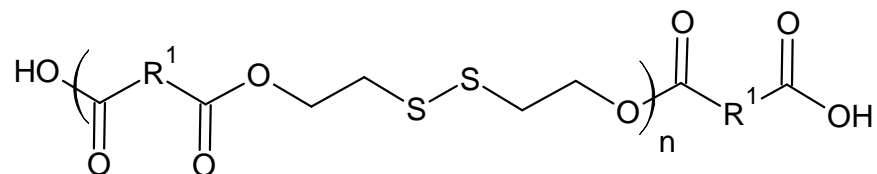


Figure 2.2.4-1. The chemical structure of carboxyl-terminated polysulfide polyesters.

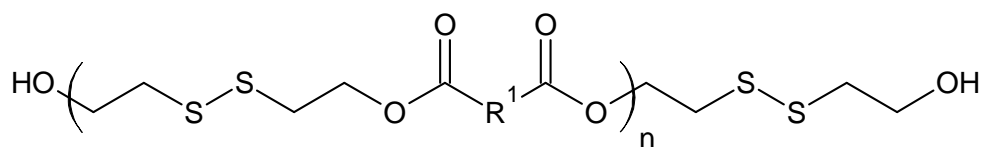


Figure 2.2.4-2. The chemical structure of hydroxyl-terminated polysulfide polyesters.

Technically, the coating, which has low VOCs, should be applied by a plural spraying system with a mixing volume ratio of 1:1. But to be convenient, the epoxy and hardener components are dissolved in xylene, which has proved to be the best solvent so far, in a rough weight concentration of 37% and 66% respectively, and sprayed by an ordinary spray gun.

In order to get an initial corrosion protection measurement, Mg pigment 3820 was added to achieve the 40% PVC, which is supposed to be able to provide a better corrosion protection according to previous work. Some mechanical properties were measured for the Mg-rich coating and the results are shown below:

CPVC=40%	Impact resistance	<5lb.cm	Thickness(μm)	155
	Conical Mandrel	Fail		123
	MEK double rubs	89		103
CPVC=0	Impact resistance	<5lb.cm	Thickness(μm)	135
	Conical Mandrel	Pass		147
	MEK double rubs	207		113

The data provided by manufacturer:

Property	Results
VOC	0
Gloss at 60° angle 3	65-70
Elongation	>32%
Dry-to-touch time	20-30 min
Impact resistance	>150 in-lb
Tensile strength	2500-2900 psi
Adhesion to “new steel subsrtate”	32000 psi

These results indicate that TZ-904 is a good working platform to produce Mg-rich anti-corrosion coatings, though some of the performance is decreased by the high Mg content.

2.3 Magnesium Alloys

Mg alloys were evaluated for their utility as active pigments in corrosion protective primers. It was found that the Mg alloys provide certain cathodic protection and barrier properties. Furthermore, it was found that the electrochemical behavior of Mg alloy pigments were different from the pure Mg powder. The more relevant experimental results are summarized in a manuscript, attached as Appendix 2.3, which will be submitted for publication during fall 2007. The Mg alloys present some issues related to the manufacturing cycle that makes them difficult to obtain. In this research study, five different Mg alloy

particle types, AM60, AZ91B, LNR96, AM503 and AZG which have similar particle size (Vol% ~55 micron meter) but different chemical composition, especially with respect to the amount of Al, Zn and Mn content, were investigated as pigments in Mg-rich primer systems. The chemical compositions of the five different Mg alloy particle types studied are shown in Table 2.3-1. Particle size and PSD of the pigments were measured by using an Accusizer 780 optical particle sizer and are reported in Tables 2.3-2.

Table 2.3-1. Chemical compositions of the Mg alloy pigments investigated.

Pigment (ASTM)	Element (atom)%						
	Mg	Al	Zn	Mn	Si	Fe	Ni
AM60	94	6	~	0.2	~	~	~
AZ91B	89.8	9	1	0.2	~	~	~
LNR91	50	50	~	~	~	~	~
AZ503*	98.1	0.002	0.006	1.88	0.004	0.006	0.0014
AZG*	91.1	5.66	2.937	0.283	0.009	0.002	0.0006

Table 2.3-2. Particle size of different Mg and Mg alloy pigments.

Pigments		Mean Size (µm)		Mode Size (µm)		Median Size (µm)	
		Num%	Vol%	Num%	Vol%	Num%	Vol%
Pure Mg	3820	3.23	14.55	1.59	16.07	2.55	11.1
Mg Alloys	AM60	15.9	71.3	2.74	68.65	5.21	67.11
	AZ91B	22.18	70.83	47.75	68.65	10.21	67.11
	LNR96	10.04	56.12	2.74	61.29	4.66	55.04
	AM503	9.68	89.89	6.78	213.5	7.89	38.17
	AZG	9.4	30.36	7.43	33.21	7.55	26.77

Coatings of Mg alloy-rich primers were formulated at two different PVCs (Table 2.3-3), in which 32% is below the critical pigment volume concentration (CPVC) and 42% is above CPVC. All paints were applied on the panel surfaces by air spray. Primer coatings were cured at room temperature for one day followed by 1 hour in 65C. The thicknesses of dry primers were about 100µm.

Potentiodynamic measurements were conducted on all of the Mg alloy-rich primers. A glass cell was clamped to the test panel (working electrode) in a horizontal position with a 7.06 cm² exposure area, a Saturated Calomel Reference Electrode and a Pt mesh counter Electrode were put into the glass cell to form a three-electrode system. Dilute Harrison's solution (DHS) was used as the electrolyte.

Table 2.3-3. Compositions of Mg-rich primers at 32% and 42% PVC.

PVC	Epon 828 (g)	Epicure 2353 (g)	MEK (g)	Mg and Mg alloy Pigments (g)					
				3820	AM60	AZ91B	LNR96	AM503	AZG
32%	20	11	15	22.98	23.78	29.06	23.24	25.89	24.44
42%	20	11	25	35.37	36.59	36.79	44.71	39.84	37.60

Potentiodynamic tests were conducted by collecting corrosion current while DC potential, whose range was from -2 volt to +2 volt vs. Open Circuit Potential, were applied to the system.

Potentiodynamic measurements are very useful for investigating the electrochemical behavior of primer systems. The results can give a quick view of the change in current density as function of applied potential. Also, through the potential dynamic curve, the mixed potential, i.e. the open circuit potential (OCP), of a primer can be obtained and the corrosion rate estimated by the Tafel coefficient. Further, it can provide information on passivation.

Figures 2.3-1 and 2.3-2 show the potential dynamic curves of Mg3820, AM60, AZ91B and LNR96-based primers at a PVC of 32% (below CPVC) and 42% (above CPVC), respectively. From these figures, it can be seen that the OCP of all Mg alloy-rich primers is less than -1.0 V which is below the OCP of bare Al and indicates that the Mg alloys all provide cathodic protection.

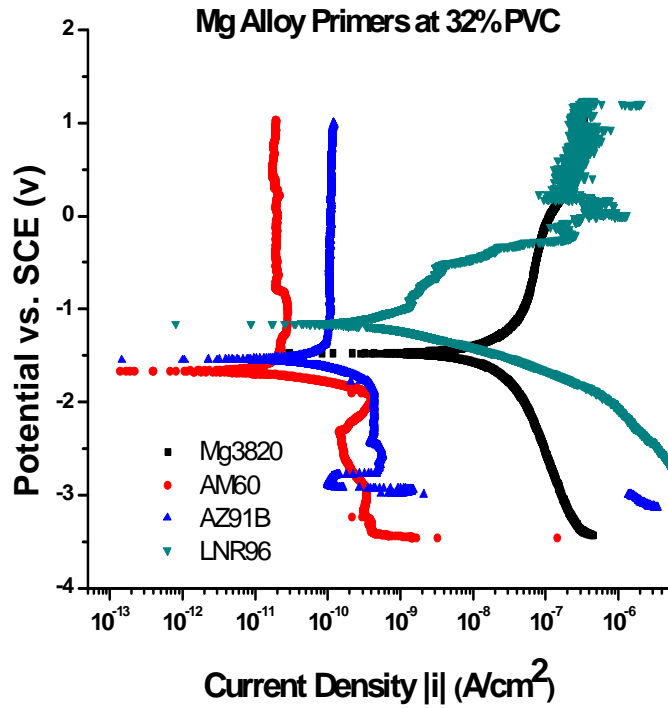


Figure 2.3-1. Potential dynamic curves for Mg alloy-rich primers at 32 % PVC.

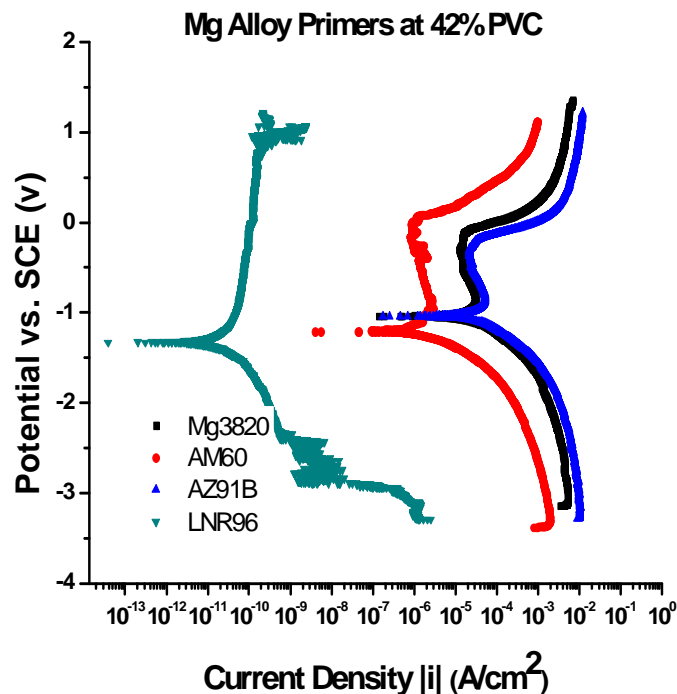


Figure 2.3-2. Potential dynamic curves for Mg alloy-rich primers at 42 % PVC.

From Figure 2.3-1, it can be seen that, at a PVC below CPVC, the OCP of Mg alloy-rich primers increased in a positive direction with increasing Al content of the alloy and the current density increased with increasing Al content. This result shows that increasing the content of the less active element, Al in this case, shifts the mixed potential toward the OCP of the bare substrate.

The current densities of Mg alloy primers were lower than that of a pure Mg primer, especially for AM60 and AZ91B, which were 5 orders of magnitude lower. This result indicated that a small amount of Al (~5%) can greatly decrease the corrosion current density. It also indicated that AM60 and AZ91B display passivating behaviour in a large range of potential (from -1.5v ~ 1 V) providing additional protection to the substrate.

From Figure 2.3-2, quite different potentiodynamic behaviour was observed for Mg alloy-based primers at 42% PVC (above CPVC) as compared to the lower PVC analogs. For primer based on pure Mg and primer based on the Mg alloy with the lowest Al content (AM60 and AZ91B), the current density increased by 3 orders of magnitude compared with that at 32% PVC (below CPVC). This behaviour can be explained by the porous structure of primers at high PVC (above CPVC). Interestingly, the current density of LNR 96 primer, which had 50% Al in the alloy, decreased greatly compared with the current density obtained at 32% PVC (below CPVC). In addition, a larger range of passivation was observed for LNR96 primer at 42% PVC than at 32% PVC.

Figures 2.3-3 and 2.3-4 show potentiodynamic curves for AM503 and AZG-based primers at a PVC of 32% (below CPVC) and 42% (above CPVC), respectively. For comparison, the potential dynamic curve for a pure Mg-based primer is also provided. Similar to primers based on the other Mg alloys, OCPs of these primers were below that of bare Al alloy indicating the ability to provide cathodic protection.

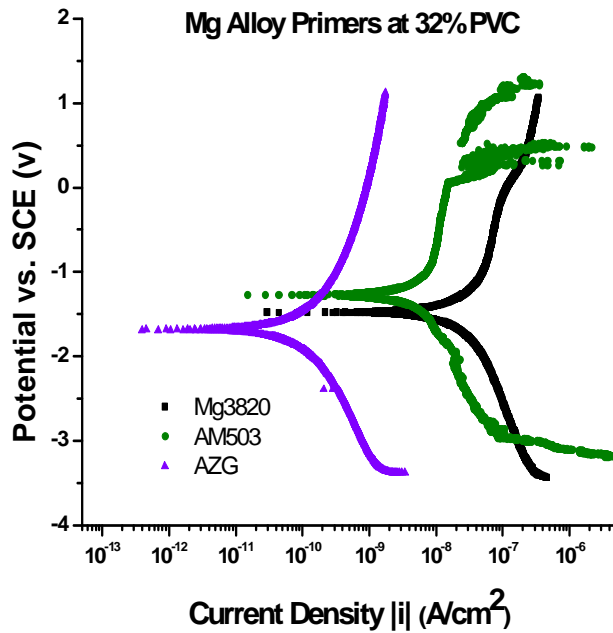


Figure 2.3-3. Potential dynamic curves of AM503 and AZG-based primers at a PVC of 32%.

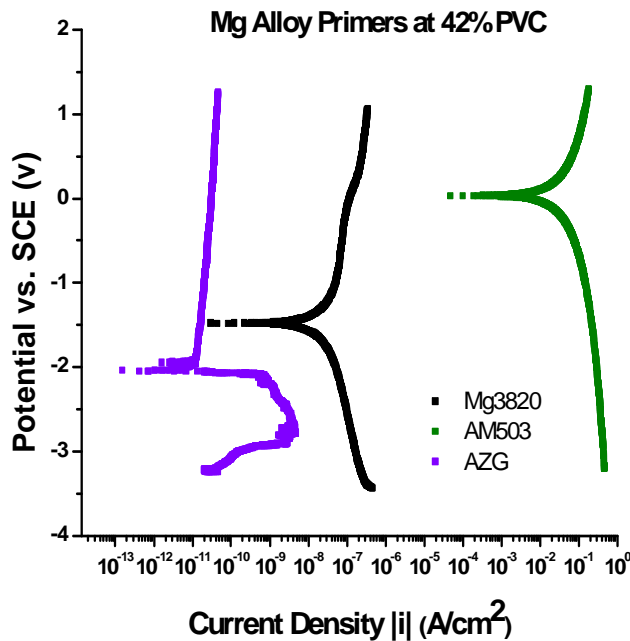


Figure 2.3-4. Potential dynamic curves of AM503 and AZG-based primers at a PVC of 42%.

The AZG primer showed unique potential dynamic behaviour. The OCP was near -2.0 V (vs. SCE), which is even lower than that of the pure Mg primer. This result may be the result of the chemical composition of the AZG alloy. From Table 2.3-1, it can be seen that AZG and AM60 have a similar Al content (~ 6%) but AZG contains about 3% Zn. Apparently, the addition of Zn results in a great decrease in OCP.

In addition, the effects of chemical composition on potentiodynamic behaviour are shown in the results obtained for the AM503 primer. AM503 consists of 98.1% Mg which is close to pure Mg. However, it showed much higher OCP than that of pure Mg primer especially at the PVC above CPVC. At 42 % PVC, the current density of the AM503 primer was much larger than that of the pure Mg primer. Obviously, the addition of less than 2% Mn could have resulted in such a different behaviour. In both cases, the small amount of Zn or Mn resulted in a significant effect on potential dynamic behaviour. Overall, corrosion protection of Mg alloy-based primers appears to be significantly affected by the third element other than Mg and Al.

In summary, our results have shown that, similar to pure Mg primer, all Mg alloy primers provide cathodic protection to the Al alloy substrate. The composition of the Mg alloy, such as the content of Al and the composition of the third element, can greatly influence performance.

3.0 Development of New Combinatorial Capabilities

NDSU has been very active in the development of combinatorial/high-throughput methods for the development of new polymers and surface coatings [Chisholm, 2007]. All aspects of the experimental process have been addressed and a full combinatorial workflow, as depicted schematically in Figure 3.0-1, has been developed. Initial efforts were focused on securing instrumentation and software and developing methods to enable the development of polymers and coatings useful for marine coatings. However, due to the Durable Hybrid Coatings for Aircraft (DHC) program, significant progress has been made toward enabling the development of aerospace coatings using the combinatorial workflow.

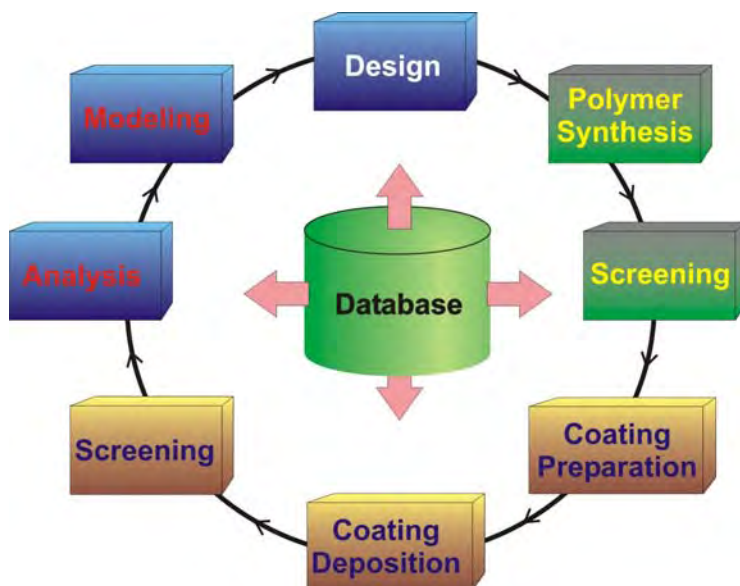


Figure 3.0-1. Schematic of the elements comprising the combinatorial workflow in place at NDSU.

At the beginning of the DHC program, some key needs for enabling the development of aerospace coatings using combinatorial methods were identified:

- 1) Robotic viscous liquid handling.
- 2) High shear mixing for pigment dispersion.
- 3) High throughput screening method for characterizing corrosion protection.
- 4) High throughput screening method for characterizing weatherability.

At present, all of these needs have been addressed; however, development status is at various stages depending on the tool.

3.1 Viscous Liquid Handling Workflow

Our current coating formulation capabilities consist of an automated powder dispenser and two liquid handling robots. The maximum viscosity that can be accurately handled with the liquid handling robots is about 250 cP [Chisholm, 2006] which necessitates pre-dilution of viscous starting materials. While pre-dilution is fine for many experimental objectives, it is a significant limitation for developing pigmented coatings since production of a pigment dispersion usually requires a viscous medium for high shear dispersion. Very recently a robotic viscous liquid handling system was purchased from Symyx was purchased using funds available from an Office of Naval Research sponsored program.

The viscous liquid handling station consists of a desktop robotic platform fitted with two arms for the mounting of end effectors and a modular deck that can be reconfigured. The apparatus is controlled by a PC and is integrated into our main database for the transfer of formulation files and data capture. The robotic arm end effectors consist of a vessel mover, positive displacement dispense tip (disposable), solvent dosing tip for 10 solvents, pH probe and conductivity probe. The modular deck has been configured with 24 mini blender cups for high shear mechanical mixing of viscous liquids and pigments, six reagent bays with heating and magnetic stirring, balance for gravimetric dispensing, disposable positive displacement tip rack, waste and washing bins.

3.2 Coating Deposition Workflow

In addition to the viscous liquid handling system, a new coating deposition system was purchased which complements the viscous liquid handling station. This system is built on the same modular platform as the viscous liquid station, but has been outfitted with different capabilities. The arm end effectors consist of a positive displacement dispensing tip (disposable), coating substrate mover, doctor blade tool, and lid remover. The deck consists of 12 mini blender cups (interchangeable from the viscous station), heated/magnetically stirred bays for reagents and a doctor blade wash station. The unit also has a plate mover/stacker attached to the side to continuously feed blank plates and store wet plates for drying. The addition of the blenders and liquid dispensing allow researchers to add reactive components at the point of coating deposition to broaden the spectrum of coating chemistries that can be performed in a high throughput fashion.

3.3 Tribology Workflow

A tribology workflow, also purchased through the ONR program, enables the high throughput measurement of friction, wear and tack on the substrates generated by the coating deposition tool. This unit is built on the same platform as the viscous liquid dispense and coating deposition tools. The robotic arms are configured with a coating substrate mover for plate manipulation and a 2 axis ball tip force probe for contacting the samples. The arms also feature a liquid dispense tip for the deposition of liquid lubricants, solvents and slurries to broaden the range of tests that can be performed on this tool. The deck contains two ball array racks for the storage of replacement balls. A new ball can be loaded for each test to eliminate the need for washing of the spherical probes between tests. A plate move/stacker is also attached to the unit to feed large numbers of panels automatically. A digital camera and laser profilometer have been incorporated into the design to monitor the groove formation over time. As with the two other stations, this one is connected to the main database for experiment control and data storage. This workflow was partially purchased with funds available within the Durable Hybrid Coating program.

3.4 High-throughput Measurements of Corrosion Protection

In order to apply the combinatorial/high-throughput methodology to the development of primers for corrosion protection, a high-throughput measurement system was required to characterize corrosion protection using relatively small samples sizes. We recently completed building and validating a high-throughput process for characterizing corrosion protection using electrochemical techniques such as impedance spectroscopy. In addition to the electrochemical measurement, the process also involves parallel dip coating for sample preparation and an imaging system for capturing images of scribed specimens after salt spray exposure. Figure 3.4-1 provides images of the equipment built. A manuscript describing, in detail, the parallel electrochemical measurement system is almost complete and will be submitted to the Journal of Combinatorial Chemistry. A draft of the manuscript is provided as Appendix 3.4.

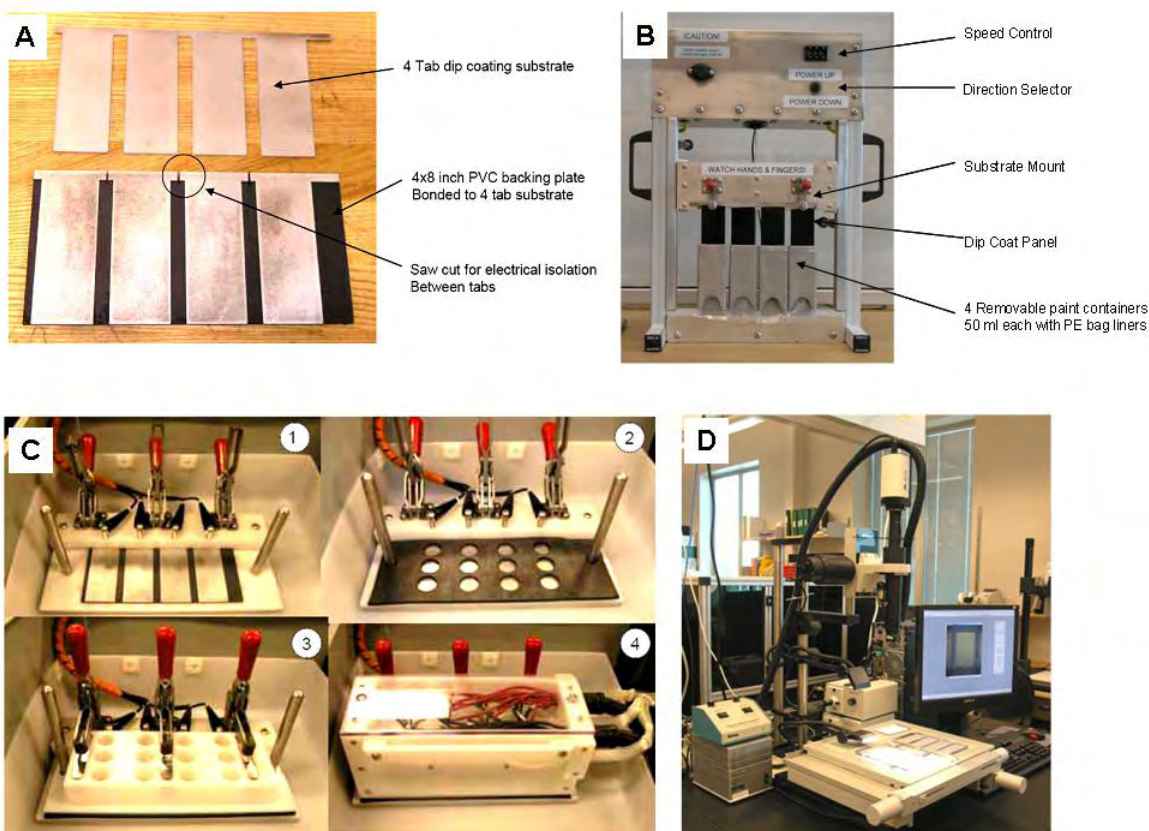


Figure 3.4-1. Images of the equipment built to enable high throughput measurements of corrosion protection. (A) Substrate illustrating the array format; (B) Parallel dip coater; (C) Parallel EIS system; (D) Imaging system.

Figure 3.4-2 displays all the components of the high-throughput EIS apparatus which consists of a Faraday cage containing an automatic electronic switch control unit and a 4 x 3 electrochemical cell array, a Gamry MultiEchem 8 workstation connected through the electronic switch system to the 4 x 3 electrochemical cell setup. The custom-made Gamry workstation contains six femtostats (FAS-2) and two potentiostats (PCI4). In this EIS setup, only four femtostats (channel 1 to 4) are interfaced to the 4 x 3

electrochemical cell array through the electronic switch unit so that four measurements can be run simultaneously.

Based on the previous design, shown in the last year's annual report, a series of modifications and engineering work was done to optimize instrument performance. First, the electronic switch unit was updated because all the electronic relays previously used had less than optimal insulation resistance (10^{10} ohm), as a result, small leaking currents made it impossible to measure high impedance coatings. Instead, a form of high resistance relay from COTO was selected, the insulation resistance of which is 10^{14} ohm.

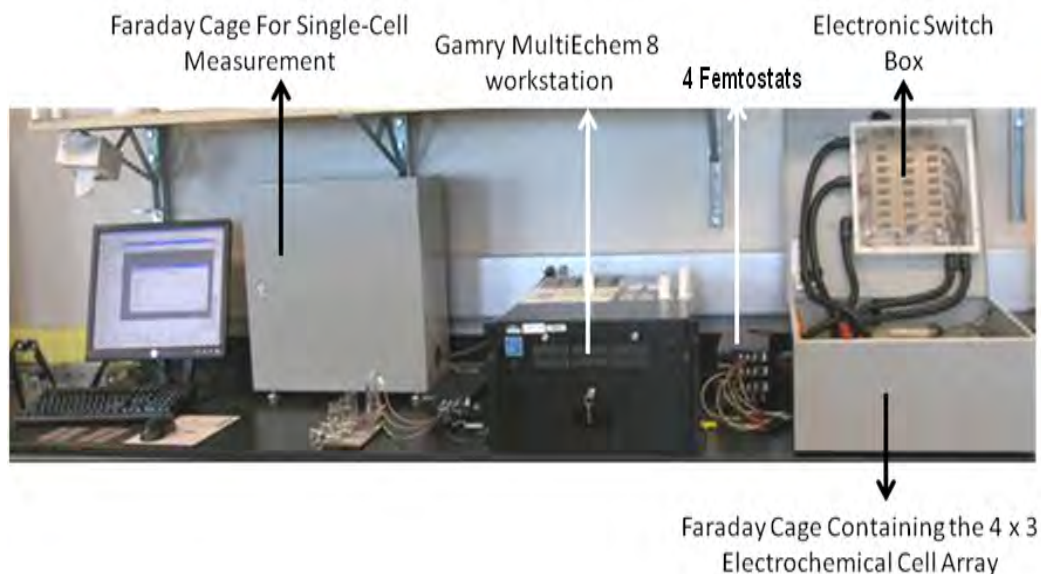


Figure 3.4-2. Image of the complete parallel EIS system.

The new relays work well with high impedance coating measurements. A diagram for the new switch unit is shown in Figure 3.4-3.

Additional modifications included a DC power supply to power the electronic switch unit to prevent ac line noise pickup, new cables for working, reference and counter electrodes were shortened to minimize their capacitive effect. High quality shielded coaxial cable was used to replace the previously used unshielded cable for all of the signal wiring. The geometry of the reference and counter electrode in each electrochemical cell was adjusted to form a relatively uniform current distribution.

During a typical run, the top row of 4 wells are measured simultaneously followed by row 2 and then row 3. This eliminates two coating patches sharing a common base (working electrode) from interfering with each other during the run. A switching device was created to perform the required connection and disconnection of the electrodes when changing rows during a test. The delay created by the sequential testing of the 3 rows presents the problem of inconsistent exposure time of the electrolyte solution with the test coatings. For example, if the researcher loads all 12 wells with electrolyte and starts the run, row 1 will be tested immediately while rows 2 and 3 will be absorbing electrolyte prior to the EIS test. Absorbed electrolyte can change the EIS behavior of the coating sample and introduce substantial error between the replicate EIS readings. To prevent this from occurring we have integrated a series of fluid delivery and extraction tubes into each well of the 12 well assemblies. With this approach, only the row subject to EIS testing is loaded with electrolyte while the others are evacuated or filled with solutions such as DI water, reference electrode conditioning solution, or other fluids of interest. This capability

will allow the entire test to be automated and allow for studies to be performed where EIS measurements are made before and after a challenge solution (acid or base) is exposed to the coating samples.

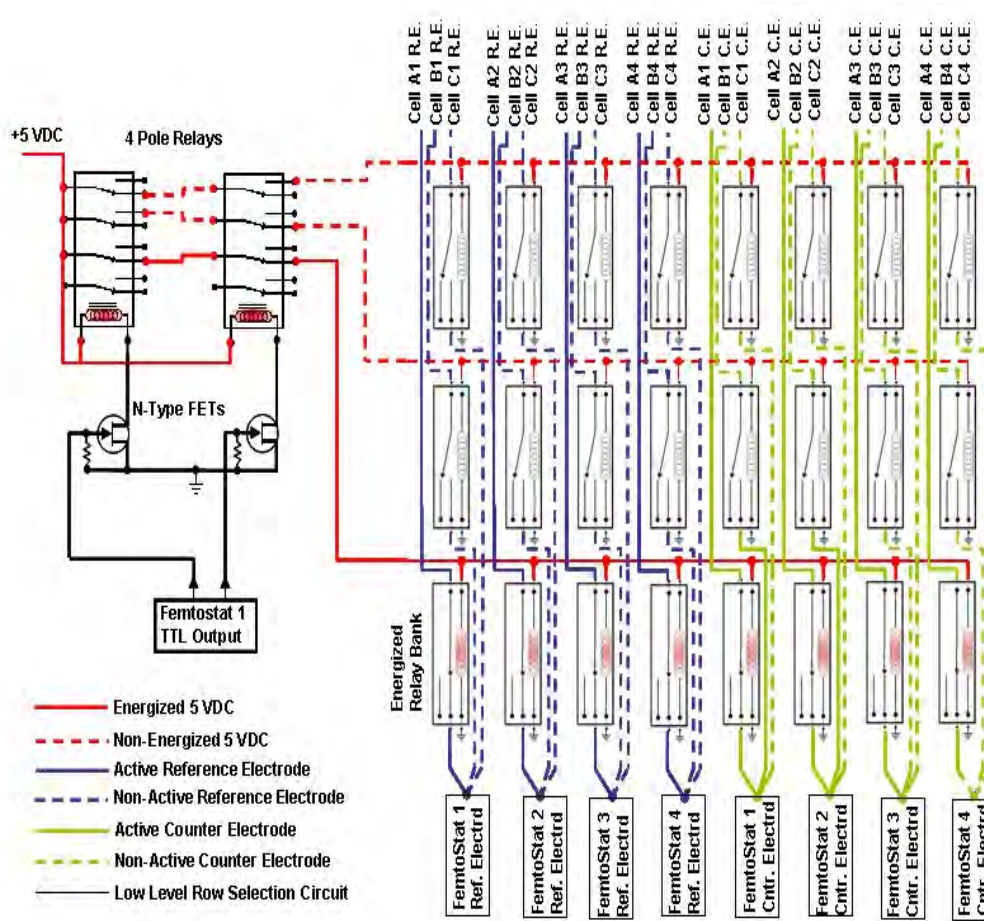


Figure 3.4-3. A schematic diagram of the switching system for the parallel EIS apparatus.

3.5 Equipment for Automated Color and Gloss Measurements

Besides providing aesthetics, topcoats also serve to provide a barrier between the environment and the substrate. Since the topcoat is in direct contact with the environment, it must have exceptional weatherability. In addition, it must have appropriate mechanical properties to resist damage due to impact or abrasion and it must adhere well to the primer layer. Recently, work was completed on the development an automated system for measuring gloss and color which will enable the high throughput characterization of weatherability. The automated color and gloss system combines an off-the-shelf spectrophotometer and gloss meter with custom robotics to provide a system that is compatible with existing array formats. The system, shown in Figure 3.5-1, is fully automated and the custom software allows for easy transfer of all data to the database for later review and consolidation.



Figure 3.5-1. A photograph of the automated color and gloss measurement system built at NDSU.

Color measurements are made using an integrating sphere spectrophotometer from X-Rite. This unit captures true color values with or without the gloss component included. The X-Rite device is fully integrated into the software for complete control of the unit without operator intervention. Gloss measurements are taken at 3 angles using a hand held device from BYK Gardner. This device is also fully integrated into the software for a completely automated system.

4.0 Plasma Deposition of Inorganic Coatings

4.1 Trimethylsilane-based Permanent Pretreatments in a Mg-rich Primer Corrosion Prevention System

In this year's effort, a trimethylsilane-based coating was investigated as a pretreatment with SiC-based thin films deposited onto Al-2024 substrates by plasma-enhanced chemical vapor deposition (PECVD). A screening study of the pressure (P) dependence of films deposited at 350 °C showed an increase in growth rate from 0.6 to 1.9 Torr. A second screening study where P was fixed at 1.9 Torr and temperature was varied from 125 to 550 °C showed decreasing growth rates with increasing temperature with an apparent transition around 300 °C. Electrochemical impedance spectroscopy (EIS) of the SiC-based films on Al-2024 after exposure to a corrosive environment (i.e., dilute Harrison solution) indicate samples coated using SiC-based films exhibit higher low frequency impedance (i.e., 100 to 1000X higher) than bare Al-2024 with open circuit potential remaining 0.1V higher for the former suggesting the SiC-based films slow the corrosion process. A Mg-rich primer was coated onto the SiC on Al-2024 with the galvanic function of the system determined by EIS. As compared to SiC on Al-2024, a similar behavior for the low frequency impedance was observed for the Mg-rich primer coated samples with some films exhibiting $1E+8$ ohm at 0.1 Hz indicating a strong barrier property. Initial gas jet erosion using acrylic media indicates the Mg-rich primer coatings are removed in preference to the Si-C films – the first step toward demonstrating a *permanent* pretreatment. When successfully developed and optimized, the value of such a hard, protective coating is the reduction of a three-component coatings system (i.e., pretreatment, primer, topcoat) to a two-component system (i.e., primer, topcoat).

This year's report is a preliminary report on the development of Si-C based coatings targeted to be *permanent* pretreatment layers on Al-2024 alloy. While films in the present study were grown at reduced pressure (i.e., $P < 2$ Torr) via PECVD (a process not amenable to application at the depot), this investigation of feasibility offers valuable initial feedback regarding the utility of gas-phase precursors and a low-temperature process in the production of SiC-based coatings that meet the electrical and durability metrics described above. We have found that this is the case and look forward to future experiments that will utilize atmospheric-pressure deposition processes such as dielectric glow discharge and atmospheric-pressure plasma jet.

4.1.1 Experimental methodology

4.1.1.1 SiC-based Film Growth by PECVD

Thin SiC-based films were grown via PECVD using 2% $\text{HSi}(\text{CH}_3)_3$ (trimethylsilane or TMS) in argon as the precursor in an Oxford 100Plus with Al-2024 alloy (Q-panel) 4"x4" substrates rubbed with 0000 steel wool immediately prior to film growth. Deposition temperatures (T_{dep}) and pressures (P_{dep}) ranged from 125-550 °C and 0.5 to 1.9 Torr, respectively, with deposition time fixed at 20 min.

4.1.1.2 Mg-rich Primer Applied to Coated Substrates

A 50% pigment volume concentration primer was applied to SiC/Al-2024 substrates using a high volume low pressure air spray method. The formulation utilized two forms of Mg powders (i.e., Eckagranules™ PK31 and Eckagranules™ PK51 (Ecka GmbH)) mixed at a 52/48 vol./vol. ratio. The epoxide binder system was comprised of 25 wt% Epon1001-CX-75 (Resolution Performance Products) dissolved in a 65/35 vol./vol. ratio methylisobutylketone/xylene (Sigma-Aldrich). Epicure3140 (Resolution Performance Products®) was employed as a polyamide curing agent and Aerosil® R974 (Degussa, Inc.) was used as dispersing agent. Figure 4.1-1 shows photographs illustrating how one half of the substrate

(i.e., 5 cm x 10 cm) is coated with Mg-rich primer/MS-derived film while the other half is covered by a TMS-derived thin film only⁴”

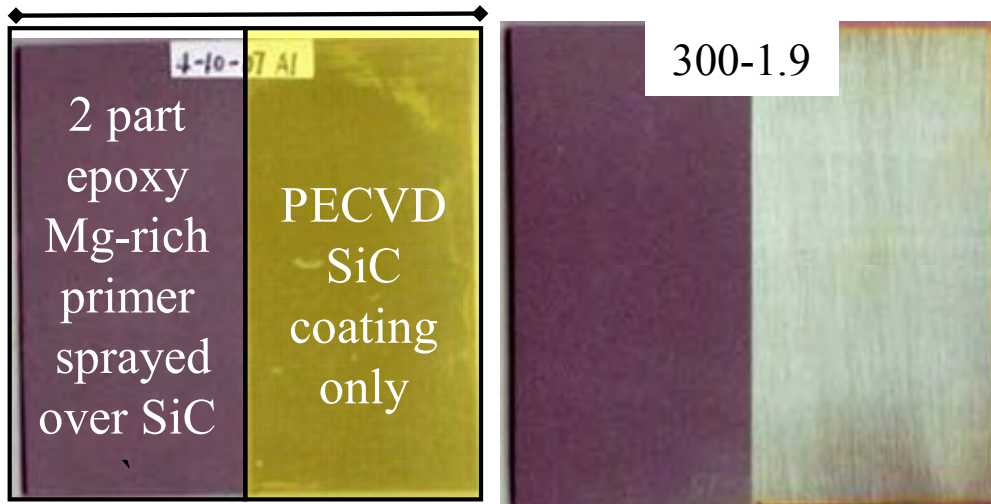


Figure 4.1-1. Photographs of test coupons used in this study.

4.1.1.3 Electrochemical Impedance Spectroscopy (EIS) Testing

The Electrochemical impedance spectroscopy (EIS) was conducted through a Gamry MultiEchem 8 Electrochemistry System coupled with EIS300 measurement software. A 5cm-long Plastic wells with inner diameter 2.54 cm were glued onto the sample surface using a 2K epoxy (Marine Goop[®]). Dilute Harrison’s solution (0.35% (NH₄)₂SO₄ and 0.05% NaCl in deionized water) was used as the test electrolyte and also served as a corrosive environment for the constant immersion test of the coatings.

4.1.2 Results and Discussion

Figure 4.1-2 shows SEM photographs of a typical TMS-derived film ($T_{\text{dep}} = 350\text{ }^{\circ}\text{C}$, $P_{\text{dep}} = 1.9\text{ Torr}$) at low (Fig. 4.2a) and high magnification (Fig. 4.2b). Marring of the Al substrate from the steel wool surface preparation step is apparent in Figure 4.1-2(a) and the surface morphology of the SiC-based coating is illustrated in Figure 4.1-2(b). Film adhesion of SiC on Al-2024 as well as Mg-rich primer on SiC on Al-2024 was qualitatively evaluated via the cross-hatch method (ASTM 3359) and all films (except 350-1.2) exhibited excellent adhesion (i.e., 5B rating).

4.1.2.1 Temperature screening study

The experimental conditions and results of the temperature screening study are given in Table 4.1-1. In this instance, pressure was fixed at 1.9 Torr and T_{dep} varied from 125 to 550 °C with upper T_{dep} limited by thermal failure of Al substrates. The real portion of the refractive index (n) increase as increasing of T_{dep} and the value varied substantially from 3.13 for films deposited at 550 °C to 1.64 for films grown at 125 °C. It appears that higher T_{dep} favors the formation of a-SiC:H. Further characterization (i.e., XPS, FTIR) is planned to substantiate chemical composition of the films. Also of note is the trend of decreasing growth rates with increasing temperature. Figure 4.1-3 shows a plot of growth rate as a function of T_{dep} . The results of this initial study tend to indicate two growth regimes that transition around 300 °C as illustrated by the two lines intersecting each other in the graph (Fig. 4.1-3). It seems plausible that the lower T_{dep} portion ($T_{\text{dep}} < 300\text{ }^{\circ}\text{C}$) of this plot represents a regime where the gas-phase precursors condense to form a partially-polymerized structure. By way of comparison, $T_{\text{dep}} > 300\text{ }^{\circ}\text{C}$ provides

enough energy such that the precursors condense and then react on the surface of the substrate to form a film.

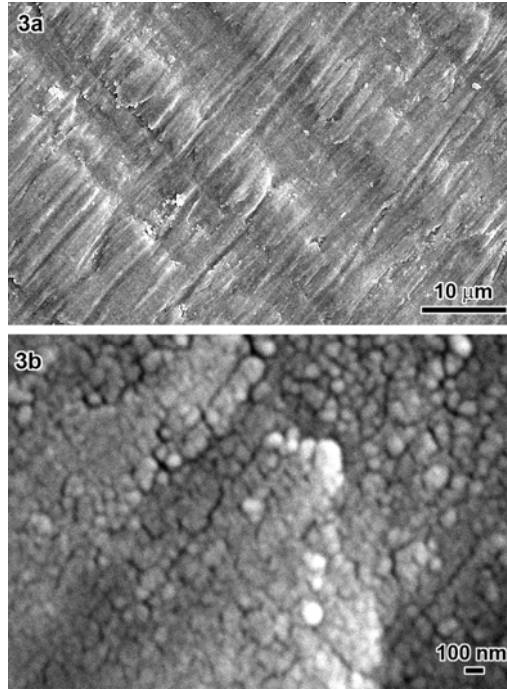


Figure 4.1-2. Scanning electron micrographs of SiC on Al-2024 at (a) 2,000 X and (b) 40,000 X magnification.

Table 4.1-1 Experimental Conditions and Characterization for the *Temperature* Screening.

Sample ID	T _{dep} (°C)	P _{dep} (Torr)	n of SiC ^[a]	SiC film t ^[a] (nm)	SiC	SiC	SiC	SiC	Mg-rich	Mg-rich	Mg-rich	Mg-rich
					10 min Z _{mod} ^[b] (Ω)	2 day Z _{mod} ^[c] (Ω)	10 min OCP ^[d] (V)	2 day OCP ^[e] (V)	10 min Z _{mod} ^[f] (Ω)	2 day Z _{mod} ^[g] (Ω)	10 min OCP ^[h] (V)	2 day OCP ^[i] (V)
Al-2024	n.a.	n.a.	n.a.	0	1E+3	3E+3	-0.654	-0.840	4E+3	7E+2	-1.178	-1.055
125-1.9	125	1.9	1.64	247	2E+5	8E+3	-0.670	-0.692	3E+7	2E+5	-1.250	-1.026
200-1.9	200	1.9	1.88	166	1E+5	2E+4	-0.690	-0.685	5E+6	3E+5	-0.910	-1.057
250-1.9	250	1.9	2.33	102	5E+4							
300-1.9	300	1.9	2.46	84	1E+5	9E+4	-0.680	-0.689	2E+7	3E+5	-1.375	-1.067
350-1.9	350	1.9	2.61	76	3E+4	3E+4	-0.660	-0.685	2E+7	3E+5	-1.250	-1.047
450-1.9	450	1.9	2.76	76	7E+3	4E+3	-0.675	-0.695	4E+6	7E+4	-1.360	-1.030
550-1.9	550	1.9	3.13	56	3E+3	1E+3	-0.695	-0.755	3E+4	5E+3	-1.305	-0.995

Legend: [a] *n* (real portion of refractive index) and *t* (film thickness) derived from ellipsometry data; [b] 0.1 Hz data for SiC on Al-2024 after 10 min in dilute Harrison solution (DHS); [c] 0.1 Hz data for SiC on Al-2024 after 2 days in DHS; [d] open circuit potential (OCP) of SiC on Al-2024 vs. standard calomel electrode (SCE) after 10 min in DHS; [e] OCP of SiC on Al-2024 vs. SCE after 2 days in DHS; [f] 0.1 Hz data for Mg-rich primer on SiC on Al-2024 after 10 min in DHS; [g] 0.1 Hz data for Mg-rich primer on SiC on Al-2024 after 2 days in DHS; [h] OCP of Mg-rich primer on SiC on Al-2024 vs. SCE after 10 min in DHS; and, [i] OCP of Mg-rich primer on SiC on Al-2024 vs. SCE after 2 days in DHS.

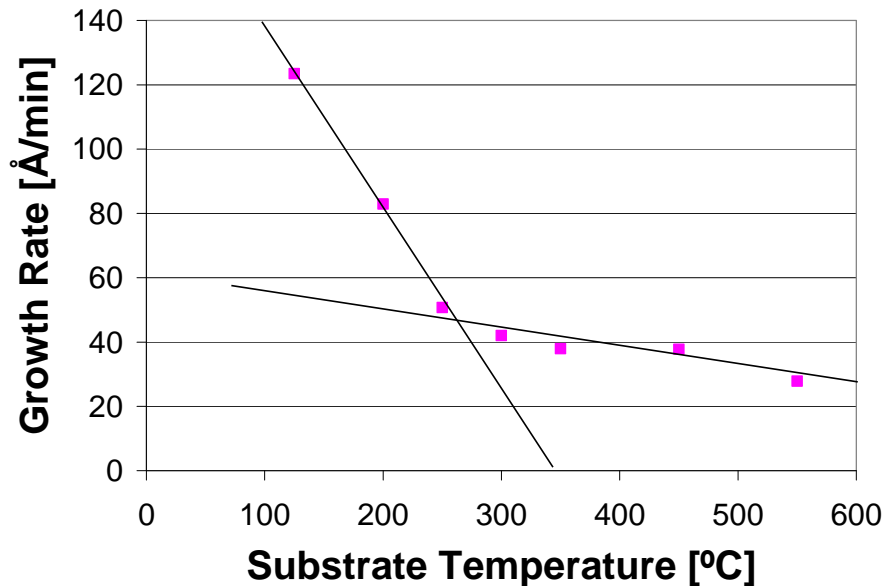


Figure 4.1-3. Growth rate as a function of T_{dep} for SiC-based films grown at 1.9 Torr.

EIS was used to evaluate the physical barrier property of the films and the impedance modulus (Z_{mod}) at 0.1 Hz was used as an indicator for the evaluation. As shown in Table 4.1-1, the SiC coated samples prepared at different deposition temperature exhibit variable impedance initially with the low frequency impedance decreasing with increasing T_{dep} . At initial point of immersion, the sample prepared at 125 °C showed the highest impedance ($2 \times 10^5 \Omega$) at 0.1 Hz – about two orders of magnitude higher than Al 2024. For T_{dep} from 200 to 350 °C, the low frequency Z_{mod} remains around $10^5 \Omega$ suggesting that the nanometer-scale thin film prepared at these conditions provide excellent barrier property. However, for $T_{\text{dep}} > 450 \text{ }^\circ\text{C}$, a significant impedance drop was noted indicating the good barrier film can't formed at this temperature range.

4.1.2.2 Pressure screening study

The experimental conditions employed for the pressure screening study as well as a compilation of the results are given in Table 4.1-2. For this study, pressure was varied from 0.6 to 1.9 Torr the latter being the highest possible given the present plasma controller. Some interesting trends are apparent from this study including increasing growth rate as a function of increased P_{dep} . Also, the optical constant of the films showed little variance possibly indicating a small effect of pressure upon film composition. The film grown at 1.2 Torr did not exhibit good adhesion. We attribute this anomaly to a stress-induced failure as the phenomenon was not observed for other pressures.

Films consisting of Mg-primer/SiC/Al-2024 showed improved barrier properties versus Mg-primer/Al-2024 with low frequency Z_{mod} at least 100X higher for the former versus the latter. After two days immersion in DHS, the 0.1 Hz Z_{mod} for all samples decreases by one or two orders of magnitude, indicating the cathodic protection of Mg-rich coating functioned. This effect was further validated by the fact that the OCP kept -1 V vs. SCE during this period of time.

Table 4.1-2. Experimental Conditions and Characterization for the *Pressure Screening*.

Sample ID	T _{dep}	P _{dep}	n of SiC ^[a]	SiC film t ^[a]	SiC 10 min Z _{mod} ^[b]	SiC 2 day Z _{mod} ^[c]	SiC 10 min OCP ^[d]	SiC 2 day OCP ^[e]	Mg-rich 10 min Z _{mod} ^[f]	Mg-rich 2 day Z _{mod} ^[g]	Mg-rich 10 min OCP ^[h]	Mg-rich 2 day OCP ^[i]
	(°C)	(Torr)		(nm)	(Ω)	(Ω)	(V)	(V)	(Ω)	(Ω)	(V)	(V)
Al-2024	n.a.	n.a.	n.a.	0	1E+3	3E+3	-0.654	-0.840	4E+3	7E+2	-1.178	-1.055
350-1.9	350	1.9	2.61	76	3E+4	3E+4	-0.660	-0.685	2E+7	3E+5	-1.250	-1.047
350-1.6	350	1.6	2.64	51	3E+5	1E+4	-0.675	-0.710	5E+7	3E+6	-0.933	-1.028
350-1.2	350	1.2	2.57	45	[j]	[j]	[j]	[j]	[j]	[j]	[j]	[j]
350-0.8	350	0.8	2.53	39	7E+5	6E+4	-0.687	-0.705	3E+7	8E+6	-1.253	-1.025
350-0.6	350	0.6	2.56	33	9E+3	8E+3	-0.683	-0.713	2E+6	2E+5	-1.230	-1.001

Legend: [a] *n* (refractive index) and *t* (thickness) derived from ellipsometry data; [b] 0.1 Hz data for SiC on Al-2024 after 10 min in dilute Harrison solution (DHC); [c] 0.1 Hz data for SiC on Al-2024 after 2 days in DHS; [d] open circuit potential (OCP) of SiC on Al-2024 vs. standard calomel electrode (SCE) after 10 min in DHS; [e] OCP of SiC on Al-2024 vs. SCE after 2 days in DHS; [f] 0.1 Hz data for Mg-rich primer on SiC on Al-2024 after 10 min in DHS; [g] 0.1 Hz data for Mg-rich primer on SiC on Al-2024 after 2 days in DHS; [h] OCP of Mg-rich primer on SiC on Al-2024 vs. SCE after 10 min in DHS; [i] OCP of Mg-rich primer on SiC on Al-2024 vs. SCE after 2 days in DHS; and, [j] film had poor adhesion.

4.1.3 Conclusions

A plasma polymerization method was used to synthesize nanometer scale SiC thin film on Al 2024. Temperature and pressure screening experiments were conducted to optimize operational conditions in the polymerization process. Several points can be concluded from this preliminary results:

1. The deposition temperature used in the process plays an important role in preparing the SiC thin film. At relative low temperature ($T_{\text{dep}} < 300$ °C), the film formation may functioned through the condensation of the gas-phase precursors. When $T_{\text{dep}} > 300$ °C, the film may be formed through sequential precursors condensation/crosslinking reaction at the surface of the substrate.
2. From our EIS study, the optimal T_{dep} to prepare the SiC film is within the range of 300 to 350 °C. The films provided better barrier property than those prepared beyond this temperature range. They also show good compatibility with Mg-rich primer in term of corrosion protection. The combination of SiC pretreatment with Mg-rich coating improve barrier properties without lossing of galvanic activity of the Mg-rich coating.
3. Our pressure screening results (in the range from 0.6 to 1.9 Torr) showed that pressure probably is not a critical factor of controlling film formation in the plasma polymerization process.

4.2 Deposition of Transparent Conductive Indium and Tin Oxides by Atmospheric Pressure Plasma Jet – Toward In-field Aircraft Canopy Repair

Transparent conductive oxides (TCOs) have found broad application over the past few decades in photovoltaics, flat panel displays, and other electronic applications. Traditionally, TCO deposition has been performed at moderate temperature using vacuum-based growth systems which is not readily applicable to deposition on inexpensive polymer substrates (e.g., Mylar) nor roll-to-roll manufacturing. The aim of this project is to develop an atmospheric pressure plasma deposition system to deposit a transparent conducting oxide (TCO) layer that is (1) highly transparent and (2) shows good conductivity. This coating would have application in the field repair of aircraft canopies where TCO layers are used to reduce the radar cross section of the aircraft. Currently, damaged canopies are repaired with conductive

epoxy, or replaced entirely. The conductive epoxy repair results in a reduction in pilot visibility and therefore is only appropriate for limited areas of the canopy. Complete canopy replacement results in the need to maintain inventory of expensive, bulky components at airbases around the world, an expensive and logistically challenging task. The proposed coating solution could be housed in equipment roughly the size of a file cabinet, with relatively reasonable cost and high portability. The following materials properties are the metrics to establish initial proof-of-concept and represent the immediate goal of this project:

- Sheet Resistance of $10 \Omega/\text{square}$ or less;
- Optical transmittance $> 80\%$ at 550 nm ; and,
- Coating durability that meets MIL-C-48497.

If the transparent conductor is indium-tin oxide (ITO), then a 100 nm thick ITO film with resistivity of $10^{-4} \Omega\text{cm}$ would be required. By way of comparison, previous reports for this approach have afforded 200 nm thick In_xO_y films with $r = 10^{-2} \Omega\text{cm}$ and sheet resistance of $500 \Omega/\text{square}$.

The current effort began in December with the delivery and qualification of a Surfex Atmospheric Pressure Plasma deposition system. This system has been used to deposit films and modify surfaces using both gaseous and liquid precursors, but not solid precursors. A picture of the APP deposition system is given in Figure 4.2-1. The system was configured to be capable of supplying two independently controlled precursors simultaneously for the production of doped materials. To date, only single component films have been deposited. This was done to allow the quantification of experimental parameters without the potential of confounding results with other variables. Experimental conditions for both precursors consisted of matrices of substrate temperature, source container/supply line temperature, oxygen/helium flow ratio, and deposition head motion during deposition. Initial attempts at deposition consisted of steadily increasing the source container temperature until some change was noted on the substrate. Often this was a simple diffraction of light when the glass slide was held at a certain angle.

Sn(II) and In(III) beta-diketonate complexes (Fig. 4.2-2) were employed as the solid precursor sources with He carrier gas, O_2 reactant gas and growth temperatures from 25°C to 250°C . Thickness measurements



- X-Y-Z robot with heated platen
- Heated single/dual-precursor delivery system

Figure 4.2-1. Picture of NDSU Atmospheric Pressure Plasma deposition facility.

by ellipsometry and x-ray reflectivity give film thicknesses of 30-70 nm over an area of 30 cm² after a 20 minute growth period. The as-deposited films exhibit light transmittance in excess of 90% over the visible spectrum while maintaining resistivities on the order of 10⁻² Ω·cm. The UV-Vis transmission spectra for several films deposited using this approach are shown in Figure 4.2-3. It is noteworthy (Fig. 4.2-3) that the films prepared using the NDSU APP system have superior transparency than a commercially-procured TCO standard from Pilkington (i.e., TEC15 glass). While the as-deposited films meet the stated targets for transparency but not for conductivity, some improvement in the electrical properties (i.e., ρ < 10⁻³ ohm·cm) were observed after thermal treatment (T ~300 °C) in a controlled gas ambient tube furnace. Additional commercial and novel precursors and doping methods are also under investigation and will be the subject of an M.S. graduate student thesis project.

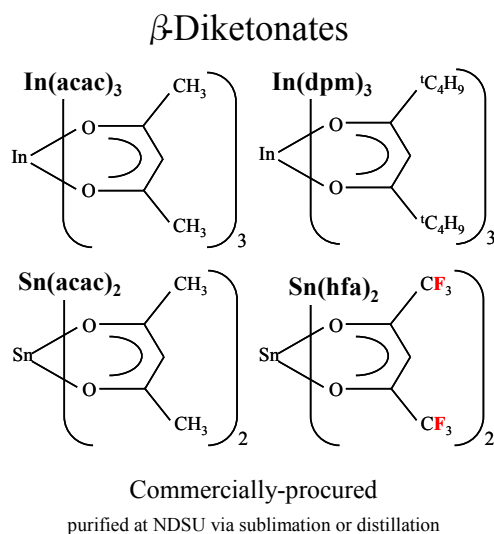


Figure 4.2-2. Precursors employed for APP film growth.

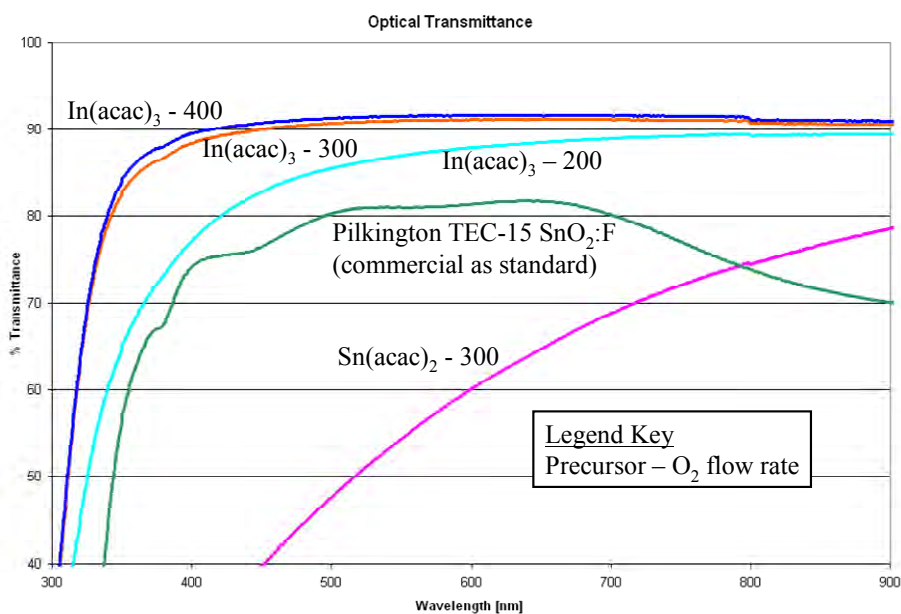


Figure 4.2-3. UV-Vis spectra for several films prepared using the NDSU APP system.

5.0 Remote Sensing for Coating Prognostics

Recently, there has been extensive development of several *in situ* sensing techniques that monitor the barrier properties of a coating. Most research in electrochemical sensors has been focused on sensor electrodes embedded in the substrate. Such sensors monitor corrosion of the metal substrate but provide no information about the film itself. Thus, they are unsuitable for monitoring corrosion within the metal-rich primer itself.

Another technique for *in situ* monitoring of a coating with *ac* involves the application of an embedded electrode or sensor within the coating. There are only a limited number of groups globally that are actively involved with the application of the embedded sensor technology (Kittel 2001, 2003; Miszyk, 2005). The Department of Coatings and Polymeric Materials at NDSU has been at the forefront in the development, feasibility demonstration, and application of embedded sensors, which consist of electrodes that act as the counter and reference but are placed between the layers of two-layered coating systems (Allahar 2005, 2006). A schematic diagram of the embedded sensor is shown in Figure 5.0-1.

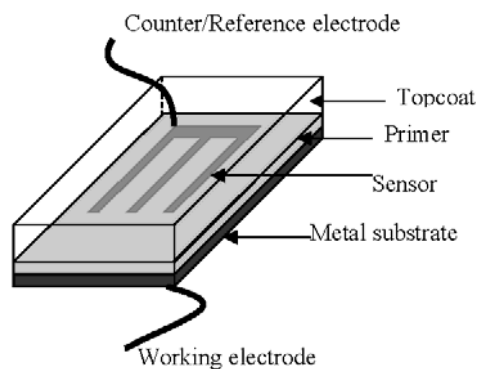


Figure 5.0-1. Schematic diagram of the embedded sensor.

An advantage of the embedded electrodes is that they are shielded from the environment by the topcoat, which prolongs the electrode life as well as reduces the noise associated with measurements. Another advantage is that electrochemical measurement of the primer and primer/metal interface can be made without being masked by high resistant topcoats.

While there have been limited studies published regarding embedded sensors, there has been no application to metal rich primers, e.g. Mg- or Zn-rich primers. The coupling of embedded sensors and coating systems with Mg-rich primers is a unique approach that allows monitoring of the electrochemical behavior of a Mg-rich coating beneath a topcoat.

Initial experiments have been carried out in order to obtain the baseline electrochemical response for the degradation of the primer in question. For the purpose of this research we have used the Mg-rich primer developed at NDSU [Nanna 2004, Battocchi^a 2006, Battocchi^b 2006]. For this primer, Mg powder with the average particle size of 25 μm (Ecka GmbH) is dispersed in a two-component epoxy-polyamide resin. A corrosion cell set-up from Princeton Applied Research was used to control the experiment geometry and enable a reliable set of results. The measurements were performed on a Gamry PCI4-300 potentiostat at 30 min intervals between consecutive runs. Figure 5.0-2 shows the low-frequency impedance modulus ($|Z|$) and the open circuit potential (E_{oc}) values plotted as a function of immersion time.

We have utilized the NDSU Pt-mesh electrode to construct a two-electrode (2E) EIS test cell, as shown in Figure 5.0-1. The metal substrate serves as the working electrode, while the Pt sensor is a combination of reference (RE) and counter (CE) electrodes, RE/CE. The primer has been applied to 6" x 3" AA2024-T3

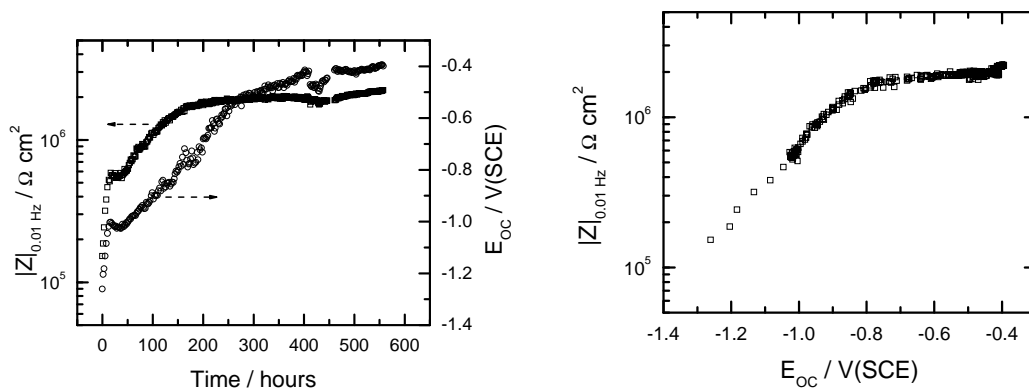


Figure 5.0-2. E_{oc} and $|Z|$ records for Mg-rich coatings on AA2024-T3 in dil. Harrison's solution.

coupons, and the Pt sensor (RE/CE) has been placed directly on top of the coating. The constant immersion will be performed in dilute Harrison's solution (0.35wt% $(\text{NH}_4)_2\text{SO}_4$ + 0.05wt% NaCl, pH=5.5) and $|Z|$ and E_{oc} monitoring will be performed as a function of immersion time.

Traditional electrochemical techniques assume homogeneous conditions over the entire working electrode surface. Aluminum alloys are particularly sensitive to localized attacks, and non-uniform electrochemical conditions are frequent on a coated surface. For a more complete interpretation of the events occurring under a coating on this type of substrate, a set of area-dependent information is necessary. For this purpose, the wire-beam electrode (WBE) has been constructed and is currently under testing at NDSU [Battocchi 2005]. The principle of this type of electrode is subdividing a metal plate into many small parts, 100 in the case shown in Figure 5.0-3, and measuring the electrochemical properties of each part by means of individual sensors [Wu 1995].

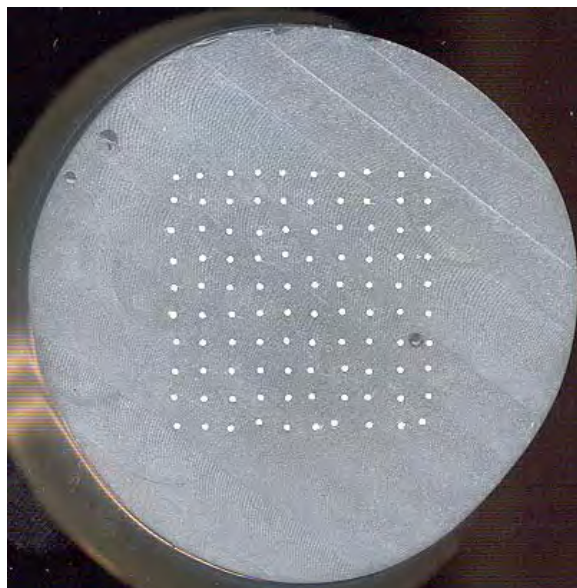


Figure 5.0.3 Cross-section of a wire-beam electrode with 100 Al wires.

To date, electrochemical studies utilizing the WBE have been primarily focused on measuring potential and current fluctuations around individual wires of this electrode assembly. This conventional WBE approach allows mapping of localized corrosion events taking place on the metal substrate.

In order to design a successful electrochemical sensor, it is imperative to understand how the geometry and dimensions of the sensor electrode influence its ability to detect small signals as a function of its separation from the substrate (WE). This task cannot be achieved by utilizing a standard, metal plate, working electrode. Therefore, we have proposed to combine the WBE with the sensor electrode (SE) embedded in the Mg-rich primer, as shown in Figure 5.0-4. This novel approach allows us to accomplish several goals aimed at understanding the electrochemical behavior of metal-rich primers upon degradation:

- map out sensor response as a function of distance from the substrate;
- estimate the “throwing power” of the embedded sensor and
- correlate the size of the sensor with the substrate area being monitored.

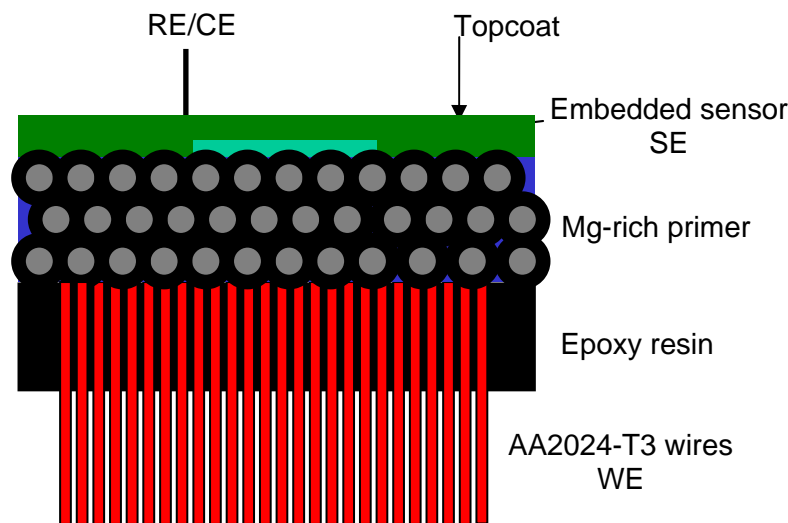


Figure 5.0-4 Schematic of WBE/SE experimental set-up.

The setup of the combined WBE/SE approach is shown in Figure 5.0-2. The WBE represents a “segmented” working electrode (WE), where one wire at a time can be activated, thus creating an electrochemical cell between the sensor electrode and this particular wire of the working electrode array. Similarly, any combination of several wires can be turned “on” to create any working surface geometry at various distances away from the sensor, limited only by the dimensions of the WBE. By switching between individual WE wires or combinations of several wires, we will be able to poll the entire area monitored by the SE for electrochemical activity.

To accomplish the task of switching 100 or more electrodes, which can be a tedious task, an electronic switch assembly was built (Figure 5.0-5) and is being referred to as the Wire-Beam Electrode Auto-Switch (WAS).

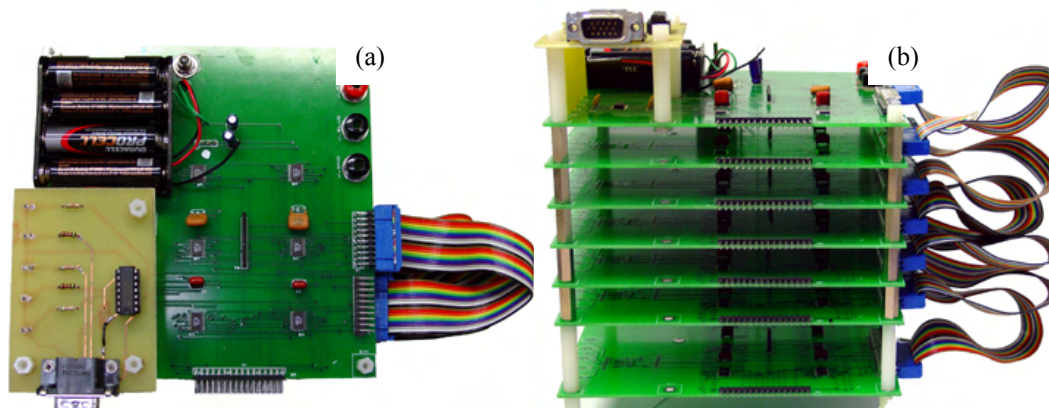


Figure 5.0-5. Wire-Beam Electrode Auto Switch: (a) top and (b) side views.

The design of the WAS accommodates WBE's of various sizes. This was accomplished through board modularity. Each measurement board accommodates a WBE of up to 16 pins. If one desires to use a WBE with between 17 and 32 pins, a second measurement board can be used and connected in series to the first board via a 16-pin ribbon cable (the cable with blue Input and Output Connectors shown in Figure 5.0-5).

The first measurement board is different from the subsequent measurement boards in that it has the components for the optical receiving network used to exchange commands with the Transmission Board (the small board with the Misc. I/O Connector in Figure 5.0-5). The subsequent boards have the corresponding solder pads for these components as well, but they are left unpopulated. Boards numbered 2 and higher get their instructions from the top measurement board in a daisy-chain fashion through the board-to-board connectors.

The Gamry PCI4-300 potentiostat PC card is connected to the auto-switch transmission board. The connection is made between the PCI4-300 interface card's D-shaped 15-pin miscellaneous I/O connector and the transmission board's corresponding 15-pin receiving port. Figure 5.0-5 (b) shows the WBE autoswitch with 7 measurement boards capable of switching an array of 112 electrodes. The actual switching is accomplished via an experimental script which is set up by the user prior to the experiment. In order to facilitate the data acquisition process and minimize the expenses associated with purchasing of expensive programming packages, Explain™ scripting language used by Gamry measurement framework was modified to incorporate the inclusion of an additional interface between the potentiostat and the electrochemical cell. The new code designed to handle the naming of the files and to program the switch states was incorporated into the Gamry measurement script for EIS. Minimal changes were made to the actual measurement portion of the script. The chart in Figure 5.0-6 shows the basic outline of the script that controls the switching system.

At present, the user must configure a simple *.ini file, which can be accomplished in any ASCII editor, like Notepad in Microsoft Windows®, etc. The *.ini file sets the global parameters for the experiment, e.g. the number of experiments/measurement, which pins/wires are activated in each experiment, etc. Then the script reads in the parameters from the *.ini file and programs the switches for Experiment 1 accordingly. Once all switches have been set, an electrochemical test is performed, and the results are stored to a date file. The program loops until all the measurements have been completed, and then exits.

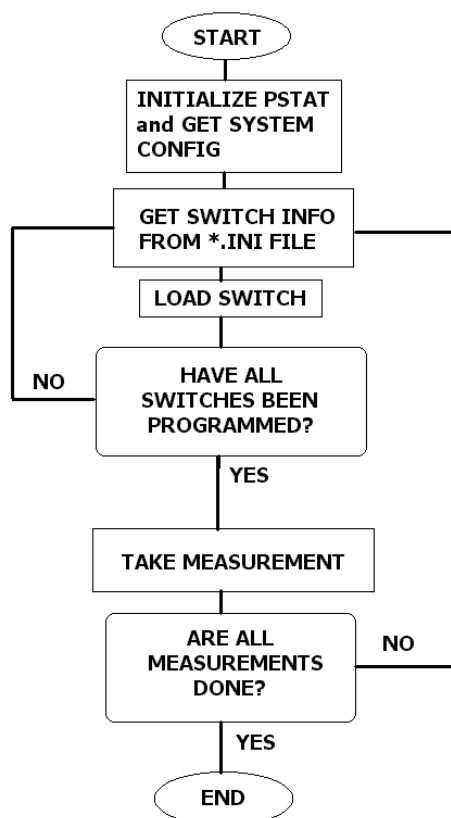


Figure 5.0-6. Schematic diagram of the switching routine.

So far, we have only adapted the EIS script for WBE, but similar modifications can be carried out for other experimental scripts available in the Gamry framework, *e.g.* Electrochemical Noise Methods, *dc* techniques, etc. In the future we will be looking at providing a simple GUI in order to generate *.ini files for a variety of electrode arrangements and experimental conditions.

6.0 References

- J. Kittel, N. Celati, M. Keddad, H. Takenouti, *New methods for the study of organic coatings by EIS. New insights into attached and free films*, Prog. Org. Coat., **2001**, 41, 93.
- J. Kittel, N. Celati, M. Keddad, H. Takenouti, *Influence of the coating-substrate interactions on the corrosion protection: characterisation by impedance spectroscopy of the inner and outer parts of a coating*, Prog. Org. Coat., **2003**, 46, 135.
- Miszcyk, T. Schauer, *Electrochemical approach to evaluate the interlayer adhesion of organic coatings*, Prog. Org. Coat., **2005**, 52, 289.
- T. C. Simpson^a, P. J. Moran, H. Hampel, G.D. davis, B.A. Shaw, C. O. Arah, T.L. Fritz, Ken Zankel, *Electrochemical Monitoring of Organic Coating Degradation During Atmospheric or Vapor Phase Exposure*, Corrosion, 46, **1990**, p. 331
- T.C. Simpson^b *et al.*, *Electrochemical impedance measurements for evaluating and predicting the testing performance of organic coatings for atmospheric exposure*, Corrosion Testing and Evaluation: Silver Anniversary Volume, ASTM STP 1000, ASTM, Philadelphia, **1990**, 397.

- G.D. Davis, C.M. Dacres, M. Shook, B.S. Wenner, *Electrochemical In-situ Sensors for Detecting Corrosion on Aging Aircraft*, Proc. Intelligent NDE Sciences for Aging and Futuristic Aircraft, ed. C. Ferregut, R. Osegueda and A. Nunez, University of Texas, El Paso, TX, **1998**, 41
- G.D. Davis, C.M. Dacres, L.A. Krebs, *In-Situ Sensor to Detect Moisture Intrusion and Degradation of Coatings, Composites, and Adhesive Bonds*, Proc. 1999 Tri-services Conference on Corrosion, Myrtle Beach, SC, **1999**.
- G.D. Davis, C.M. Dacres, et al., Mater. Perform., **2000**, 39, 46.
- K. N. Allahar, Quan Su, G. P. Bierwagen, D. Battocchi, V. J. Gelling, D.E. Tallman, *Examination of the feasibility of the use of in-situ corrosion sensors in army vehicles*, submitted to Proc. 2005 Tri-services Corrosion Conference, Orlando, FL **2005**.
- K. Allahar, Quan Su, G. Bierwagen, D. Battocchi, V. Johnson Gelling, D. Tallman, *Further Studies of Embedded Electrodes for In-Situ Measurement of Corrosion Protective Properties of Organic Coatings*, NACE Corrosion/2006 Conference, March **2006**, San Diego CA.
- K. Allahar, Quan Su, G. P. Bierwagen, *Monitoring of the AC-DC-AC degradation of organic coatings by embedded sensors*, accepted for NACE Corrosion/2007 Conference, March **2007**, Nashville, TN.
- K. N. Allahar, Quan Su, G. P. Bierwagen, D. Battocchi, V. J. Gelling, D.E. Tallman, *Examination of the feasibility of the use of in-situ corrosion sensors in army vehicles*, submitted to Proc. 2005 Tri-services Corrosion Conference, Orlando, FL **2005**.
- K. Allahar, Quan Su, G. Bierwagen, D. Battocchi, V. Johnson Gelling, D. Tallman, *Further Studies of Embedded Electrodes for In-Situ Measurement of Corrosion Protective Properties of Organic Coatings*, NACE Corrosion/2006 Conference, March **2006**, San Diego CA.
- M.E. Nanna, G.P. Bierwagen, *Mg-rich coatings: A new paradigm for Cr-free corrosion protection of Al aerospace alloys*, JCT Research, **2004**, 1(2), 69-80.
- D. Battocchi^a, A.M. Simões, D.E. Tallman, G.P. Bierwagen, *Electrochemical behaviour of a Mg-rich primer in the protection of Al alloys*, Corros. Sci., **2006**, 48, 1292-1306.
- D. Battocchi^b, A.M. Simões, D.E. Tallman and G.P. Bierwagen, *Comparison of testing solutions on the protection of Al-alloys using a Mg-rich primer*, Corr. Sci, **2006**, 48, 2226-2240.
- D. Battocchi, J. He, G.P. Bierwagen, and D.E. Tallman, *Emulation and study of the corrosion behavior of Al alloy 2024-T3 using a wire beam electrode (WBE) in conjunction with scanning vibrating electrode technique (SVET)*, Corrosion Science, **2005**, 47(5), 1165-1176.
- C. L. Wu, X. J. Zhou, Y. J. Tan; *Progress in Organic Coatings*, **1995**, 25, 379-389.
- G.G. Perrault, in *Encyclopedia of the Elements*, Vol. VIII, Ed. A.J. Bard, pp. 262, Marcel Dekker, New York, NY (**1978**)
- D. A. Kramer, "Magnesium, its Alloys and Compounds," U.S. Geological Survey Open-File Report 01-341
- B. D. Freeman, A.J. Hill; Free Volume and Transport Properties of Barrier and Membrane Polymers in Structure and Properties of Glassy Polymers, edited by Martin Tant and Anita J. Hill, Oxford University Press, ACS Symposium Series, 710, Chapt. 21, **1998**.
- M.L. Williams, R. F. Landel, J. D. Ferry; J. Amer. Chem. Soc., **1955**, 77, 3701
- H. Fujita, Fortschr. Hochpolym. Forsch., **1961**, 3, 1
- D. Patterson, A. Robard; Macromolecules, **1969**, 2(6), 672
- D. Turnbull, M.H. Cohen; J. Chem. Phys., **1961**, 34, 120
- J. D. Ferry, Viscoelectric Properties of Polymers, John Wiley and Sons, New York; Chapter 11, **1980**.
- T.G. Fox, P. J. Flory; J. Polym. Sci., **1954**, 14, 315
- J. J. Aklonis, W. J. MacKnight; Introduction to Polymer Viscoelasticity, John Wiley and Sons, New York, Chapters 3 & 4, **1983**.
- W. Wrasidlo; Advances in Polymer Science: Thermal Analysis of Polymers, Vol. 13, Springer-Verlag, New York, **1974**. 29.
- A. J. Kovacs; Fortschr. Hochpolym. Forsch, **1963**. 3, 394.
- L. C. E. Struik; Physical Aging in Amorphous Polymers and Other Materials, Elsevier Scientific Publishing Company, Amsterdam, **1978**.

- P. E. Mallon; Application to Polymers in Positron and Positronium Chemistry, World Scientific, Singapore, Chapter 10, **2003**.
- B. J. Chisholm, D. C. Webster., “The Development of Coatings Using Combinatorial/High-Throughput Methods: A Review of the Current Status.”, *J. Coat. Technol. Res.*, **2007**, 4(1), 1-12.
- B. J. Chisholm, D. A. Christianson, D. C. Webster; “Combinatorial Materials Research Applied to the Development of New Surface Coatings II: Process Capability Analysis of the Coatings Formulation Workflow.” *Progress in Organic Coatings*, **2006**, 57(2), 115-122.

7.0 Program Management

The Durable Hybrid Coatings program has the following management structure:

- Technical Manager for Department of Coatings and Polymeric Materials activities: Dante Battocchi, Research Assistant Professor, Department of Coatings and Polymeric Materials.
- Technical Manager for Center for Nanoscale Science and Engineering activities: Dr. Bret J. Chisholm, Senior Research Scientist, Center for Nanoscale Science and Engineering.
- Technical Manager for inorganic hard coatings Studies: Dr. Douglas L. Schulz, Senior Research Scientist, Center for Nanoscale Science and Engineering.
- Senior Scientific Advisor: Dr. Gordon Bierwagen, Professor, Department of Coatings and Polymeric Materials. [PI of record]
- Program Manager and management POC for AFRL: Dr. Gregory J. McCarthy, Director, Center for Nanoscale Science and Engineering.

Additional senior research staff include:

- Dr. Kerry N. Allahar, Research Assistant Professor, Department of Coatings and Polymeric Materials.
- Dr. Vsevolod “Séva” Balbyshev, Research Scientist, Center for Nanoscale Science and Engineering.
- Dr. Jie “Jim” He, Research Associate, Center for Nanoscale Science and Engineering.
- Mr. James Bahr, Senior Research Engineer, Center for Nanoscale Science and Engineering.
- Mr. Robert Sailer, Research Engineer, Center for Nanoscale Science and Engineering.

The Durable Hybrid Coatings program at AFRL was initiated in July 2004, and with the supplement for new work added in 2007, the end date is now May 2010. Progress through September 30th is reported annually, with a Final Report due after the close of the program.

The following table summarizes expenditures on the program through September 2007.

Durable Hybrid Coatings
Cooperative Agreement FA8650-04-1-5045
Annual Report for Period ending September 30, 2007

	Jul-04 to Aug-06	Sep-06 to Sep-07	Total Expenditures	Budget	Balance
Personnel	\$323,788	\$555,556	\$879,344	\$1,853,593	\$974,249
Direct Operating Costs	\$122,398	\$200,066	\$322,464	\$426,002	\$103,538
Subcontracts	\$89,816	\$30,552	\$120,368	\$162,247	\$41,879
Capital Equipment	\$129,820	\$94,438	\$224,259	\$481,529	\$257,270
Indirect (F&A) Costs	\$205,479	\$314,451	\$519,929	\$991,429	\$471,500
Total	\$871,301	\$1,195,063	\$2,066,364	\$3,914,800	\$1,848,436

Technical Appendix

Positron Annihilation Studies

Bret Mayo

Center for Nanoscale Science and Engineering

Understanding of the parameters that impact the performance of any protective coating has broadened over time with the introduction of ever more sophisticated analytical tools such as AFM, DMA, FTIR, etc. These tools complement a variety of more qualitative tools such as gloss assessment, pencil hardness, solvent rubs, and cross-hatch adhesion tests. Many of the analytical tools only give a glimpse of what is happening in the coating because they can only examine the surface. However, there is a great deal of information to be gleaned by a probe beneath the surface of the coating for at least three reasons: 1) some surface properties change in response to changes beneath the surface which are “telegraphed” through the bulk of the coating to the surface; 2) the morphology at or near the surface can change in response to temperature, mechanical stress, or contact with water; and 3) with many coatings, the surface will erode over time, continually exposing new material which may be very different from the original pristine surface. If it were possible to probe beneath the surface nondestructively, the information yield would be even richer because the same sample could be analyzed, exposed to natural or laboratory stresses, and then analyzed again.

Free volume (FV, sometimes referred to as molecular free volume or fractional free volume) can be defined as the specific volume of a material minus the volume occupied by constituent molecules or atoms. The occupied volume in polymers has been estimated at 1.3 times the van der Waals volume of the constituent monomers in a polymer (Freeman 1998).

The concept of molecular FV and its relationship to a multiplicity of properties in materials has been discussed for decades. For example, Williams, Landel and Ferry (Williams 1955) and Fujita (Fujita 1961) discussed the temperature dependence of polymer viscosity and diffusion in terms of FV. Patterson and Robard (Patterson 1969) discussed polymer compatibility and numerous researchers (Cohen and Turnbull (Turnbull 1961), Ferry (Ferry 1980), Fox and Flory (Fox 1954), Aklonis and Macknight (Aklonis 1983), and Wrasidlo (Wrasidlo 1974) have discussed the glass transition in terms that relate physical properties to theoretical FV. Tiny volume changes in glassy polymers over time were noted by Kovacs (Kovacs 1963) and their effects on mechanical properties were studied in detail by Struik (Struik 1978). Virtually all of these early researchers recognized the importance of FV and developed theoretical relationships without being able to accurately and directly measure it. Dilatometry, diffusion studies with an assortment of probe molecules and modeling using Bondi’s group contribution method were some of the approaches used to varying degrees of satisfaction.

Positron annihilation spectroscopy (PAS) is a novel, nondestructive technique which can be used to study molecular FV at the surface as well as probing into the bulk of the coating. Because it is profoundly sensitive to voids down to a molecular level, it is one of the best techniques to directly probe polymer FV. Furthermore, since it can provide the average FV site size as well and the relative number of FV sites, it can provide information about FV distribution in a material which is something that was impossible to achieve before, but may in fact be more important to the performance of a material. The value of the technology is rapidly being realized as it becomes better understood and more widely applied. It is perfectly complementary to many conventional techniques in terms of the size range of FV sites it can probe, but spans a much broader depth of penetration (See Resolved Defect Size, Figure 1). In terms of

the FV void concentration, it encompasses many conventional techniques (See Defect Concentration, Figure 1).

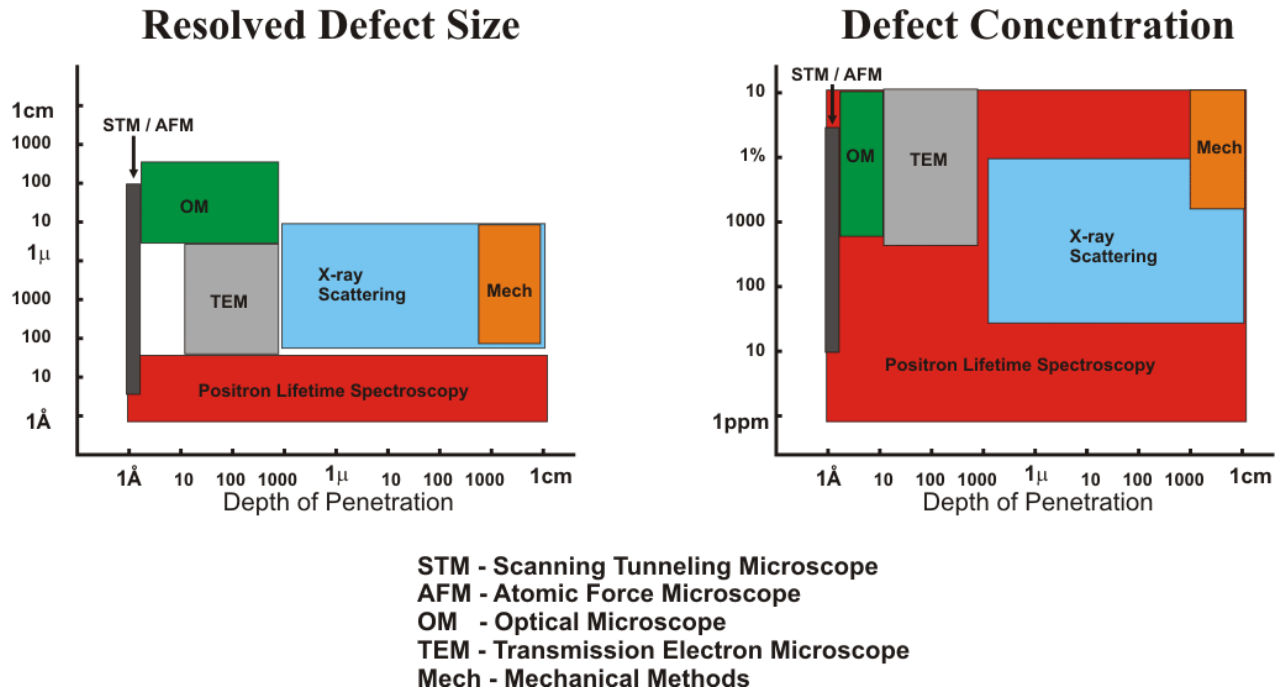


Figure 1. Comparison of PAS with Conventional Analytical Techniques (Mallon 2003).

PAS is nondestructive and requires no special sample geometry or surface preparation, so it can potentially yield more meaningful information more easily than conventional techniques. For example, analyses could be performed just after preparation, during and after curing, and after exposure to environmental stress on the same set of samples without changing the samples in any way. Being able to make measurements of the samples *in situ* while they are being exposed to some stress could be a distinct advantage to understanding the influence of FV on performance properties. Furthermore, because it is so sensitive to small changes, accelerated test methods may not be necessary to provide meaningful information in a reasonable timeframe.

Since PAS has not been utilized to any great extent to characterize polymer coatings, initial experiments with the newly installed PAS system (procured through another grant) involved systematically varying the composition of a polyurethane coating and comparing results obtained with PAS to results obtained using dynamic mechanical analysis (DMA). A set of three coatings were prepared and cured at 50°C for four hours. Table 1 provides a description of the oligomeric triols used for the experiment and Table 2 provides the compositional details of the coatings prepared.

Glass transition temperature (T_g), plateau modulus, and crosslink density of the coating films were determined using DMA and the data obtained is shown in Table 3. As expected, T_g and crosslink density were found to decrease with increase oligomeric triol molecular weight.

PAS was conducted on free films. In order to assess reproducibility, measurements were repeated twice on the same samples at weekly intervals. Each sample measurement was done in triplicate. The data obtained are shown as Run 1 and Run 2 in Figures 2, 3, and 4.

Table 1. A description of the oligomeric triols used for the experiment.

Polyol	Number average MW	Hydroxyl number	Hydroxyl equiv. wt.
Tone 301	300	187	300
Tone 305	540	311	561
Tone 310	900	180	100

Table 2. The compositional details of the coatings prepared.

Tolonate HDT-LV, Rhodia Chemicals 1 drop dibutyl tin dilaurate 0.5g acetone	1.83g	1.83g	1.83g
Tone 301, Dow Chemicals	1.0g	-	-
Tone 305, Dow Chemicals	-	1.8g	-
Tone 310, Dow Chemicals	-	-	3.0g

Table 3. Data obtained from DMA.

Sample crosslinker	301	305	310
Tg (from tan delta)	56.21	7.79	-8.26
Plateau modulus	21.06	18.95	18.4
Crosslink density	0.020445	0.018396	0.017862

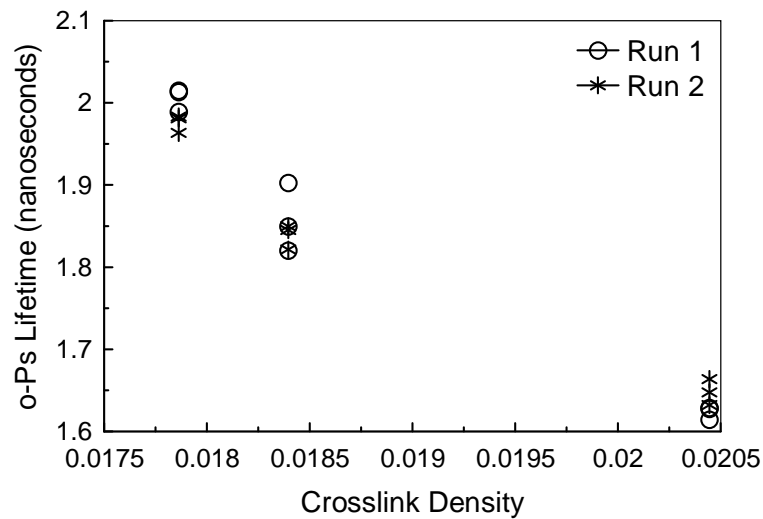


Figure 2. o-Ps lifetime as a function of crosslink density as determined by DMA.

Figure 2 shows o-Ps lifetime data which reflects free volume site size. Intuitively, one would expect the crosslink density to follow the trend shown, i.e., the shorter the chain length of the trifunctional crosslinker, the higher the crosslink density.

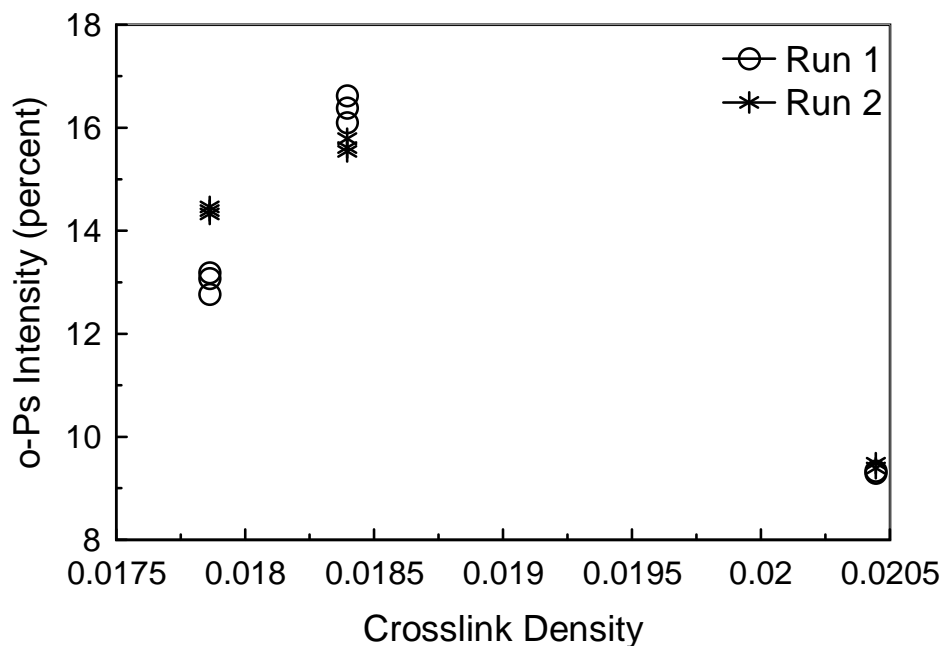


Figure 3. o-Ps intensity as a function of crosslink density.

Figure 3 shows the o-Ps intensity as a function of the crosslink density. Interestingly, o-Ps intensity, which is related to the number of free volume sites, showed a non-linear relationship with crosslink density. Because the total free volume parameter is a combination of the lifetime and intensity parameters, a non-linear relationship was also observed between total free volume and crosslink density, as shown in Figure 4. Further work is required to understand these results.

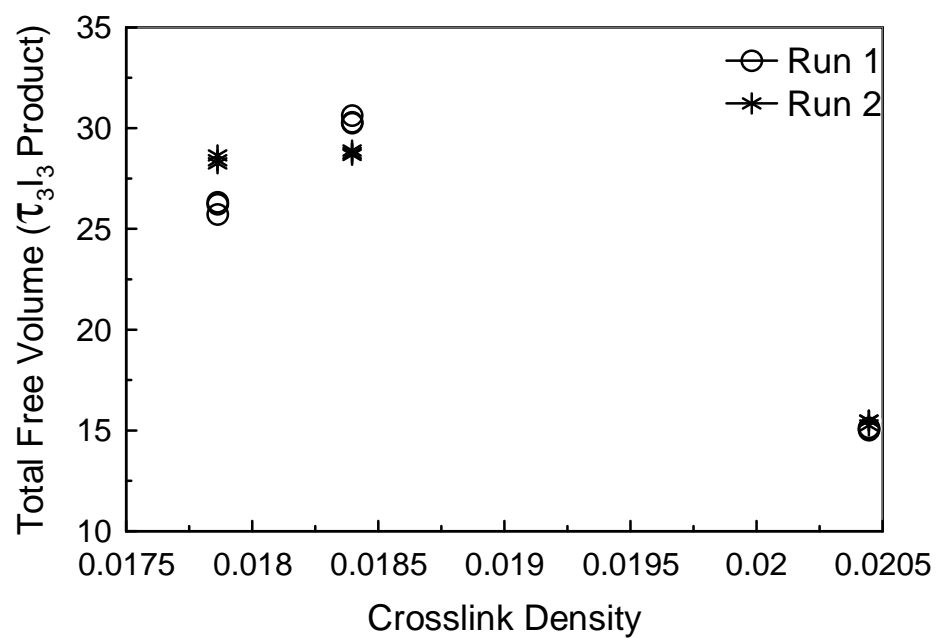


Figure 4. Total free volume as a function of crosslink density.

THE DEVELOPMENT OF A TWO-COMPONENT, MAGNESIUM-RICH PRIMER FOR CONTROLLING CORROSION OF ALUMINUM ALLOYS

Jun Li, Jie He, Bret J. Chisholm, Missy Berry, Dante Battocchi, and Gordon P. Bierwagen

North Dakota State University
Fargo, ND 58102

Presented at the
The Waterborne Symposium
Advances in Intelligent Coatings Design
February 14 - 16, 2007
New Orleans, LA, USA

Symposium Sponsored by
The University of Southern Mississippi
Department of Polymer Science

ABSTRACT

It has recently been shown that commercially-available magnesium particles can be used to produce primers that provide corrosion protection to aluminum alloys by serving as a sacrificial metal. A polymer binder system that has enabled exceptionally good performance with magnesium particles was based on a three-component binder system comprised of an epoxy resin, di-isocyanate, and aminofunctional silane. Due to the complexity of the three-component system and variability in pot-life, a simpler one- or two-component binder system was desired that could provide equivalent or better performance than the three-component system. As a result, research was conducted to develop a two-component Mg-rich primer that provides excellent corrosion protection to aluminum alloys. As part of the investigation, several variables associated with the coating formulation were examined using open circuit potential measurements, electrochemical impedance spectroscopy, salt spray exposure testing, and scanning electron microscopy in conjunction with the energy dispersive X-ray technique. The results showed that all of the variables investigated which included epoxy resin molecular weight, curing agent functionality, epoxy/NH ratio, and Mg content significantly affected coating performance. An optimized formulation for the two-component primer was identified, which showed very similar corrosion protection performance to the extensively studied three-component, hybrid binder system for Mg-rich primers.

Introduction

Chromate containing coatings have been extensively used for corrosion control of aluminum (Al) alloys designed for aerospace applications. However, due to environmental concerns and adverse health effects surrounding use of chromates, there is an intensive effort to find suitable replacements for chromate-based coatings. Recently, a novel magnesium-rich (Mg-rich) primer coating specifically designed for corrosion protection of Al alloys was developed by Bierwagen and coworkers.^[1-3] Corrosion protection for these coatings results from galvanic coupling between the Mg and Al. The Mg particles dispersed in the polymer binder serve as a sacrificial anode, which cathodically interacts with the Al substrate (as cathode) to protect it from corrosion.

The Mg-rich coating which showed the best performance in the original studies was based on a three-component binder system comprised of an epoxy resin, diisocyanate, and an aminofunctional silane. Due to the complexity of the three-component system and variability in pot-life, a simpler two-component binder system was desired. As a result, two-component epoxy-based binder systems were targeted for investigation.

In order for the Mg to provide cathodic protection to the aluminum substrate, it is necessary to create continuous electronic conduction pathways between Mg particles and the Al substrate. These pathways facilitate electron transfer between the two metals and can be controlled by optimizing Mg content. Qualitatively, if the Mg content in the coating is much less than the critical pigment volume concentration (CPVC), the Mg particles will not be in electrical contact with the Al and, as a result, cathodic protection will be significantly reduced. In contrast, if the Mg content far exceeds the CPVC, significant void space will be created within the coating, leading to relatively high permeability of the coating. As a result, Mg content optimization was also required to obtain a high performance, two-component Mg-rich primer.

Experimental

Materials. The Al alloy of interest was AA2024-T3 which is an aerospace aluminum. AA2024-T3 panels were obtained from Q-Panel Lab Products. A Mg powder obtained as a 52/48 vol./vol. blend of Eckagranules™ PK31 (mean particle size distribution (PSD) of 30 μm) and Eckagranules™ PK51 (PSD of 70 μm) was used as received from Ecka GmbH. The epoxides, Epon874-CX-90 and Epon1001-CX-75, and curing agents, Epicure3140 and Epicure3292-FX-60, were obtained from Resolution Performance Products®. Both epoxides are bisphenol-A-based diepoxides with Epon874-CX-90 possessing a relatively low molecular weight (MW) and the Epon1001-CX-75 possessing a relatively high MW. Epon874-CX-90 contains 10 wt.% MIBK/xylene (50/50 vol./vol) while Epon1001-CX-75 contains 25 wt.% MIBK/xylene (65/35). Epicure3140 is a solventless polyamide curing agent and Epicure3292-FX-60 is a polyamine curing agent containing 40 wt.% n-butanol/xylene (50/50). Table 1 provides a further description of the epoxy resins and curing agents. Dispersing agent, Aerosil® R974, was purchased from Degussa. Methylisobutylketone (MIBK) and xylene were obtained from Sigma-Aldrich Company. The topcoat used was DEFT MIL-PRF-85285C, which is glossy polyurethane.

The two-component Mg-rich coatings investigated were comprised of a component containing epoxy resin, Mg particles, MIBK, and dispersing agent, and another

component containing curing agent and xylene. Table 2 displays the composition of each of the coatings prepared. The acronyms used to identify the coatings were chosen to allow for easy identification of the coating composition. For example, the acronym L-Ad-1-50 indicates that the epoxy resin used in the coating was based on the low molecular weight epoxy resin (“L”), amide functional curing agent (“Ad”), 1/1 mole/mole epoxy/NH ratio (“1”), and 50 volume percent Mg (“50”).

Table 1. Properties of the epoxy resins and curing agents utilized. *The capital letters indicate Gardner-Holdt viscosity according to ASTM D 1545-98. †Equivalent weight is grams of resin per mole of functional group.

	Viscosity (Poise)	Equivalent Weight †	Density (lb/gal)	Amine Value (mg KOH/g)
Epon874-CX-90	X-Z ₁ *	245-275	9.1	----
Epon1001-CX-75	Z ₁ -Z ₆ *	450-550	9.1	----
Epicure3140	30-40	95	8.1	360-390
Epicure3292-FX-60	Z-Z ₂ *	140	8.5	390-420

Table 2. Formulations of the primers investigated.

Raw Material	L-Ad- 1-40	L-Ad- 1-45	L-Ad- 1-50	L-Ad- 1-55	L-Ad-1- 60	L-Ad- 0.87-45	L-Ad- 0.87-55	L-Ad- 1.18-45
	Weight, g							
Epon874- CX-90	58	58	58	58	58	58	58	58
Epon1001- CX-75	×	×	×	×	×	×	×	×
Epicure3140	19	19	19	19	19	21.9	21.9	16.2
Epicure3292 -FX-60	×	×	×	×	×	×	×	×
Mg powder	72	88	108	132	163	93	139	85
Aerosil® R974	0.7	0.9	1	1.3	1.6	1	1.5	1
MIBK	32	37	42	50	65	40	52	40
Xylene	7	9	10	13	16	9	15	8

Raw Material	L-Ad-1.18-55	L-Am-1-0	L-Am-1-50	H-Ad-1-0	H-Ad-1-20	H-Ad-1-50	H-Am-1-0	H-Am-1-20	H-Am-1-50
Weight, g									
Epon874-CX-90	58	58	58	×	×	×	×	×	×
Epon1001-CX-75	×	×	×	67	67	67	67	67	67
Epicure3140	16.2	×	×	9.5	9.5	9.5	×	×	×
Epicure3292-FX-60	×	46	46	×	×	×	23	23	23
Mg powder	128	×	123	×	23	95	×	24	99
Aerosil® R974	1.5	0.5	1	0.5	0.5	1	0.5	0.5	1
MIBK	52	20	60	20	22	45	20	30	45
Xylene	12	5	25	5	10	20	5	10	20

Procedures. Substrate panels were pretreated prior to coating application by: 1) immersing them for 20 minutes at room temperature in an aqueous alkaline solution comprised of 0.4 wt.% sodium hydroxide, 2.8 wt.% tetrasodium pyrophosphate, and 2.8 wt.% sodium bicarbonate; 2) rinsing the panels with deionized (DI) water; 3) immersing in a deoxidizer solution comprised of 35% n-butyl alcohol, 25% isopropyl alcohol, 15% ortho-phosphoric acid (85%), and 25% DI water for 2 minutes at room temperature; 4) rinsing with DI water; and 5) allowing the panels to dry at ambient conditions.^[4]

Primer compositions were applied to pretreated panels using a high volume/low pressure spray method.^[5] Solvent flash and curing were done at ambient conditions. All primed specimens were allowed to cure for at least one week before top coating. The average dry film thicknesses of the Mg-rich primers were about 100±25 microns. The high gloss polyurethane topcoat was applied by spray coating and the average film thickness was 50±15 microns.

Characterization. Electrochemical impedance spectroscopy (EIS) was used to evaluate electrochemical properties of coated specimens using a Gamry Femtostat/PCI4 Electrochemical Workstation in conjunction with dilute Harrison's solution (0.35 wt% (NH₄)₂SO₄ and 0.05 wt% NaCl) as the electrolyte. A single sinusoidal potential 10 mV in amplitude was superimposed on the open-circuit potential (OCP). Measurements were made between 10 mHz and 100 kHz from high to low frequency. The sample area of the working electrode was 3.5 cm². A saturated calomel electrode (SCE) was used for the reference electrode and a platinum mesh was used as the counter electrode.

Scanning electron microscopy (SEM) and energy-dispersive X-ray (EDX) analysis were performed with a JEOL JSM-6300V microscope (JEOL, Ltd., Tokyo, Japan) equipped with a Thermo EDS detector using a VANTAGE Digital Acquisition Engine. An accelerating voltage of 15 kV, a take-off angle of 29.08, and a 100 s count were used. Samples were mounted on Al mounts and coated with gold using a Technics Hummer II sputter coater.

Testing. Salt spray exposure tests were conducted according to ASTM B117 using a Q-FOG CCT-1100 salt fog chamber obtained from Q-PANEL. The salt fog was

generated from a 5 wt. % NaCl solution with a pH ranging from 6.5 to 7.2. The fog deposition rate ranged from 1 to 2 ml/h and the temperature of the chamber was kept constant at 35°C. The coated specimens (3 inch by 6 inch) were scribed using a tungsten carbide cutter (Robert Bosch Tool Corporation). The scribe was X-shaped with a top width of 4 cm, a height of 10 cm, and width of 1 mm and penetrated through all coating layers to expose the substrate. The outer edges and backside of the specimens were protected by covering them with Polyken 231 tape (Covalence Adhesives). After a desired amount of salt spray exposure, specimens were removed from the chamber and rinsed thoroughly with DI water before visually inspecting the coatings for corrosion. In addition to visual inspection, EIS was conducted on some specimens. After visual inspection and an EIS measurement, specimens were immediately returned to the salt spray chamber for further testing.

Results and Discussion

Since Mg is critical to corrosion protection, initial experimentation was focused on characterizing the effect of Mg content on coating properties using representative two component-binder systems and EIS to determine CPVC by measuring the change of coating pore resistance as a function of Mg volume content (PVC).^[6] Low frequency impedance (0.01 Hz) of the coatings was used as an indicator of coating pore resistance. Figure 1 displays a representative plot of low frequency impedance as a function of PVC. A distinct drop in impedance was observed when the PVC was changed from 45 to 50%, indicating that the CPVC lies within this range. From theoretical calculations made for the three-component Mg-rich system, the calculated CPVC was 47.5 %, a value quite similar to our experimental result.^[3] It is interesting to note that the impedance increased to some extent after the PVC exceeded CPVC, indicating that the polymer binder concentration was too low to completely coat all of the surface area of the Mg particles. Due the presence of exposed Mg surfaces within the coating, it would be expected that rapid Mg oxidation would occur by reaction with water or ionic species (Cl^- , SO_4^{2-} , etc.) diffusing through the coating,^[2] generating oxidation products that fill void space and therefore increase coating pore resistance. Similar behavior may be responsible for the increase in impedance that was observed at a given PVC when electrolyte exposure time was increased beyond three days.

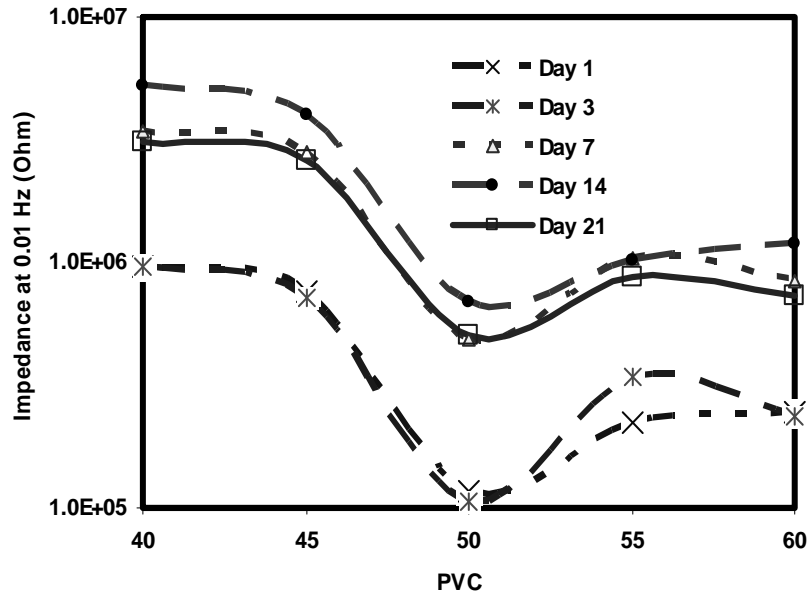


Figure 1. Impedance at low frequency (0.01Hz) as a function of PVC and exposure time for a series of Mg-rich primers based on the low MW epoxy resin, amide curing agent, and 1/1 epoxy/NH ratio.

The galvanic coupling between the Mg particles in the coating and the Al substrate was also characterized by measuring OCP above and below the CPVC. As shown in Figure 2, galvanic coupling was only obtained for a short period of exposure (1 to 2 hours) for the coating containing 40% PVC. A large fluctuation of potential was also found during this period, indicating ineffective electrical contact between Mg particles and the Al substrate.^[7] The OCP stabilized at -0.7 V after about four hours of exposure, which is basically the OCP of Al 2024. For the 50% PVC coating, a lower and more stable OCP was obtained, indicative of the formation of effective electric contact between Mg particles and the Al substrate. From these results, it was clear that 50% PVC was approximately the optimum for the two component primers of interest.

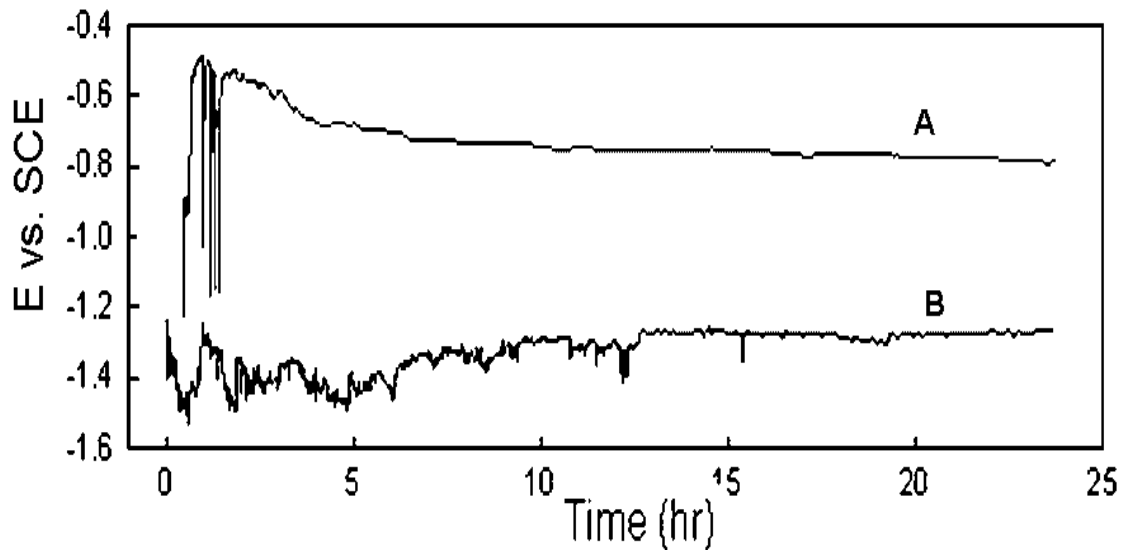


Figure 2. A short term OCP measurement for Mg-rich primers, L-Ad-1-40 (A) and L-Ad-1-50 (B), on Al 2024 using dilute Harrison's solution.

After having determined the approximate Mg content needed to obtain galvanic coupling between the Mg particles and Al substrate, the effect of the various factors associated with polymer binder composition were investigated. The factors investigated included epoxy/NH ratio, epoxy resin MW, and curing agent functionality.

Figure 3 shows the effect of epoxy/NH ratio on coatings produced at different Mg contents above and below the CPVC. As expected, impedance of coatings containing 45% PVC were higher than corresponding coatings containing 55% PVC because increasing the Mg content above CPVC increases conductivity and coating porosity. With regard to the effect of epoxy/NH ratio, the data shown in Figure 3 shows that, at a given PVC, coatings formulated using a 1/1 epoxy/NH ratio showed the highest impedance over the entire frequency range. This behavior suggests that use of an equal molar ratio of epoxy groups to NH groups results in the highest crosslink density and, thus, the highest barrier properties.

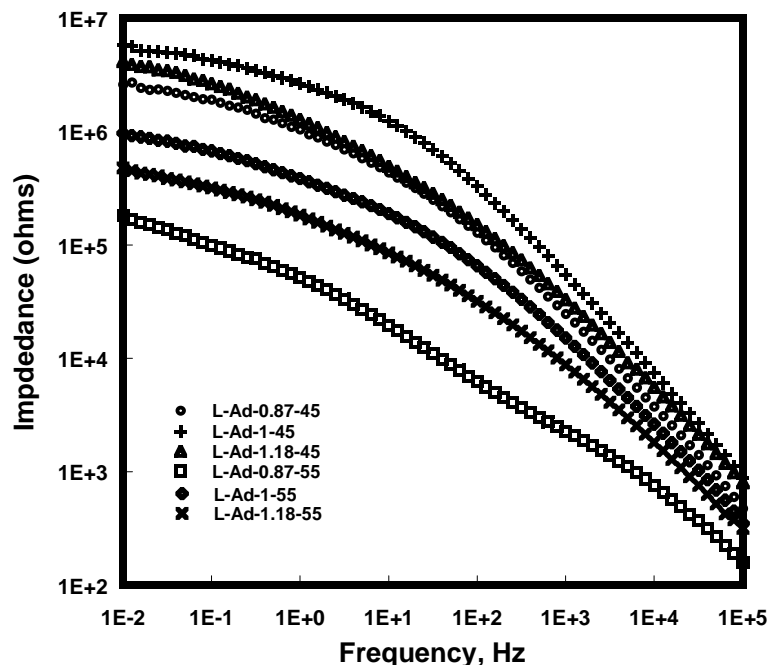


Figure 3. Bode plots of impedance for Mg primers exposed for 1 day to dilute Harrison's solution.

Based on the results obtained with respect to the effect of epoxy/NH ratio, epoxy/NH ratio was held constant at 1.0 for further experimentation. The effect of epoxy resin MW on corrosion protection of topcoated samples was evaluated using EIS. As shown in Figure 4, before the exposure test and after two weeks exposure to dilute Harrison's solution, the coating system based on the high MW epoxy resin showed significantly higher low frequency impedance than the coating system based on the low MW epoxy resin. This result indicates that the coating system based on the high MW epoxy resin possessed better barrier properties than the coating system based on the low MW epoxy resin. Since the higher MW epoxy resin possesses a higher epoxy equivalent weight (Table 1), the higher barrier properties for this coating system may be due to the lower concentration of the hydrophilic curing agent required to cure the resin.

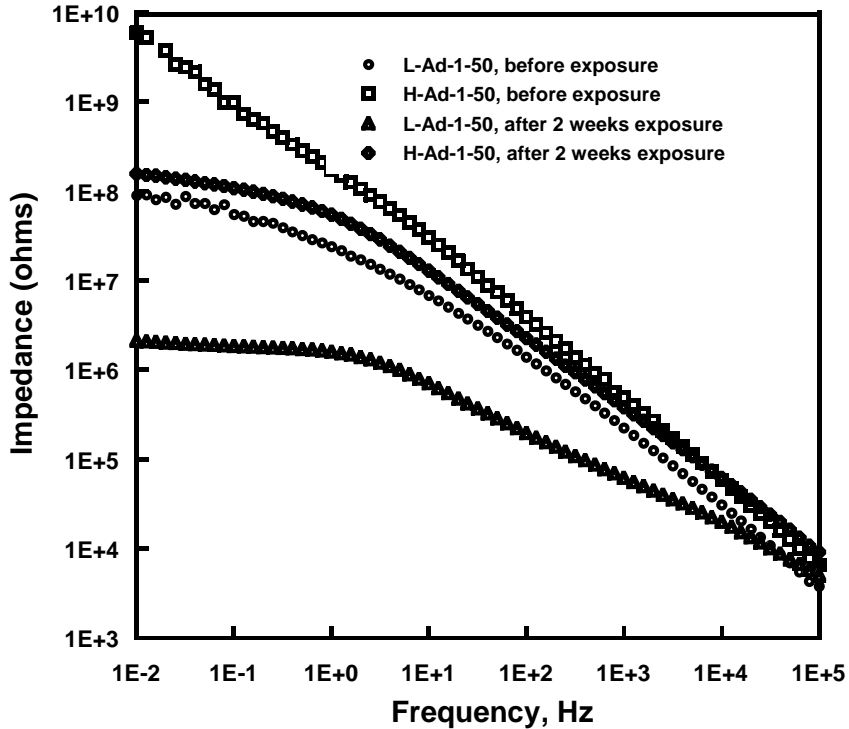


Figure 4. Bode plots for polyurethane topcoated samples illustrating the effect of epoxy resin MW in the Mg-rich primer layer.

Using the high MW epoxy resin, the effect of curing agent composition on corrosion protection was investigated. The experiment compared an aminofunctional curing agent to an amidofunctional curing agent using EIS and B117 salt spray to characterize corrosion protection. Figure 5 displays Bode plots for coatings as function of curing agent composition, Mg content, exposure time. The coatings in their “as produced” state (prior to longer term exposure to dilute Harrison’s solution) showed essentially no difference in impedance behavior with respect to the effect of curing agent composition. However, after two weeks of exposure, higher impedance was consistently found with the use of the polyamide curing agent suggesting that the polyamide cured epoxy provides better barrier properties than the amino-cured epoxy.

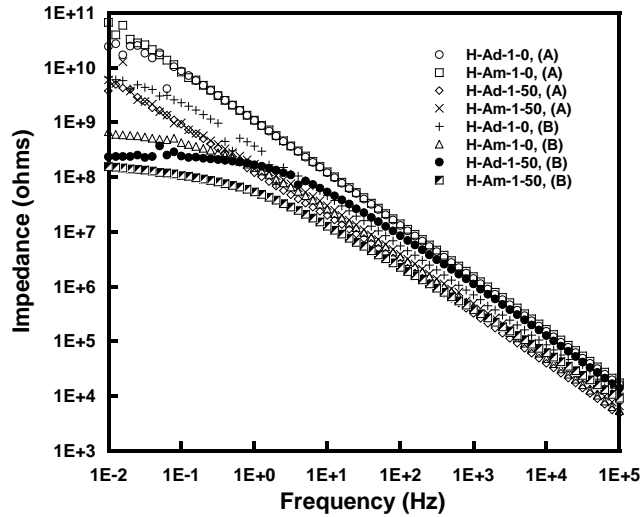


Figure 5. Bode plots of impedance for polyurethane topcoated epoxy primers on Al 2024 before (A) and after two weeks of exposure to dilute Harrison's solution (B).

Figure 6 displays images of coating samples tested using 3000 hours of B117 salt spray exposure. All of the coating samples based on the aminofunctional curing agent exhibited blistering even at 50% PVC while samples prepared using the amide-functional curing agent generally showed much less blistering. For the coating system based on the amide-functional curing agent and 50% PVC, no blistering or corrosion was observed after 3000 hours of salt spray exposure.

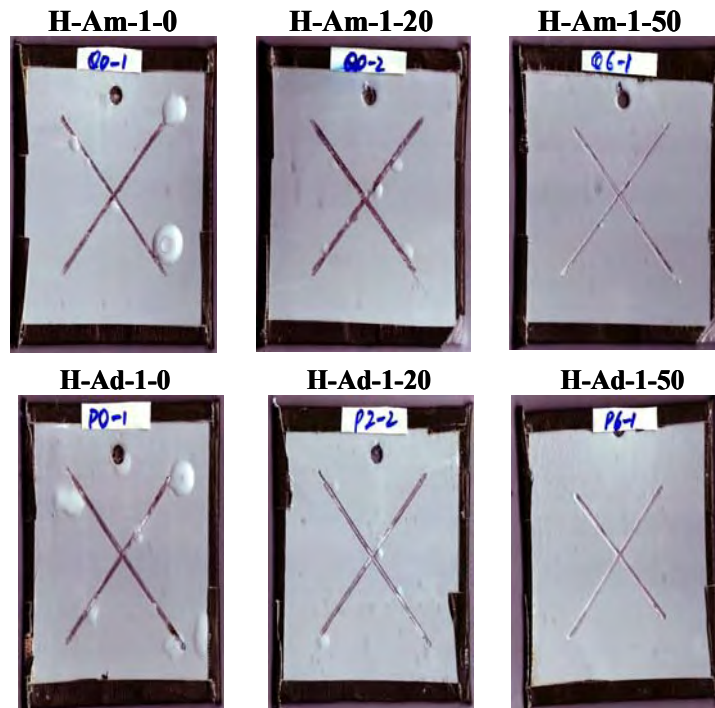


Figure 6. Images of topcoated two-component Mg-rich primer samples after 3000 hours of B117 salt spray exposure.

In addition to measuring the corrosion protecting capabilities of the coatings, the effect of primer curing agent composition on adhesion was measured. As shown in Figure 7, the coatings based on the amidofunctional curing agent consistently displayed higher adhesion than the coatings based on the aminofunctional curing agent. The superior corrosion protection provided by the polyamide curing agent may be at least partly due to better adhesion.

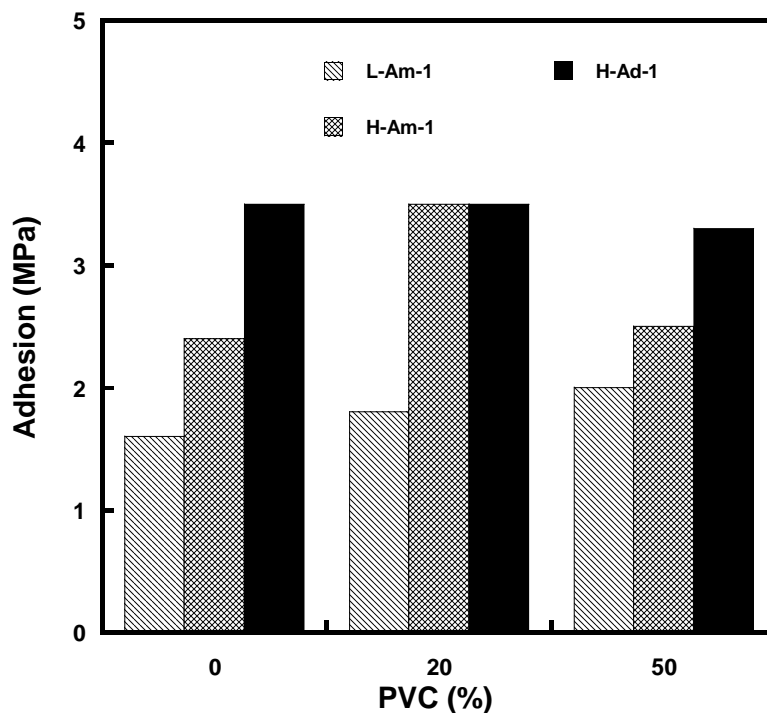


Figure 7. Pull-off adhesion results obtained for topcoated samples illustrating the effect of curing agent composition and PVC.

Since the primary objective of the work described in this document was to develop a two-component Mg-rich primer that possessed the excellent corrosion protective attributes of the previously described three-component Mg-rich primer,^[3] a comparison between the three-component and the optimized two-component Mg-rich primer was made using B117 salt spray. Figure 8 displays representative images before and after 3,000 hours of salt spray exposure for a sample based on the three-component Mg-rich primer and an analogous sample based on the optimized two-component Mg-rich primer (H-Ad-1-50).

After 3000 hours of salt exposure, no blistering or coating delamination was observed indicating that the two-component Mg-rich primer provides at least the same corrosion protection performance as the three-component Mg-rich system.

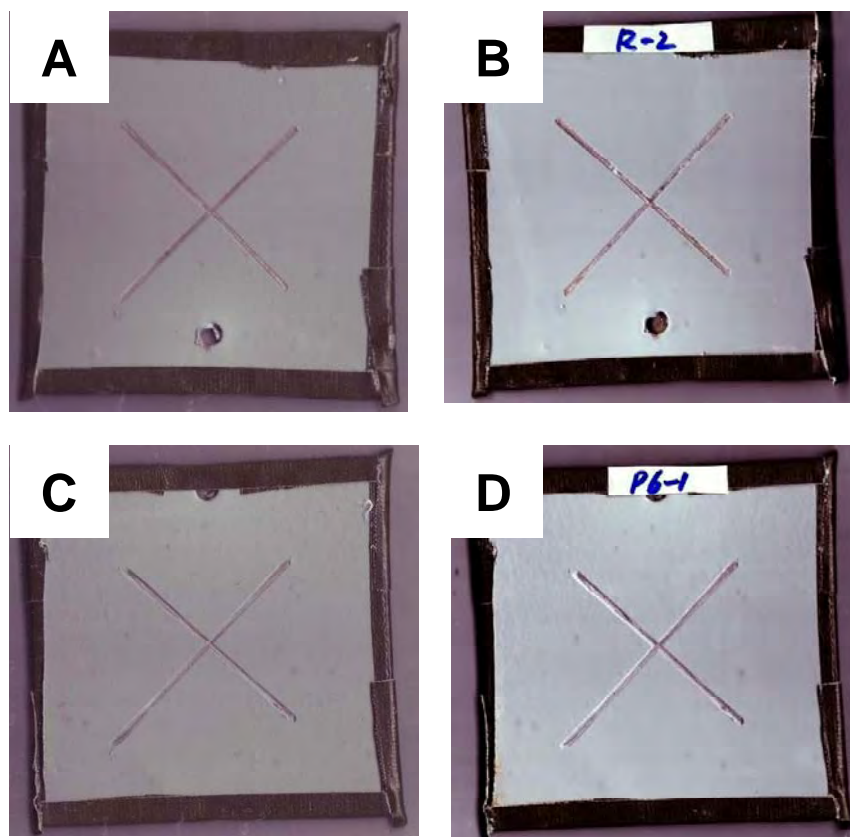


Figure 8. Representative images before and after 3,000 hours of salt spray exposure for a topcoated three-component Mg-rich primer on Al 2024 (A = before salt spray and B = after 3,000 hours salt spray) and a topcoated two-component Mg-rich primer (H-Ad-1-50) on Al 2024 (C = before salt spray and D = after 3,000 hours salt spray).

Based on the promising salt spray results obtained for the two-component Mg-rich primer developed, further characterization of this composition was conducted using electrochemical methods and SEM-EDX. A long term OCP measurement was conducted to observe the variation in conductivity with exposure time for the Mg-rich primer on Al 2024. As illustrated in Figure 9 and similar to the results previous observed by Bierwagen and coworkers,^[3] the OCP can be divided to three regimes. Regime 1 corresponds to the change in OCP during the initial 7 days of exposure in which the OCP was the mixed potential between pure Mg (-1.6 V) and bare Al 2024 (-0.6 V). During this time period, the Mg-rich coating interacts with the Al substrate predominantly through a cathodic protection mechanism. After 7 days of exposure, the OCP slowly increased from -0.9V to -0.6V over a 43-day period (Regime 2). The slow increase in potential during Regime 2 was attributed to the consumption of Mg in the coating, reducing the galvanic interaction between Mg particles and the Al substrate. The OCP shifted out of the cathodic protection domain and basically stabilized at -0.6V (OCP of bare Al 2024) after 50 days of immersion (Regime 3). This time period for the OCP transition from -1.25 V to -0.6V is assumed to be the life-time of the primer (50 days) for

activate cathodic protection, which is much longer than that reported for the three-component Mg-rich primer (30 days).^[3]

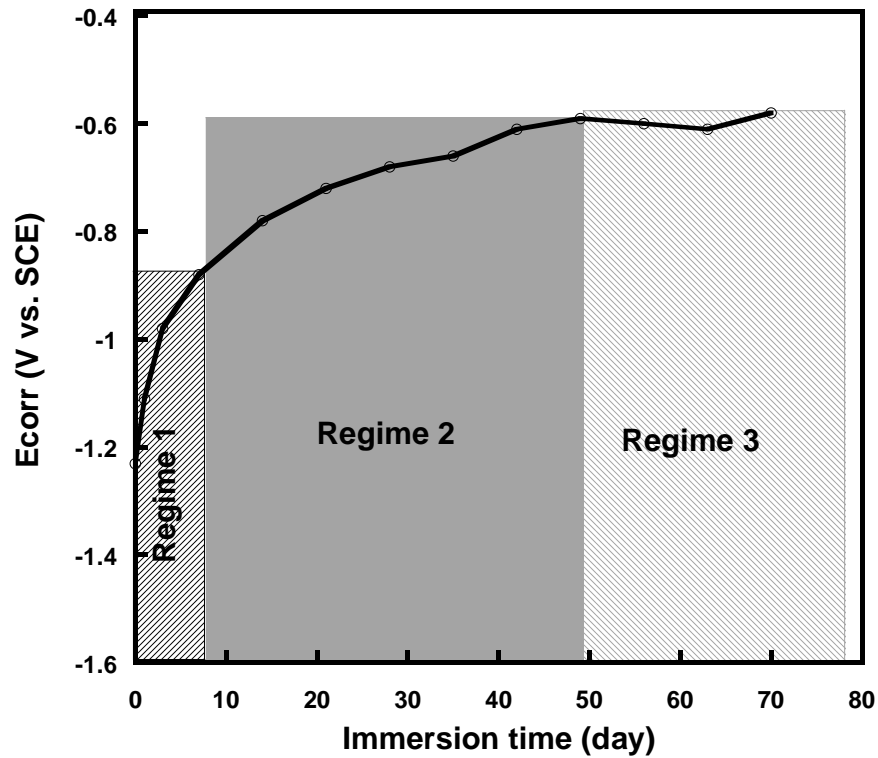


Figure 9. A long term OCP measurement of the optimized two-component Mg-rich primer, H-Ad-1-50, on AA2024-T3 using dilute Harrison's solution.

A long term study of corrosion protection for the coating system based on the two-component Mg-rich primer and the polyurethane topcoat was conducted by using EIS in conjunction with salt spray exposure. As shown in Figure 10, the coating system showed excellent barrier properties prior to salt spray exposure. The low frequency impedance was quite high (more than 10^9 ohm) and the linearity of the Bode plot indicated highly capacitive behavior. As salt spray exposure time increased, the coating resistance slowly decreased as indicated by the reduction in low frequency impedance. However, after 125 days of salt spray exposure, the low frequency impedance only dropped about one order of magnitude, indicating that the coating system maintained good barrier properties over the course of the exposure. This conclusion was supported by visual observation of the coating which showed no evidence of coating delamination, blistering, or corrosion products.

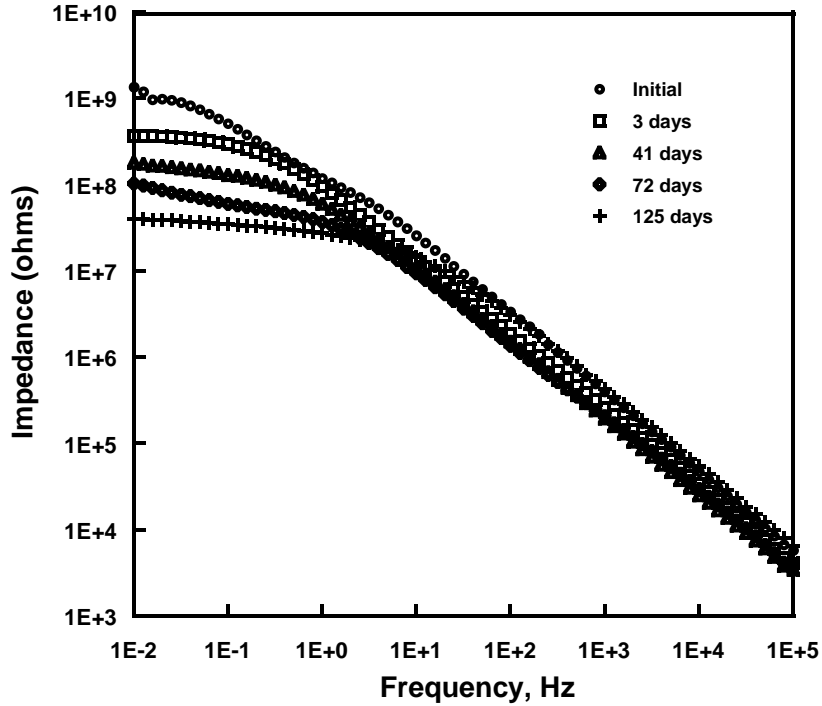


Figure 10. Bode plots of the topcoated, optimized Mg-rich primer, H-Ad-1-50, as a function of salt spray exposure time.

SEM and EDX were used to correlate corrosion performance of the two-component Mg-rich coating with coating morphology. Figure 11 shows a surface and cross section SEM image of the coating before salt spray exposure. From both the surface SEM image and the cross section image, it can be seen that the Mg particles were in direct contact with one-another allowing for the efficient electron transfer needed for galvanic protection. In addition, the cross section image shows a high concentration of Mg particles in direct contact with the Al substrate allowing for galvanic coupling with the substrate.

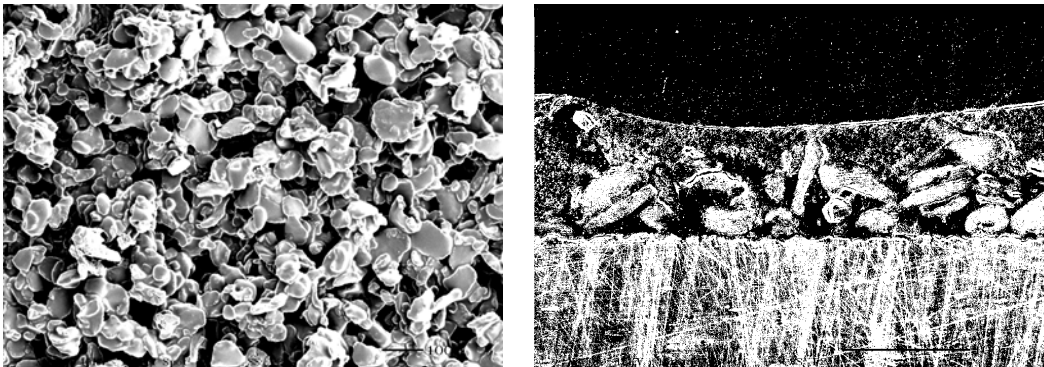


Figure 11. Surface (left) and cross-section (right) SEM image of sample H-Ad-1-50 coated on Al-2024.

Figure 12 shows a cross section image of the coating system after 3,000 hours of salt spray exposure and provides EDX mapping for Mg, Al, oxygen, and chlorine. From Figure 12, a higher oxygen content was found in the primer than in the topcoat, indicating the generation of Mg oxidation products as a result of salt spray exposure. The Mg oxide or derivative compounds may affect corrosion performance by at least two mechanisms. Similar to zinc-rich coatings for the galvanic protection of steel, Mg corrosion products may fill porosity within the primer and, thereby, enhance barrier properties of the coating.^[8-10] The Mg oxide generated as a result of Mg oxidation may also precipitate at the substrate and modify the Al surface by filling pores within the Al oxide layer, increasing the stability of the oxide layer to ions (Cl⁻).^[11] Due to the excellent corrosion performance of the coating system, no Al species were found in the primer or topcoat as shown by EDX Al mapping (Figure 12).

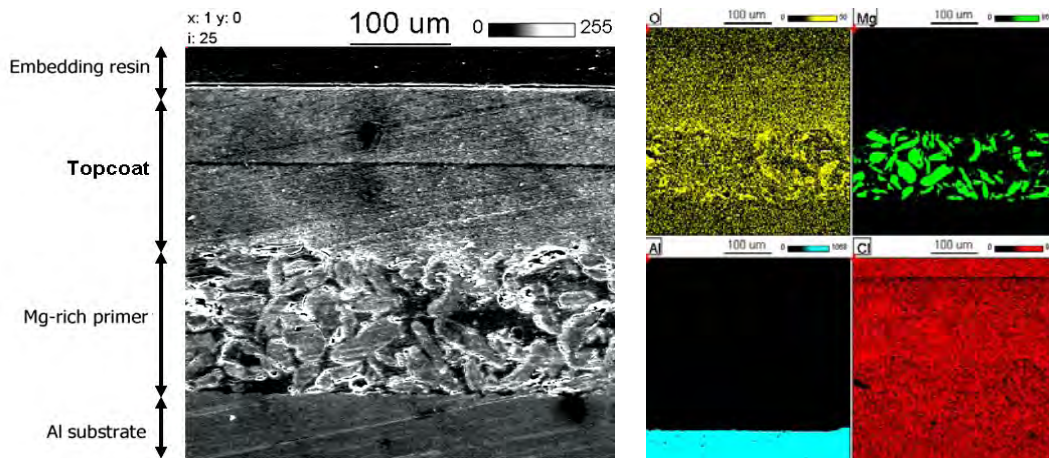


Figure 12. SEM cross section image (left) and EDX mapping (right) of sample H-Ad-1-50 after 3,000 hours of salt spray exposure.

Conclusions

A two-component Mg-rich primer coating was developed that showed excellent corrosion protection of Al 2024 when used in conjunction with a polyurethane topcoat. The development involved an investigation of the effects of most all of the compositional variables on corrosion protection. The variables investigated were epoxy resin MW, curing agent functionality, epoxy/NH ratio, and Mg content. A number of techniques such as OCP measurement, EIS, B117 salt spray, pull-off adhesion, SEM, and EDX were used to study and evaluate corrosion protection. All of the variables investigated had a significant effect on coating system performance and an optimized coating composition was identified that showed very good corrosion protection for at least 3,000 hours of B117 salt spray exposure. The optimized coating composition was based on the high MW epoxy resin, amide-functional curing agent, 1.0 epoxy/NH ratio, and Mg volume content of 50%. Detailed characterization of the optimized coating system clearly showed that corrosion protection occurs through galvanic coupling between Mg in the primer and the Al substrate. In addition, SEM-EDX mapping results in conjunction with electrochemical measurements indicate that Mg oxidation products may also be playing a

role in corrosion protection by increasing barrier properties over the lifetime of the coating.

References

- [1] D. Battocchi, A. M. Simoes, D. E. Tallman, G. P. Bierwagen, *Corrosion Science* **2006**, *48*, 1292.
- [2] D. Battocchi, A. M. Simoes, D. E. Tallman, G. P. Bierwagen, *Corrosion Science* **2006**, *In Press*, *Corrected Proof*.
- [3] M. E. Nanna, G. P. Bierwagen, *J. Coatings Technology Research* **2004**, *1*.
- [4] L. M. Farrier, S. L. Szaruga, *Materials Characterization* **2005**, *55*, 179.
- [5] W. D. o. N. Resources, (Ed.: W. H. W. M. Program), **1993**, pp. PUBL.
- [6] R. E. Lobnig, W. Villalba, K. Goll, J. Vogelsang, I. Winkels, R. Schmidt, P. Zanger, J. Soetemann, *Progress in Organic Coatings* **2006**, *55*, 363.
- [7] A. E. Hughes, R. J. Taylor, B. R. W. Hinton, *Surface and interface analysis* **1997**, *25*, 223.
- [8] S. M. A. Shibli, R. Manu, *Surface and Coatings Technology* **2006**, *201*, 2358.
- [9] *Focus on Powder Coatings* **2004**, *2004*, 3.
- [10] H. Marchebois, C. Savall, J. Bernard, S. Touzain, *Electrochimica Acta* **2004**, *49*, 2945.
- [11] C. Dornfest, F. C. Redeker, M. A. Fodor, C. Brekaw, H. S. Tomizawa, *Vol. 648866* (Ed.: E. P. Appl.), **1995**.

A Combinatorial/High-Throughput Workflow for the Development of Hybrid Organic-Inorganic Coatings

Bret J. Chisholm,^{1,2} Missy Berry,¹ James Bahr,¹ Jie He,¹ Jun Li,² Seva Balbyshev,¹ Duhua Wang,² and Gordon P. Bierwagen²*

¹The Center for Nanoscale Science and Engineering

²Department of Coatings and Polymeric Materials

North Dakota State University

1805 Research Park Drive

Fargo, ND 58102

Abstract

Interest in hybrid organic-inorganic (HOI) materials has grown rapidly in the last two decades. The appeal of this broad class of materials can be attributed to the unique combinations of properties that can be achieved by combining an inorganic phase with an organic phase. HOI materials can be divided into two basic categories: homogeneous systems derived from monomers or miscible organic and inorganic components, and heterogeneous, phase-separated systems with domains ranging from angstroms to micrometers in size. The structure of the inorganic component is dependent on the interaction of many variables such as pH, water content, overall solution concentration, solvent composition, temperature, and time. Due to the complexity of HOI materials, a combinatorial/high-throughput approach to the development of novel materials is highly desired. The authors have recently developed a combinatorial workflow for the synthesis and characterization of HOI coatings. Initial experimentation conducted with the workflow was focused on the development of primers for corrosion protection derived from a HOI binder system and magnesium particles. Both homogeneous and heterogeneous HOI binders were investigated. With just one iteration of the combinatorial workflow, heterogeneous, moisture-curable HOI binders were identified that enabled the formation of magnesium-rich primers that provided excellent corrosion protection to an aerospace aluminum alloy (Al 2024).

*To Whom Correspondence Should be Addressed

Bret.Chisholm@ndsu.edu

Introduction

In the past two decades, research in the area of hybrid organic-inorganic (HOI) materials has exploded both in industry and academia. To illustrate this point, Loy¹ noted that the number of patents and publications containing the term “hybrid organic-inorganic” increased from fewer than five in 1985 to over 528 in the year 2000, including 85 patents. The interest in this broad class of materials can be attributed to the unique combinations of properties that can be achieved by combining an inorganic phase with an organic phase. HOI materials can be divided into two basic categories: homogeneous systems derived from monomers or miscible organic and inorganic components, and heterogeneous, phase-separated systems with domains ranging from angstroms to micrometers in size. Thus, the definition of HOI materials excludes polymeric compositions containing inorganic fillers or fibers, such as polymer composites.

The most common method for producing HOI materials is the sol-gel process, which is a solution method.² With this process, the inorganic phase is produced by hydrolysis and condensation of metal alkoxides. Many of the advantageous properties of HOI materials can be attributed to the sol-gel process which often results in the formation of a very fine inorganic phase, often interconnected three-dimensionally, within an organic polymer. A tremendous number of variables, most of which strongly influence material properties, are involved in a sol-gel process. These variables include metal-alkoxide composition and/or organometal-alkoxide composition [Si, Al, Ti, Zr, as well as their mixtures that result in co-condensed mixed metal-oxides, and organogroup chemical composition], alkoxide concentration, water:alkoxide ratio, pH, temperature, and solvent composition. While other additional factors can be considered, the combination of the most basic variables that are listed above constitute a huge multidimensional compositional space. The complexity of the chemistry involved in a sol-gel process coupled with the high sensitivity of the compositional variables to material composition makes the prediction of material properties based on first principles very difficult. As a result, an extensive amount of experimentation is typically required to develop a HOI material with a desirable set of material properties. Based on these considerations, the applications of combinatorial/high throughput methods to the development of HOI materials appeared to be a very worthwhile endeavor.

The author's and their colleagues have created an extensive combinatorial workflow for the development of new polymers and coatings for applications such as environmentally-friendly marine coatings and coatings for corrosion protection.^{3,4} This document describes more recent efforts to create a combinatorial workflow for the development of HOI coatings designed to provide corrosion protection to aluminum alloys. The primary function of the combinatorial workflow was to develop a HOI binder system for magnesium (Mg) particles for the production of high performance primers for the protection of aluminum alloys from corrosion.^{5,6}

The rationale for an investigation of HOI binders for Mg-rich coatings came from prior work conducted on the development of zinc (Zn)-rich coatings for the protection of steel substrates via a cathodic protection mechanism in which the Zn serves as a sacrificial anode.⁷ Two general class of Zn-rich coatings have been commercialized which are distinguished by their binder chemistry. The two general classes are two-component, epoxy-based Zn-rich coatings and Zn-silicate coatings. The Zn-silicate

primers are based on a silicate binder system derived from alkoxysilanes using a sol-gel process in which curing occurs at ambient temperature through silanol condensation. In general, it has been found that Zn-silicate primers provide longer service-life compared to epoxy-based Zn-rich primers.⁷

Since Mg has a higher oxidation potential than aluminum (Al), Mg particles can serve as a sacrificial anode to provide cathodic protection to Al substrates in analogy to the protection of steel substrates with Zn particles.^{5,6} Mg-rich primers for the protection of aluminum alloys based on organic binder systems have been previously investigated and found to provide very good protection.⁵ This document describes initial efforts to develop Mg-rich primers based on HOI binders using a combinatorial approach.

Experimental

Materials. All reagents were used as received. Methyltrimethoxysilane (MeTMS), ureidopropyltrimethoxysilane (UpTMS), 3-aminopropyltrimethoxysilane (ApTMS), diethylphosphatoethyltriethoxysilane (DTES), phenethyltrimethoxysilane (PhEtTMS), (3-glycidoxypropyl)trimethoxysilane (GpTMS), and 2-(3,4-epoxycyclohexyl)ethyltrimethoxysilane (CyTMS) were all purchased from Gelest Incorporated. Glacial acetic acid, propylene glycol monomethyl ether (PMA), tetrabutylammonium fluoride (1.0 M in tetrahydrofuran), and tetraethoxysilane (TEOS) were purchased from Sigma Aldrich Company. Water was purified via reverse osmosis. Isopropyl alcohol (IPA) was manufactured by Burdick & Jackson and purchased from VWR International. Colloidal silica was purchased from Nissan Chemical. The specific grade of colloidal silica was Snowtex-O. Magnesium powder was obtained from Ecka Granules and had an average particle size of 25 microns. AntiTerra 204, a wetting agent, was obtained from BYK Chemie. Bentone 38, an anti-settling agent, was obtained from Elementis Specialties. Aerosil R812, a viscosity modifier, was obtained from Degussa. Mica 325WG was obtained from Georgia Industrial Minerals Inc. The substrate used for corrosion testing was Al 2024-T3 obtained from Q-Panel. The polyurethane topcoat used together with experimental Mg-rich primer compositions was MIL-PRF-85285C obtained from Deft Chemical Coatings. Salt water used for corrosion screening by immersion testing was 3 weight percent sodium chloride in water purified by reverse osmosis.

Sols used to produce homogeneous HOI coatings were synthesized as follows: IPA, water, acetic acid, TEOS, and trialkoxysilane were added sequentially to an 8-mL scintillation vial, containing a stir bar, using the liquid handling robot. The solutions were allowed to stir overnight at room temperature. Detailed formulations for all of the homogeneous sols prepared are provided in Appendices 1 and 2.

Sols used to produce heterogeneous HOI coatings were synthesized as follows: IPA, colloidal silica, and trialkoxysilane were added sequentially to an 8-mL scintillation vial, containing a stir bar, using a liquid handling robot. The solutions were allowed to reflux for a total of 2 or 24 hours. In the cases where tetrabutylammonium fluoride (TBAF) was used, it was added after the first hour of reflux. Detailed formulations for all of the heterogeneous sols prepared are provided in Appendix 3.

Mg-rich primers based on HOI binders were prepared using the formulation shown in Table I. This formulation provides a primer composition comprised of 80

weight percent Mg particles. The solids content of the HOI solutions or colloidal dispersions were adjusted with PMA to be 10 % by weight.

Instrumentation and Software. Symyx[®] Discovery Tools[™] is a package of software used for experiment design, equipment operations, data storage, and analysis. A Symyx[®] Discovery Tools[™] liquid handling robot was used for producing arrays of sols while a second Symyx robot was used to cast sols into stamped aluminum arrays. Library Studio[®] was used to design all experiments run with the automated robots. The instruments were run using either an Impressionist[®] procedure or Epoch[®] protocol. Solvents were removed from samples using the Genevac[®] EZ-2 parallel evaporator. Salt spray corrosion testing was done in a Q-FOG cyclic corrosion tester (model SSP, 1100 liter capacity) according to ASTM method B117. Electrochemical impedance spectroscopy (EIS) measurements were taken with a potentiostat from Gamry Instruments. The software used was Gamry Framework (version 4.35). Data analysis was accomplished using Gamry EChem Analyst (version 1.35).

Methods. The combinatorial workflow implemented for developing HOI binders for Mg-rich primers for corrosion protection was based on a tiered material screening process as illustrated in Figure 1. Sols were prepared robotically using the Symyx liquid handling robot. The compositions used to produce the sols are shown in Appendices 1-3. After having prepared the sols, their stability was evaluated 24 hours later. Sols that produced homogenous solutions or homogenous, stable, colloidal dispersions were robotically cast into embossed wells of the four inch by eight inch aluminum panels shown in Figure 2 using the Tecan Freedom EVO liquid handling robot. Each well was 2.5 cm by 3.8 cm and approximately 1.0 mm deep 750 μ L of solution was pipetted into a well. The array of solutions were then placed in a low flow, vented cabinet to allow for solvent evaporation and curing at ambient conditions for 24 hours. After the 24 hour period for solvent evaporation and curing, film formation and curing characteristics were rapidly assessed using visual and physical observation. Compositions that produced tack-free films that had no visible signs of cracking were taken through a second solution processing step in which PMA was added to a given sol at a weight equivalent to a factor of 1.75 relative to the total weight of solids and the mixture solvent stripped using the parallel rotary evaporator to largely remove the lower boiling solvents, IPA and water, rendering the HOI material in PMA. After this solution processing step, stability of the sols was assessed using visual observation and only those sols that displayed good stability were carried forward to secondary screening.

Secondary screening consisted of the preparation of larger volumes of the sols selected from primary screening using two carousel reactors and manual solution preparation. The solvent exchange process for each sol was done using a conventional rotoevaporator using a temperature of 60°C and pressure of approximately 5 mm Hg. With these larger volume sols, tabs machined from a standard 4 inch by 8 inch aluminum panel, as shown in Figure 3, were dip coated using the parallel dip coater such that each tab contained a different coating composition. The dip coated coatings were then allowed to cure and the barrier properties of the coatings characterized using salt water immersion as a screen. The compositions that showed the best barrier properties were used for formulation experiments involving the use of Mg particles for cathodic protection. Traditional, manual methods of experimentation were used for Mg-rich primer formulation experiments.

Results and Discussion

General Aspects of the Combinatorial Workflow. The combinatorial workflow created to develop new HOI Mg-rich primers for corrosion protection of aluminum alloys is shown schematically in Figure 1. The workflow was based on a tiered screening process in which initial screening involved the synthesis and characterization of sols produced from hydrolysis and condensation reactions of alkoxysilane functional monomers in solution. The results of the initial screening resulted in the identification of sols that displayed both solution stability and cured that films that were tack-free and free of macroscopic cracks. Only those compositions that showed these desirable characteristics were selected for further experimentation.

The next step in the tiered process involved exchange of water and low boiling alcohols (IPA and methanol) present in the sols with the higher boiling solvent, PMA. This process was required to largely remove water from the materials to further drive condensation reactions and minimize water induced oxidation of Mg particles during Mg-primer formulation. After completing the solvent exchange, solution stability was again screened since some of the previously stable solutions may have gelled or formed a precipitate. Those compositions that produced stable solutions or colloidal dispersions after undergoing the solvent exchange process were carried forward for further screening referred to as “secondary” screening.

Secondary screening involved scale-up of solution volumes to 50 mls, dip coating on to the aluminum alloy substrate of interest, curing at ambient conditions, and measuring relative corrosion protection using partial immersion of coated specimens in salt water. Those compositions showing the best corrosion resistance based on visual observation were selected for use in Mg-rich primer formulation experiments in which the HOI solutions were utilized as the coating binder material.

Experiments Involving the Development of Mg-rich Primers Based on a Homogeneous HOI Binder System. Initial high throughput experiments for the development of HOI-based Mg-rich primers were focused on binders based on a homogenous HOI network derived from trialkoxysilanes and tetraethoxysilane (TEOS) using a sol-gel process as shown schematically in Figure 4. The experimental design utilized for the first screening experiment was based on variations in trialkoxysilane composition, molar ratio of trialkoxysilane to TEOS, and molar ratio of water to TEOS. Figure 5 provides the chemical structure of the trialkoxysilanes investigated while Figure 6 provides a schematic illustration of the experimental design.

The rationale for the selection of the amino-, ureido-, and phosphonato-functional trialkoxysilanes was based on the need for relatively polar or reactive functional groups in order to provide for good adhesion of the primer to the substrate and good wetting and adhesion of the topcoat to the primer. Methyltrimethoxysilane (MeTMS) was included to serve primarily as a negative control to determine the effect of a relatively nonpolar, nonreactive organic functional group on coating performance.

Figure 7 displays the results obtained with regard to solution stability and cured film characteristics. As previously discussed, solution stability was simply characterized by visual observation. Figure 8 displays representative images of sols that were produced

during the experiment. It can be seen that, for this experiment, solution stability was easily characterized using visual observation.

From Figure 7, some general trends between the responses and chemical composition can be readily discerned. Most notable, all of the sols derived from ApTMS were unstable and resulted in the formation of a precipitate or gel. This result was not completely unexpected since the isoelectric point for silicate particles is at a pH of approximately 4 and addition of ApTMS to the acidic IPA/water/TEOS mixture increased pH from approximately 3 to approximately 10. For sols based on UpTMS, most the sols were unstable, with the exception of two sols derived from the highest water/alkoxysilane ratio and a molar excess of UpTMS to TEOS. These two sols all produced cured films that were both tack-free and free of visible cracks.

For sols based on MeTMS, two trends were apparent. First, sols containing the highest level of water tended to be unstable while those containing lower water levels provided stable sols. For a sol-gel process, water/alkoxysilane ratio strongly influences structure of organosilicate oligomers. Use of an excess of water tends to produce spherical particles whereas more linear structures are produced when alkoxysilane groups are in molar excess.²

The second trend observed involved the effect of TEOS/MeTMS molar ratio on cured film characteristics. For coatings prepared using a molar excess of MeTMS to TEOS, cured films were obtained that were tack-free after 24 hours and had no visible signs of cracks, while coatings prepared using a stoichiometric ratio of MeTMS to TEOS or a molar excess of TEOS produced cured films that had visible cracks. An increased tendency for cracking with a relative decrease in MeTMS concentration is consistent with expectations since crosslink density and, thus, shrinkage during cure would increase with decreasing MeTMS concentration.

All of the sols produced using DTES were stable; however, most of the coatings were insufficiently cured after 24 hours at ambient conditions as indicated by their tacky surface. Only coatings produced using an excess of TEOS relative to DTES showed sufficient cure after 24 hours. This result may be due to the fact that DTES, unlike the other trialkoxysilanes, is a triethoxysilane. It is well known that ethoxysilanes hydrolyze slower than methoxysilanes.² The slower hydrolysis rate associated with ethoxysilanes may ultimately result in a reduction in cure rate if significant concentrations of ethoxysilane groups are still present in the sol at the time of coating application.

Since many of the coatings based on MeTMS cracked while many based on DTES were tacky and under-cured in 24 hours, primary screening was extended to include coatings based on blends of MeTMS and DTES as the organosilane component. The experimental design for this follow-up experiment is shown schematically in Figure 9. All fifty of the sols displayed good solution stability. As shown in Figure 10, approximately 70 % of the compositions produced crack-free and tack-free films. These compositions were carried forward to the solvent exchange process. All of the PMA-based sols were stable and, thus, all of these compositions were carried forward to secondary screening.

As indicated in Figure 10, five coating compositions were identified using salt water immersion screening as being the best with respect to providing a promising barrier coating for inhibiting corrosion. Figure 11 displays representative images of both a good

and a poor performing coating with respect to salt water immersion testing. These five compositions were used for Mg-rich coating formulation experiments.

Four of the five binder compositions identified using high throughput screening were successfully utilized to produce Mg-rich primers that displayed good solution stability. Corrosion protection of topcoated samples prepared using Mg-rich primers derived from the four promising HOI binder candidates was assessed using B117 salt spray in conjunction with electrochemical impedance spectroscopy. Figure 12 displays Bode plots of the four samples of interest both before and after 2,500 hours of B117 salt spray exposure. All four of the samples showed similar impedance before salt spray exposure; however, after 2,500 hours of salt spray, considerable differentiation was observed. The coating based on binder “88,” as described in Figure 12 and Appendix 2, was found to possess the highest impedance after 2,500 hours of B117 salt spray exposure. Figure 13 displays images of a scribed specimen both before and after 2,500 hours of salt spray. As shown in Figure 13, no corrosion away from the scribed area or blistering in the scribed area was observed after 2,500 hours of salt spray. However, some corrosion product was observed in the scribe. This level of performance obtained after a single iteration of the combinatorial workflow was a very nice result.

Experiments Involving the Development of Mg-rich Primers Based on a Heterogeneous HOI Binder System. In addition to coating binders based on sols derived from a blend of trialkoxysilanes and TEOS, HOI binders derived from colloidal silica nanoparticles were also investigated. These binders can be considered heterogeneous HOI binders since the chemistry utilized, shown schematically in Figure 14, results in silicate nanoparticles dispersed in a continuous phase derived from hydrolysis and condensation of a trialkoxysilane.

Three different trialkoxysilanes were used for the experiment: PhEtTMS, GpTMS), and CyTMS. The two epoxy-functional trimethoxysilanes were chosen because successful functionalization of the silica nanoparticles would enable the investigation of a two-component, epoxy-amine cured binder system in addition to a moisture-cured binder system. Figure 15 provides a schematic representation of the experimental design utilized.

All of the colloidal dispersions were stable after adding the trialkoxysilane and refluxing to drive alkoxy silane hydrolysis and silanol condensation. However, during the solvent exchange process, colloidal stability was lost for all of the materials based on the epoxy-functional trialkoxysilanes. In addition to these materials, four of the materials based on PhEtTMS also formed a precipitate during the solvent exchange process. Thus, as shown in Figure 16, only eight out of the 36 materials originally produced, resulted in stable colloidal dispersions in PMA. These eight materials were used for Mg-rich primer formulation experiments.

Impedance spectroscopy and B117 salt spray exposure were used to evaluate corrosion protection of topcoated specimens. As shown in Figure 17, the difference in low frequency impedance between samples was marginal before salt spray exposure; however, after 1,000 hours salt spray, significant differences were observed (Figure 18). Coatings “119” and “121,” were found to possess the highest impedance after 1,000 hours of salt spray. Both of these specimens were based on HOI binders derived from the highest ratio of PhEtTMS to silica.

With regard to B117 corrosion testing, all of the specimens based on heterogeneous HOI binders were found to have much less corrosion in the scribed area than specimens based on homogeneous HOI binders. In fact, as shown in Figure 19, sample 121 showed no significant corrosion in the scribe after 3,100 hours of salt spray exposure. The “bump-like” defects shown in Figure 19, which might be mistaken for blisters, were the result of clumps of Mg particles present in the primer layer. The vortex mixing used to produce the Mg-rich primers did not allow for the level of Mg dispersion that could have been achieved with high shear mechanical mixing or ball milling. None-the-less, the Mg-rich primer based on the heterogeneous HOI binder provided excellent cathodic protection in spite of the poor Mg dispersion. This level of protection is at least as good as the level of protection that can be obtained using conventional chromate-based primers. The much better corrosion protection provided by the heterogeneous HOI binder system as compared to the homogeneous HOI binder system is very interesting and will be the subject of further investigation.

Conclusion

Using the combinatorial/high-throughput workflow, new Mg-rich primers based on a HOI binder system were explored. Approximately 150 unique HOI compositions were rapidly screened based on solution stability, cured film characteristics, and corrosion protection. Based on these screening results, promising HOI compositions were identified for further investigation in Mg-rich primers. Interestingly, it was found that the use of heterogeneous HOI binders based on colloidal silica provided dramatically better corrosion protection than homogeneous HOI binders derived from TEOS. It was found that an Mg-rich primer based on a heterogeneous HOI binder derived from the highest ratio of PhEtTMS to silica gave excellent corrosion protection with essentially no visible evidence of corrosion in the scribe after 3,100 hours of B117 salt spray exposure.

Acknowledgement

The authors thank the Air Force Research Laboratory for funding through cooperative research agreement, FA8650-04-1-5045.

References

1. Loy, D. A. *MRS Bulletin* **2001**, 26(5), 364.
2. C. J. Brinker and G. W. Scherer, “Sol-Gel Science,” Academic Press, San Diego, CA, 1990.
3. Webster, D. C.; Bennet, J.; Kuebler, S.; Kossuth, M. B.; Jonasdottir, S. *JCT Coat. Tech.*, **2004**, June, 34.
4. Chisholm, B. J.; Christianson, D. A.; Webster, D. C. *Prog. Org. Coat.*, **2006**, 57, 115.
5. M. E. Nanna and G. P. Bierwagen, *J. Coat. Technol. Res.*, **1**, 69 (2004).
6. D. Battocchi, A. M. Simoes, D. E. Tallman, G. P. Bierwagen, *Corrosion Science* **2006**, 48, 1292.
7. N. C. Fawcett, *Polym. Matr. Sci. Eng.*, **53**, 855-859 (1985).

Table I. Formulation used for preparing Mg-rich primers.

Order of Addition	Raw Material	Weight percent
1	HOI solution (10% solids)	60
2	AntiTerra 204	0.3
3	Bentone 38	0.7
4	Aerosil R812	0.3
5	Mica 325WG	1.7
6	Mg powder	37

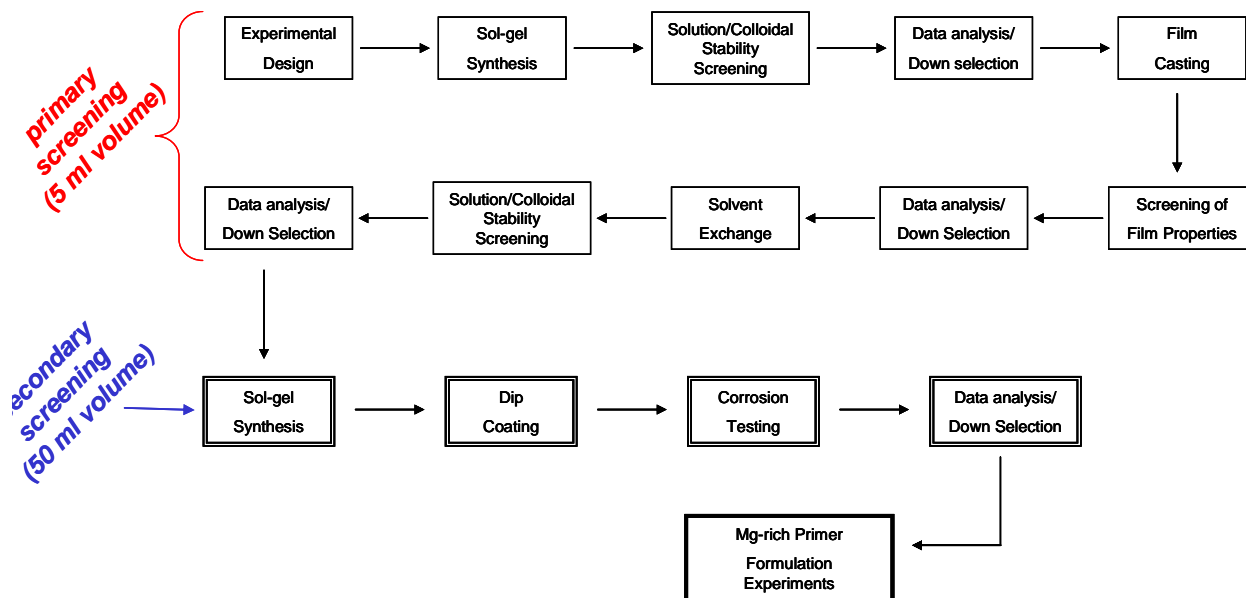


Figure 1. A schematic of the combinatorial workflow used to development new Mg-rich primers based on HOI binder systems.



Figure 2. Photograph of the array template used to prepare coating films with a robotic film casting technique.

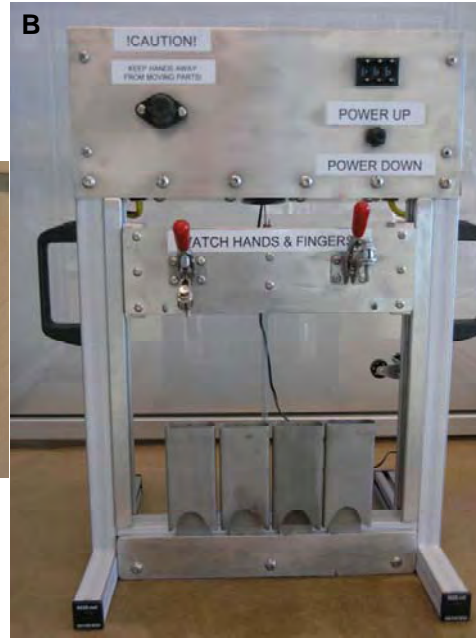


Figure 3. (A) Photograph of substrate used for parallel dip coating. (B) Photograph of the parallel dip coater.

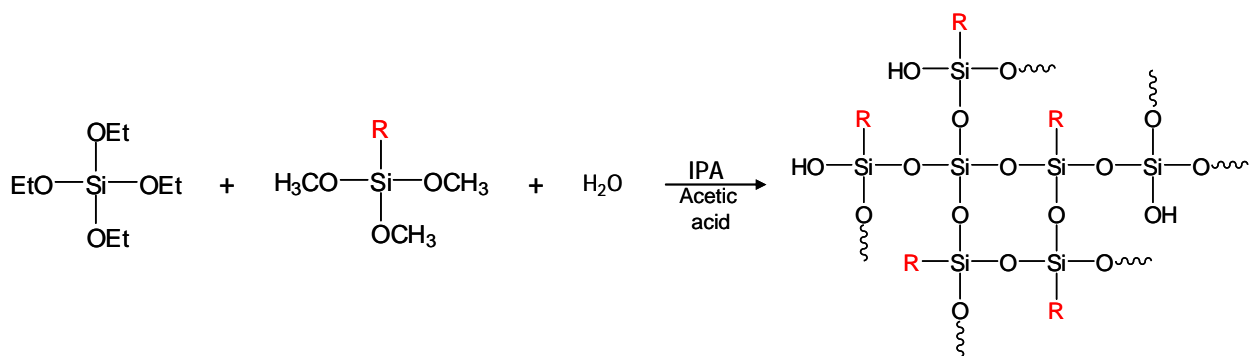


Figure 4. Schematic of the synthesis of homogeneous HOI materials.

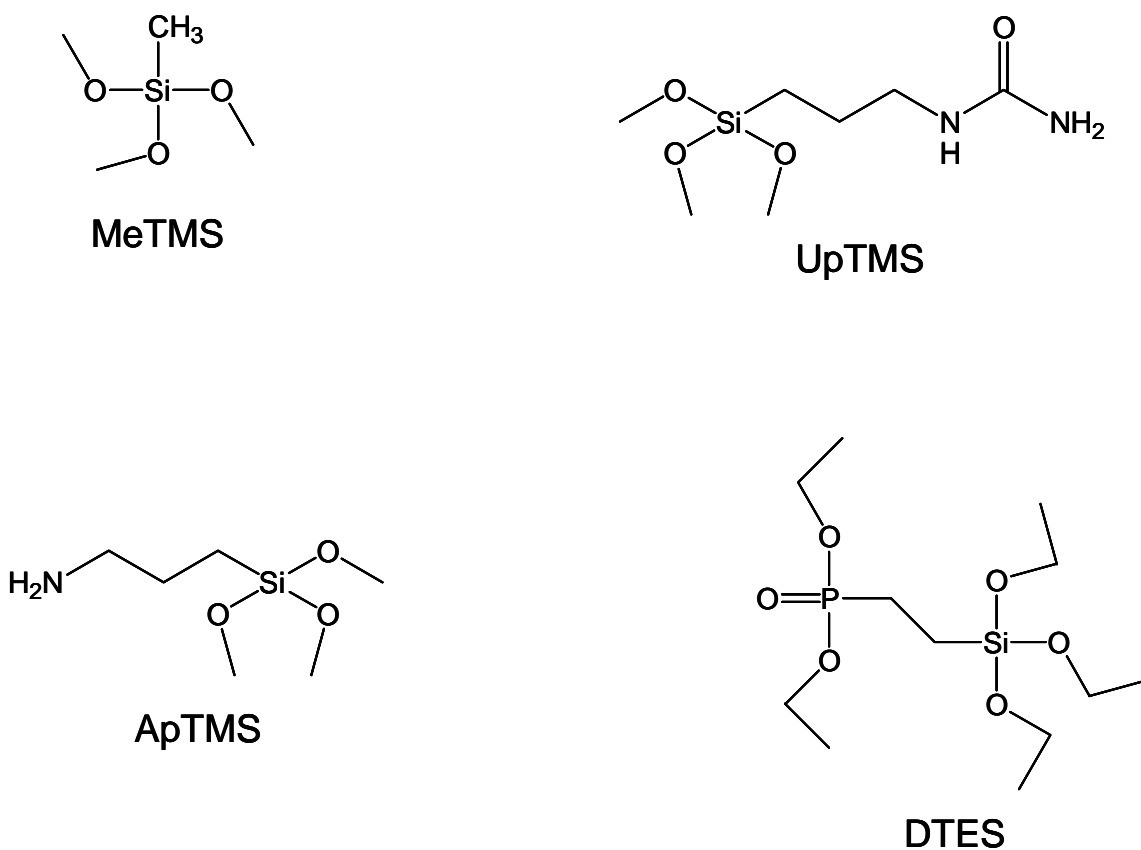


Figure 5. Chemical structure of the trialkoxysilanes investigated for the production of homogeneous HOI binders.

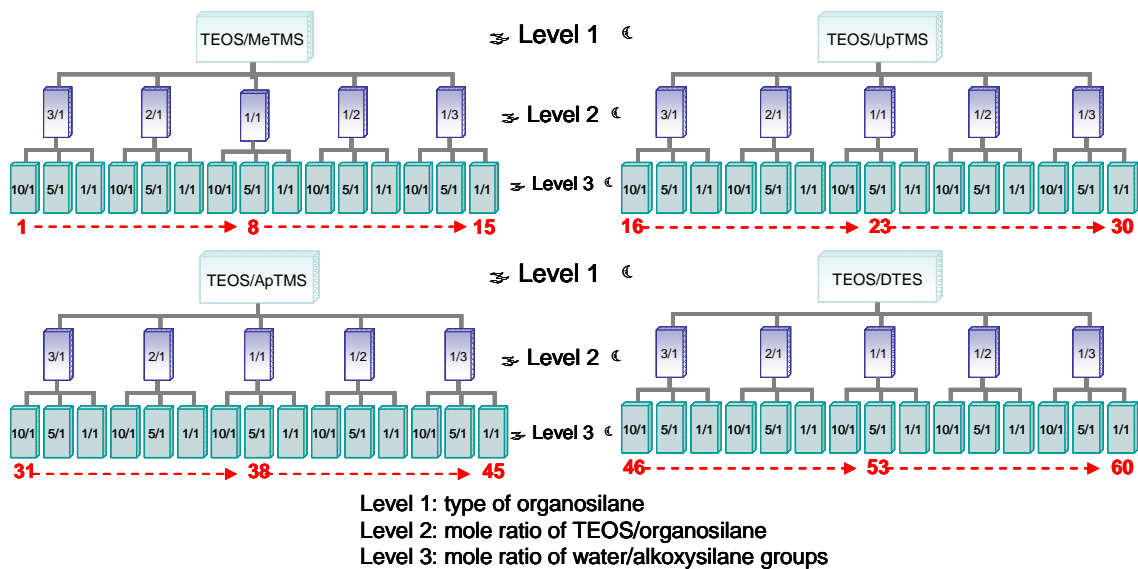


Figure 6. An illustration of the experimental design used to screen homogeneous HOI materials.

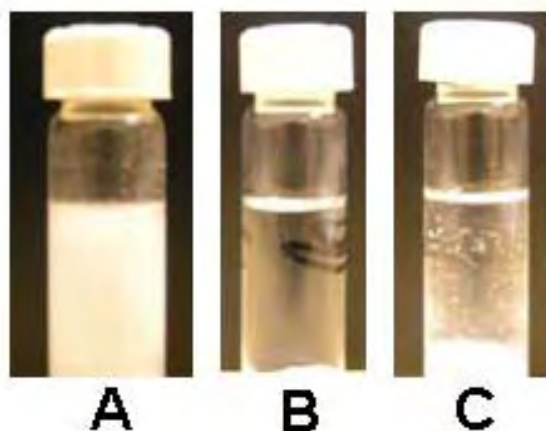


Figure 8. Photographs of representative sols that resulted in the formation of gels (A), homogeneous solutions (B), and precipitates (C).

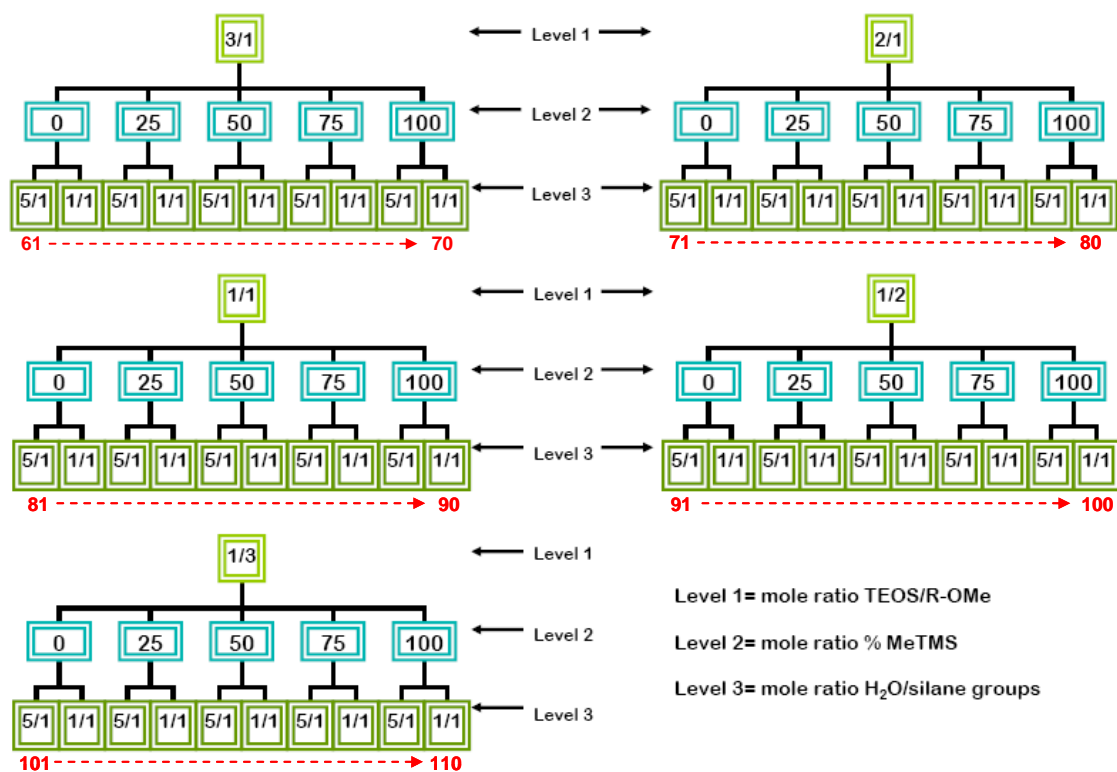


Figure 9. An illustration of the experimental design used to screen HOI materials derived from blends of MeTMS and DTES.

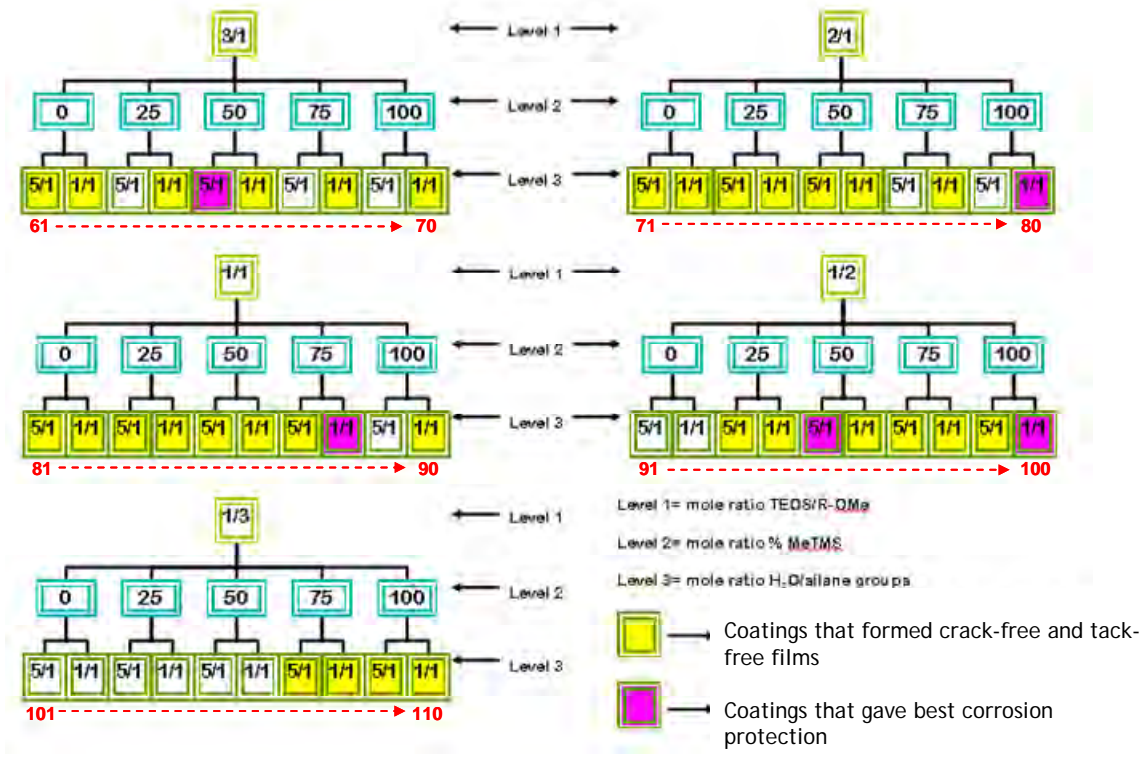


Figure 10. Results obtained for solution stability screening and screening of cured film characteristics.

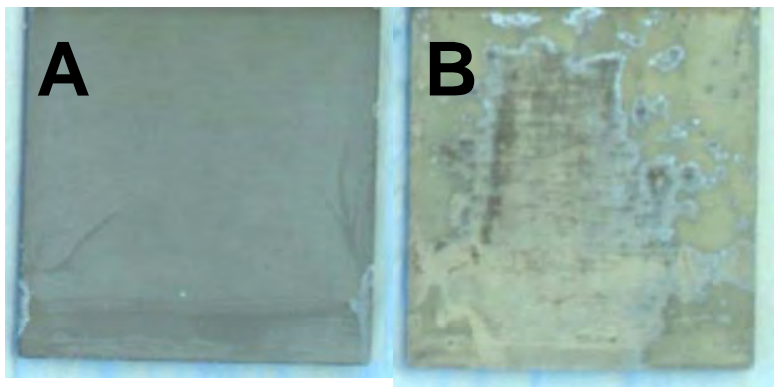


Figure 11. Images of coated aluminum samples displaying relatively good (A) and relatively bad (B) performance with respect to corrosion protection upon salt water immersion.

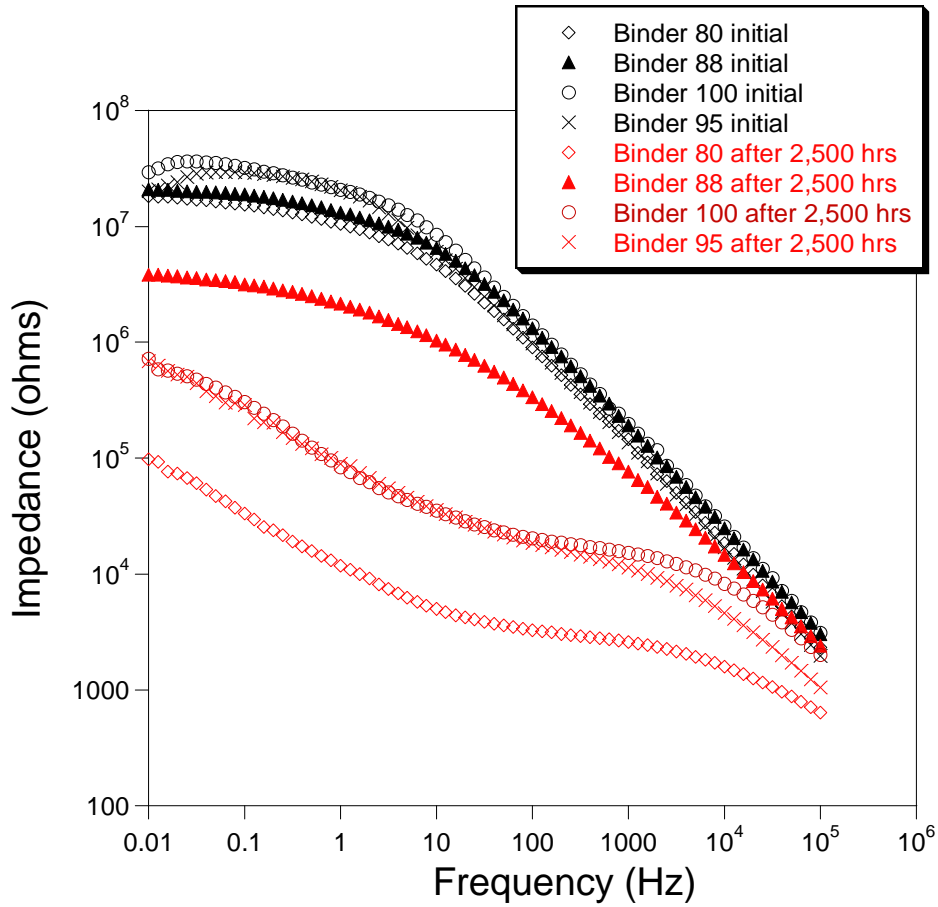


Figure 12. Bode plots of topcoated Mg-rich primers based on the most promising homogeneous HOI binder systems. The data corresponds to materials before and after 2,500 hours of B117 salt spray exposure.

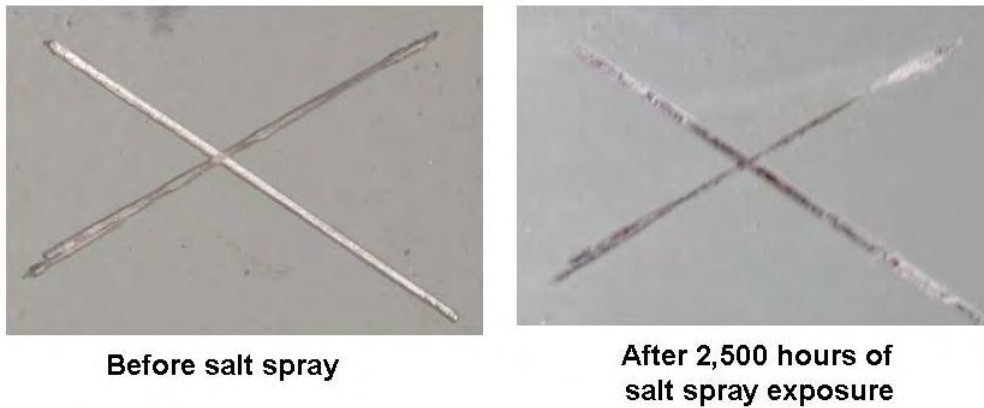


Figure 13. Images illustrating the corrosion protection of a topcoated Mg-rich primer based on HOI binder number 88.

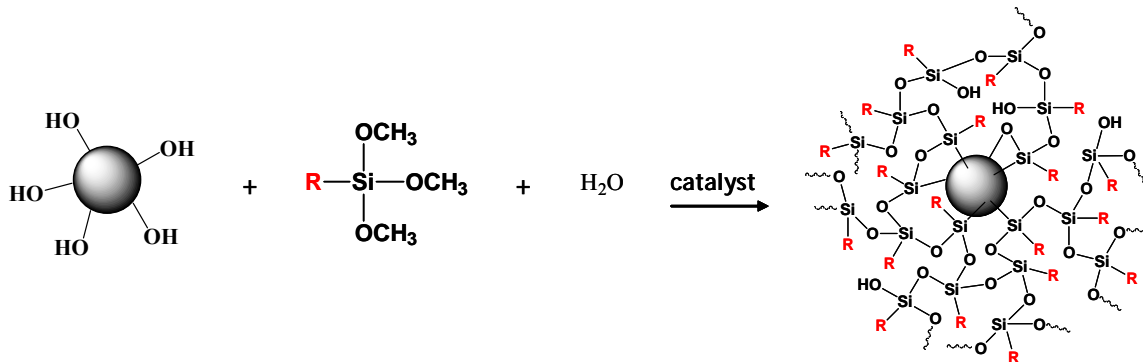


Figure 14. Schematic describing the synthesis of the heterogeneous HOI materials using colloidal silica.

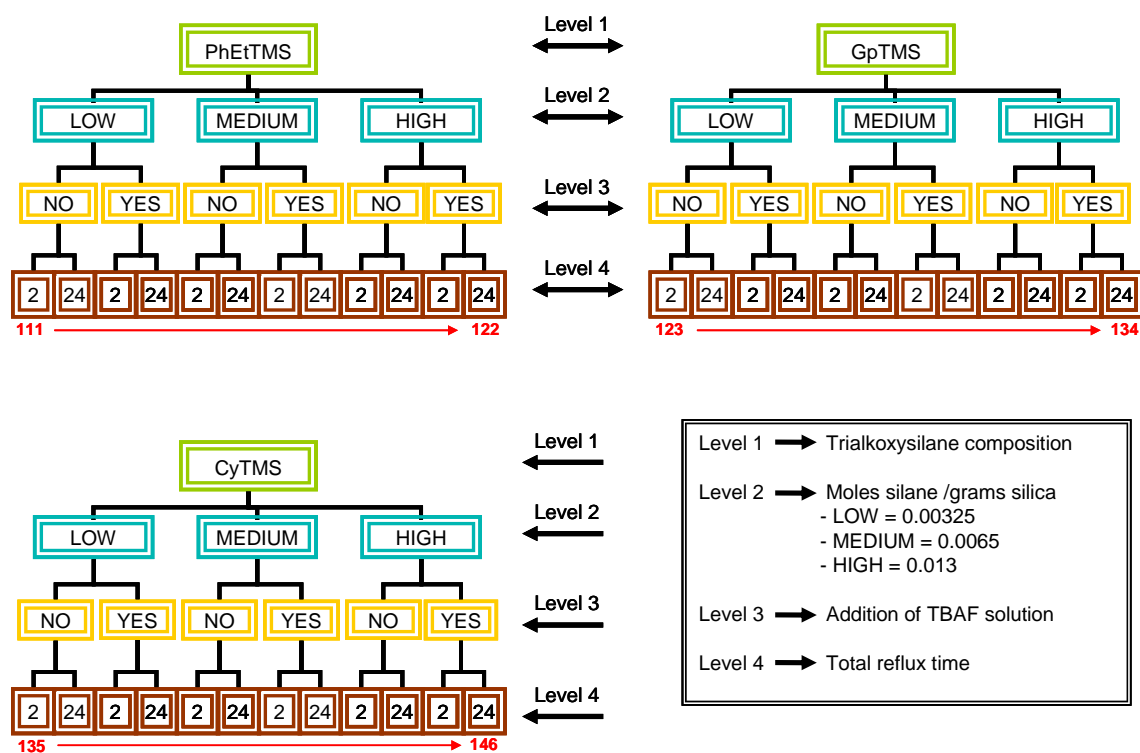


Figure 15. Provides a schematic representation of the experimental design utilized to investigate heterogeneous HOI materials.

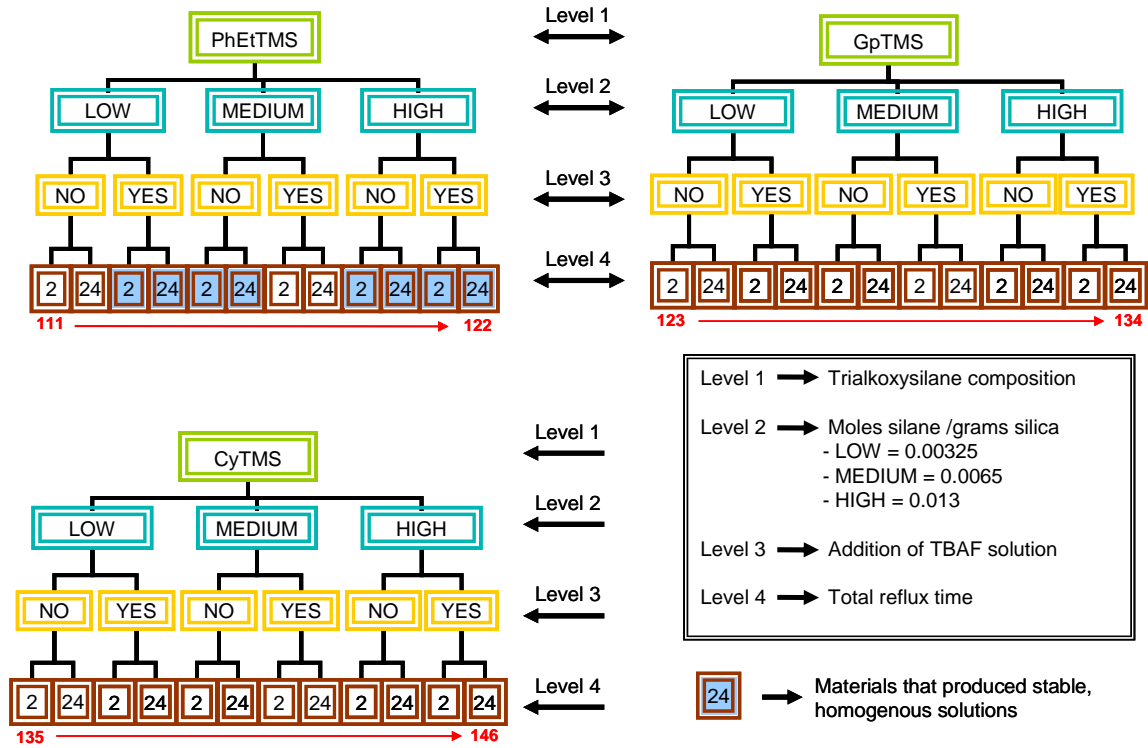


Figure 16. Results of colloidal stability screening for heterogeneous HOI materials.

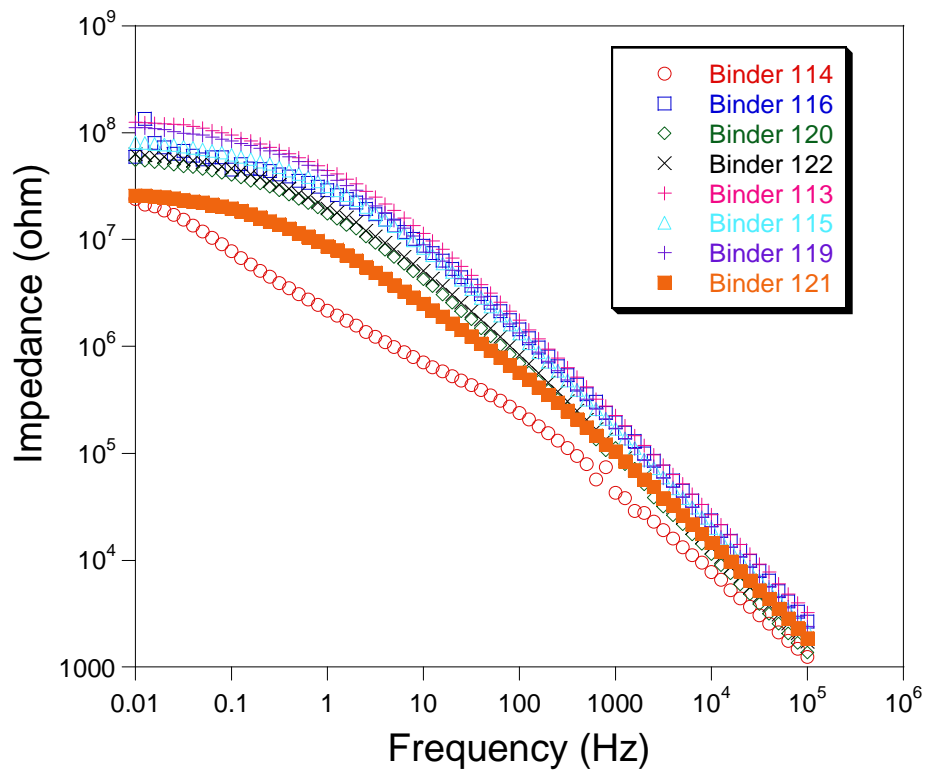


Figure 17. Bode plots of topcoated Mg-rich primers based on heterogeneous HOI binders before salt spray exposure.

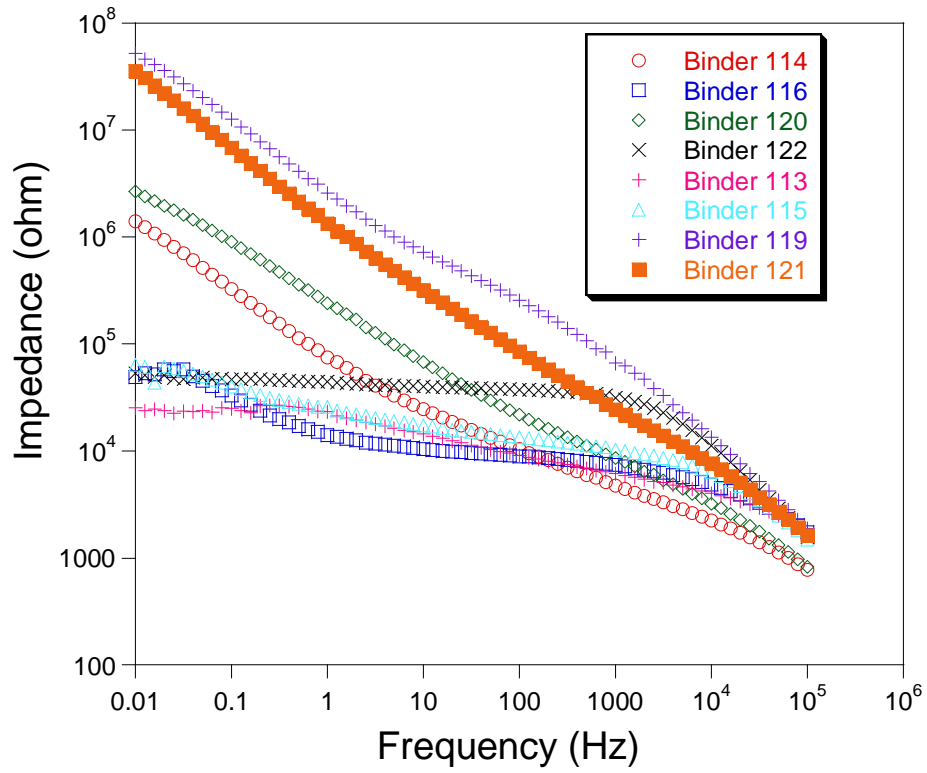


Figure 18. Bode plots of topcoated Mg-rich primers based on heterogeneous HOI binders after 1,000 hours of salt spray exposure.

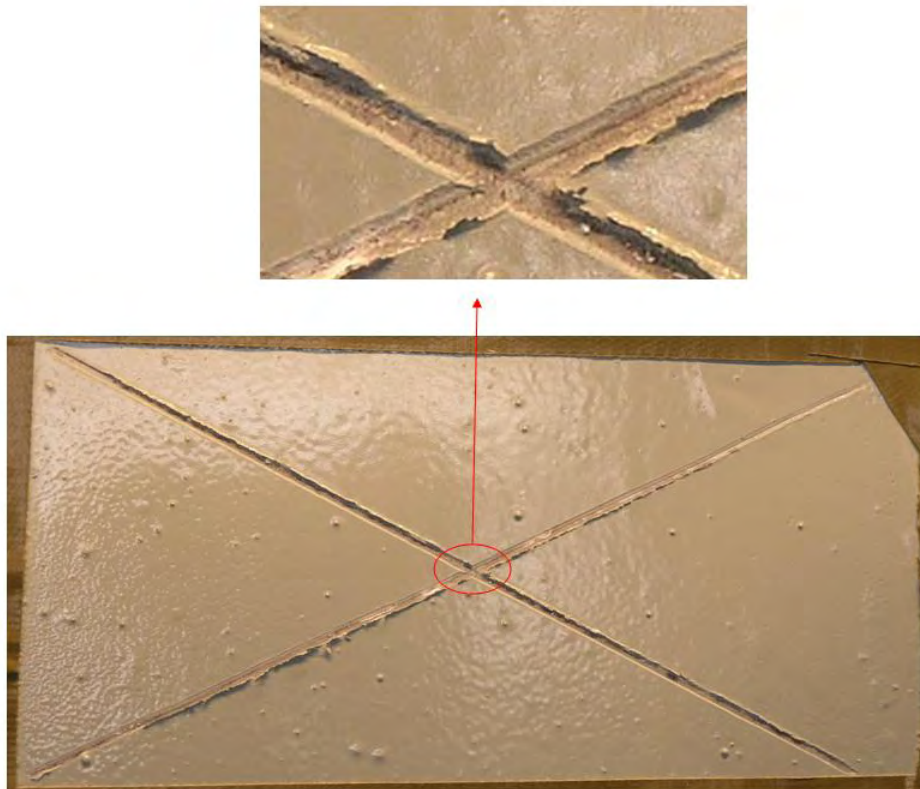


Figure 19. Image of a topcoated specimen derived from HOI binder 121 after 3,100 hours of salt spray exposure.

Appendix 1. Coating formulations for the experiment described in Figure 6. All values are in units of microliters.

Coating No.	IPA	H2O	Acetic acid	TEOS	MeTMS	UpTMS	ApTMS	DTES
1	240	3900	52	900	204	0	0	0
2	2190	1950	52	900	204	0	0	0
3	3750	390	52	900	204	0	0	0
4	202	3825	51	800	272	0	0	0
5	2114	1912	51	800	272	0	0	0
6	3644	382	51	800	272	0	0	0
7	143	4163	54	680	463	0	0	0
8	2224	2082	54	680	463	0	0	0
9	3890	416	54	680	463	0	0	0
10	63	4403	56	500	680	0	0	0
11	2264	2201	56	500	680	0	0	0
12	4025	440	56	500	680	0	0	0
13	14	4021	51	350	714	0	0	0
14	2025	2011	51	350	714	0	0	0
15	3633	402	51	350	714	0	0	0
16	773	3345	52	800	0	246	0	0
17	2446	1673	52	800	0	246	0	0
18	3784	335	52	800	0	246	0	0
19	911	3187	51	700	0	323	0	0
20	2505	1594	51	700	0	323	0	0
21	3780	319	51	700	0	323	0	0
22	1269	3117	54	550	0	507	0	0
23	2828	1559	54	550	0	507	0	0
24	4075	312	54	550	0	507	0	0
25	1512	2763	53	350	0	645	0	0
26	2894	1382	53	350	0	645	0	0
27	4000	276	53	350	0	645	0	0
28	1584	2531	51	250	0	692	0	0
29	2849	1265	51	250	0	692	0	0
30	3862	253	51	250	0	692	0	0
31	513	3630	52	850	0	0	236	0
32	2328	1815	52	850	0	0	236	0
33	3780	363	52	850	0	0	236	0
34	568	3515	51	750	0	0	312	0
35	2325	1757	51	750	0	0	312	0
36	3731	351	51	750	0	0	312	0
37	695	3382	51	570	0	0	475	0
38	2386	1691	51	570	0	0	475	0
39	3739	338	51	570	0	0	475	0
40	858	3372	53	400	0	0	666	0

41	2544	1686	53	400	0	0	666	0
42	3892	337	53	400	0	0	666	0
43	921	3277	52	300	0	0	749	0
44	2559	1639	52	300	0	0	749	0
45	3870	328	52	300	0	0	749	0
46	1089	2987	51	700	0	0	0	355
47	2582	1494	51	700	0	0	0	355
48	3777	299	51	700	0	0	0	355
49	1311	2809	52	600	0	0	0	456
50	2716	1405	52	600	0	0	0	456
51	3840	281	52	600	0	0	0	456
52	1630	2370	50	400	0	0	0	608
53	2815	1185	50	400	0	0	0	608
54	3763	237	50	400	0	0	0	608
55	1964	2102	51	250	0	0	0	760
56	3016	1051	51	250	0	0	0	760
57	3857	210	51	250	0	0	0	760
58	2328	2179	56	200	0	0	0	912
59	3417	1090	56	200	0	0	0	912
60	4289	218	56	200	0	0	0	912

Appendix 2. Coating formulations for the experiment described in Figure 9. All values are in units of milliliters.

Coating No.	IPA	H2O	Acetic acid	TEOS	MeTMS	DTES
61	2.535	1.480	0.051	0.700	0.000	0.335
62	3.719	0.296	0.051	0.700	0.000	0.335
63	2.460	1.571	0.051	0.740	0.040	0.266
64	3.717	0.314	0.051	0.740	0.040	0.266
65	2.331	1.640	0.050	0.770	0.083	0.185
66	3.644	0.328	0.050	0.770	0.083	0.185
67	2.239	1.753	0.050	0.820	0.132	0.098
68	3.642	0.351	0.050	0.820	0.132	0.098
69	2.142	1.888	0.051	0.880	0.189	0.000
70	3.652	0.378	0.051	0.880	0.189	0.000
71	2.648	1.387	0.051	0.600	0.000	0.431
72	3.757	0.277	0.051	0.600	0.000	0.431
73	2.540	1.486	0.051	0.640	0.051	0.345
74	3.729	0.297	0.051	0.640	0.051	0.345
75	2.395	1.587	0.050	0.680	0.109	0.244
76	3.665	0.317	0.050	0.680	0.109	0.244
77	2.277	1.736	0.051	0.740	0.179	0.133
78	3.666	0.347	0.051	0.740	0.179	0.133
79	2.105	1.886	0.050	0.800	0.257	0.000
80	3.614	0.377	0.050	0.800	0.257	0.000
81	2.852	1.218	0.051	0.420	0.000	0.604
82	3.826	0.244	0.051	0.420	0.000	0.604
83	2.713	1.345	0.051	0.460	0.074	0.496
84	3.789	0.269	0.051	0.460	0.074	0.496
85	2.504	1.473	0.050	0.500	0.161	0.359
86	3.682	0.295	0.050	0.500	0.161	0.359
87	2.346	1.693	0.051	0.570	0.275	0.205
88	3.701	0.339	0.051	0.570	0.275	0.205
89	2.064	1.916	0.050	0.640	0.412	0.000
90	3.597	0.383	0.050	0.640	0.412	0.000
91	3.001	1.060	0.051	0.260	0.000	0.748
92	3.849	0.212	0.051	0.260	0.000	0.748
93	2.830	1.196	0.050	0.290	0.093	0.625
94	3.787	0.239	0.050	0.290	0.093	0.625
95	2.632	1.376	0.050	0.330	0.212	0.474
96	3.733	0.275	0.050	0.330	0.212	0.474
97	2.354	1.603	0.050	0.380	0.367	0.273
98	3.636	0.321	0.050	0.380	0.367	0.273
99	2.030	1.962	0.050	0.460	0.592	0.000
100	3.599	0.392	0.050	0.460	0.592	0.000

101	3.096	0.998	0.051	0.190	0.000	0.820
102	3.894	0.200	0.051	0.190	0.000	0.820
103	2.860	1.118	0.050	0.210	0.101	0.679
104	3.755	0.224	0.050	0.210	0.101	0.679
105	2.737	1.349	0.051	0.250	0.241	0.539
106	3.816	0.270	0.051	0.250	0.241	0.539
107	2.482	1.640	0.052	0.300	0.434	0.323
108	3.794	0.328	0.052	0.300	0.434	0.323
109	2.016	1.993	0.051	0.360	0.695	0.000
110	3.610	0.399	0.051	0.360	0.695	0.000

Appendix 3. Coating formulations for the experiment described in Figure 15. All values are in units of milliliters.

Coating No.	IPA	Snowtex-O	PhEtTMS	GpTMS	CyTMS	TBAF	Reflux time
111	2.548	1.770	0.284	0	0	0	2
112	2.548	1.770	0.567	0	0	0	2
113	2.548	1.770	1.135	0	0	0	2
114	2.548	1.770	0.284	0	0	0.00354	2
115	2.548	1.770	0.567	0	0	0.00354	2
116	2.548	1.770	1.135	0	0	0.00354	2
117	2.548	1.770	0	0.287	0	0	2
118	2.548	1.770	0	0.574	0	0	2
119	2.548	1.770	0	1.149	0	0	2
120	2.548	1.770	0	0.287	0	0.00354	2
121	2.548	1.770	0	0.574	0	0.00354	2
122	2.548	1.770	0	1.149	0	0.00354	2
123	2.548	1.770	0	0	0.369	0	2
124	2.548	1.770	0	0	0.739	0	2
125	2.548	1.770	0	0	1.478	0	2
126	2.548	1.770	0	0	0.369	0.00354	2
127	2.548	1.770	0	0	0.739	0.00354	2
128	2.548	1.770	0	0	1.478	0.00354	2
129	2.548	1.770	0.284	0	0	0	24
130	2.548	1.770	0.567	0	0	0	24
131	2.548	1.770	1.135	0	0	0	24
132	2.548	1.770	0.284	0	0	0.00354	24
133	2.548	1.770	0.567	0	0	0.00354	24
134	2.548	1.770	1.135	0	0	0.00354	24
135	2.548	1.770	0	0.287	0	0	24
136	2.548	1.770	0	0.574	0	0	24
137	2.548	1.770	0	1.149	0	0	24
138	2.548	1.770	0	0.287	0	0.00354	24
139	2.548	1.770	0	0.574	0	0.00354	24
140	2.548	1.770	0	1.149	0	0.00354	24
141	2.548	1.770	0	0	0.369	0	24
142	2.548	1.770	0	0	0.739	0	24
143	2.548	1.770	0	0	1.478	0	24
144	2.548	1.770	0	0	0.369	0.00354	24
145	2.548	1.770	0	0	0.739	0.00354	24
146	2.548	1.770	0	0	1.478	0.00354	24

DEVELOPMENT OF HYBRID ORGANIC-INORGANIC BINDER FOR MG-RICH PRIMER

Séva Balbyshev, Missy Berry, Jun Li and Bret J. Chisholm

*The Center for Nanoscale Science and Engineering
North Dakota State University, Fargo, ND*

Abstract

Recently Mg-rich pigmentation has been developed as an attractive alternative to chromated primers for corrosion control of Al alloys. Mg pigments incorporated in an organic binder protect Al alloys by acting as a barrier to corrosive environment and by acting as a cathodic protector. The authors have investigated hybrid organic-inorganic (HOI) binders for Mg-rich primer based on organically-modified colloidal silica. Such binders benefit from the unique combination of properties when organic and inorganic phases are combined. The inorganic component promotes adhesion and increases barrier properties of the film, while the organic phase imparts flexibility and compatibility with subsequent polymer layers. Colloidal silica particles have been functionalized via sol-gel process. Numerous sol-gel processing variables strongly affect material properties. These include, but not limited to, silica/organosilane ratio, organosilane and solvent chemical composition, reaction time, and catalyst concentration. The combinatorial/high throughput workflow has been used to assist in optimization of the processing parameters in order to identify promising hybrid organic-inorganic binder systems for the development of Mg-rich primers. The candidate binders have been investigated by liquid state ^{29}Si NMR. Electrochemical behavior of the film has been evaluated by electrochemical impedance spectroscopy.

Introduction

Current coating systems for aircraft corrosion protection are based on a traditional chromate surface treatment, primer, and topcoat. To date, the corrosion protection of aluminum alloys has relied extensively on potent hexavalent-chromium compounds, which are included in both surface preparation/treatments and organic primers. However, the toxicity and carcinogenic properties of chromium has caused federal agencies, in particular the EPA, to impose severe restrictions on its use.¹ Corrosion protection of aluminum-skinned aircraft and development of improved environmentally benign surface treatments for aluminum aerospace alloys are critical needs for the aerospace industry. Recently developed metal-rich coatings for corrosion protection of aircraft aluminum alloys rely on magnesium powder dispersed in an organic binder.² It has been shown that this environmentally friendly formulation of Mg-rich coatings can provide exceptional protection for aluminum-based alloys.^{3,4} In these metal-rich coatings, Mg particles embedded in a polymeric matrix act as a sacrificial anode; Mg undergoes anodic dissolution and thus protects the underlying metal from corrosion.

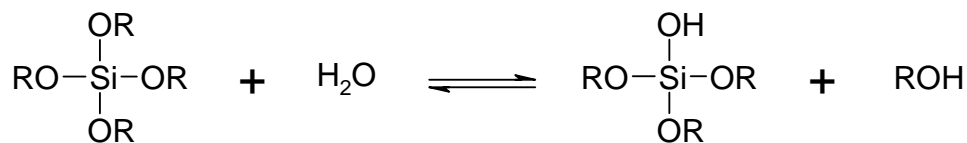
Selection of binder is crucial to successful design of Mg-rich coatings. A primary failure mechanism in traditional coating systems results from a lack of hydrolytic stability at the substrate-coating interface. The loss of adhesion here allows accumulation of water and ions at this interface, which may result in a corrosion cell. For corrosion protection, hybrid organic-inorganic (HOI) binder systems are of particular interest. HOI binders enable strong covalent bonding at the metal oxide/coating interface and

could dramatically improve the long-term hydrolytic stability. In addition to providing robust interface bonding via the inorganic component, the organic phase of HOI binders imparts flexibility and compatibility subsequent polymers layers.

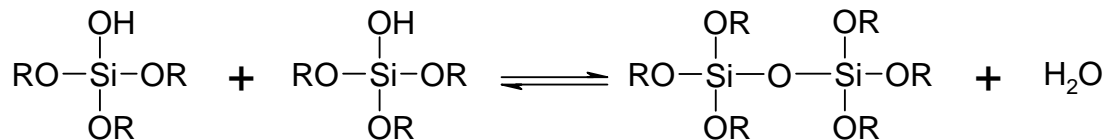
Organic-inorganic hybrid materials prepared by sol-gel approach have rapidly become a fascinating new field of research in materials science. The explosion of activity in this area in the past decade has made tremendous progress in both the fundamental understanding of the sol-gel process and the development and applications of new organic-inorganic hybrid materials. A large amount of sol-gel research, including the work presented here, is based on silicon precursors because of their balance of reactivity and ease of handling, as well as their ready availability.⁵

Silane sol-gel chemistry consists primarily of hydrolysis and condensation reactions of alkoxy silane precursors that form nano-porous gels as the reactions proceed. The hydrolysis reactions are typically catalyzed by acid or base conditions, producing a hydrolyzed silanol of the general form $(RO)_xSi(OH)_{4-x}$ and an alcoholic by-product as shown in Scheme 1. Subsequent condensation reactions occur to form siloxane bridges resulting in a substantial increase in molecular weight as shown in Scheme 2.

Scheme 1: Hydrolysis



Scheme 2: Condensation



The molecular structure, degree of organization, and properties that can be obtained for these sol-gel derived materials depend on the chemical nature of their components, but they also rely on the synergy between these components. Synthesis of such hybrid organic-inorganic compounds via sol-gel process and, in turn, the properties of the resulting films are influenced by a variety of parameters. These variables include the choice of silane, relative ratio of organic and inorganic components, alkoxide:solvent ratio, choice of solvent, pH, and temperature, to name a few. Therefore, tremendous amount of experimental work is required for development of hybrid organic-inorganic compounds with desired properties for a particular application. Previously, combinatorial/high throughput approach has been applied to help address this complex multidimensional matrix of experimental parameters.⁶ Since many more compounds and formulations can be explored simultaneously, this method greatly accelerates the process of new material discovery. Combinatorial/high throughput experimentation is based upon the concept of a workflow, which is a series of process steps taken during the course of an experiment starting with experimental design and ending with modeling of the data, as illustrated in Figure 1.

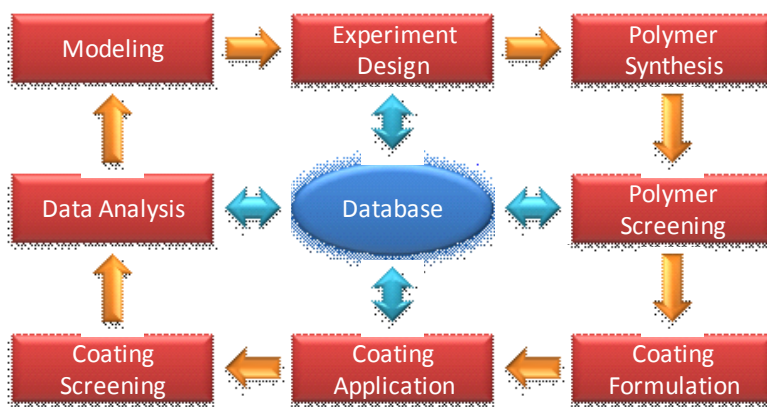


Figure 1. Schematic diagram of combinatorial workflow.

We use the combinatorial workflow to optimize the sol-gel processing parameters and identify promising hybrid organic-inorganic binder systems for the development of Mg-rich primers. This work expands on the effort on the application of combinatorial/high throughput methods to the development HOI coatings for the protection of aluminum alloys initiated by Chisholm *et al*⁶.

In the first phase of combinatorial/high throughput approach described by Chisholm *et al*⁶, several mixtures of tetraethyl-orthosilicate (TEOS) and four trifunctional methyl silicates formulated via the sol-gel process were screened. In this research effort we further investigate HOI binder systems based on organically modified colloidal silica formed via the sol-gel process. In this modified approach, a trifunctional silicon alkoxide is hydrolyzed according to Scheme 1 and undergoes condensation with itself and the nanophased silica particles in aqueous solution, as described in Scheme 2. SnowtexTM colloidal silica is a commercial product that is made by growing mono-dispersed, negatively charged, amorphous silica particles in water. Schematic diagram of SnowtexTM colloidal silica is shown in Figure 2.

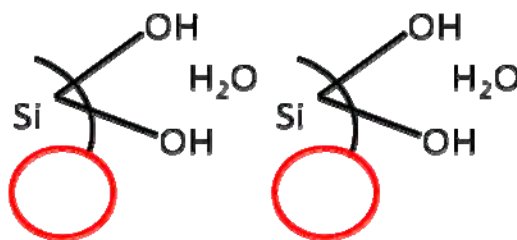


Figure 2. Schematic representation of Snowtex® colloidal silica.

Experimental

All reagents were used as received. The organosilanes were received from Gelest Inc. Propylene glycol monomethyl ether acetate (PMA), isopropyl alcohol, and tetrabutyl ammonium fluoride (TBAF) were purchased from Sigma Aldrich. Chromium (III) *tris*-acetylacetonate ($\text{Cr}(\text{acac})_3$) and deuterated acetone were obtained from Alfa Aesar. Snowtex-O colloidal silica used in the research effort was a

product of Nissan Chemical. According to the manufacturer's specification, the nanoparticles were 10-20 nm in size with a silica content of 20% by weight.

Sol mixtures for stability studies were synthesized on a combinatorial/high throughput formulations station developed by Symyx® Discovery Tools and shown in Figure 3. In the first step, colloidal silica was dispensed into 8 mL scintillation vials by a liquid robot using disposable pipette tips and magnetic stirring. It was then diluted by IPA followed by quick addition of a trifunctional silane at room temperature. During this step, hydrolysis of trifunctional silanes took place and, possibly, some initial siloxane bond started to form. The reaction temperature was then raised to 100°C to further drive the condensation reaction. The three organofunctional silanes selected for investigation are shown in Figure 4. They are phenethyltrimethoxysilane (PhETMS), 3-glycidoxypopyl-trimethoxysilane (GPTMS), and 2-(3,4-epoxycyclohexyl)ethyltrimethoxysilane (EchETMS).

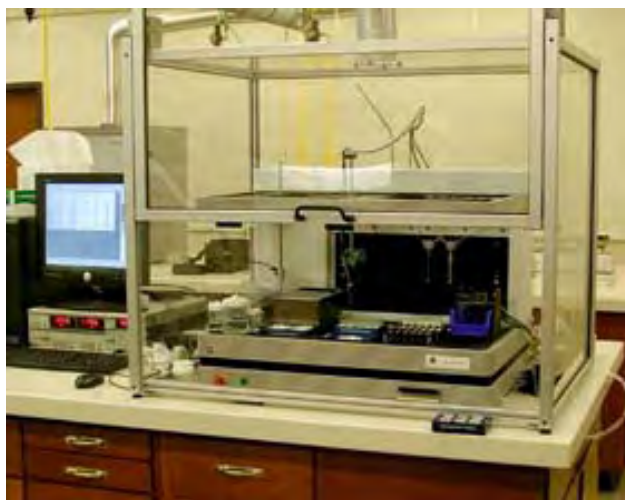


Figure 3. Symyx® coating formulation system – liquid handling robot.

Oxidation of Mg by water reduces the effectiveness of the primer, and the reduction of hydrogen creates a hazard during primer formulation. For the HOI binder solutions based on nanophased silica to be used for Mg-rich primers, an additional step was involved after sol-gel reactions were completed in solution and before film application. In this step, the mixture of the reacted silica and a trifunctional silane was diluted by PMA. The amount of PMA added was based on 1.75 times the total mass of silica (Snowtex-O) and silane. Dilution with a higher boiling solvent enables evaporation of the IPA/water azeotrope from the mixture. The removal of water promotes further condensation of silica and the silane and prepares the HOI binder for the addition of Mg pigment. Solvents were removed from the mixtures in the Genevac EZ-2 Personal Evaporator.

After removal of water and solvent, binder compositions were screened by visually inspecting the solution stability. Sols with homogeneous solutions or stable colloids were carried forward to film application. Films from the most promising candidates were cast in multiwell stamped aluminum panels on a Symyx® coating application station. Film formation characteristics were studied visually, and binder compositions that produced tack-free, crack-free films upon ambient cure were further investigated for use as Mg-rich binders.

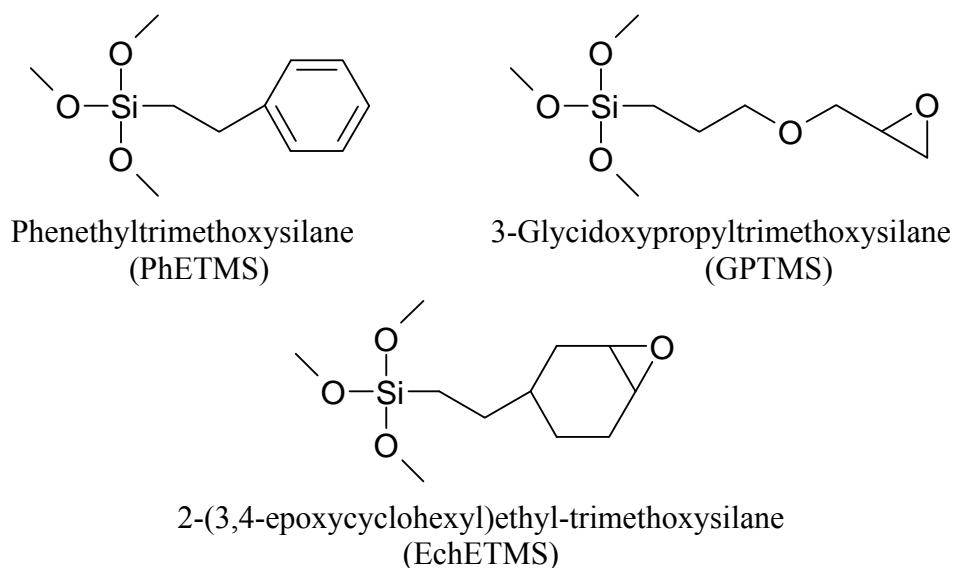


Figure 4. Trifunctional silicon alkoxides.

The HOI binders for Mg-rich primers were scaled up to 50 mL and synthesized in a Radleys Carousel 6 reaction station. Silicon NMR (^{29}Si) spectra were collected on a JEOL ECA-400 NMR spectrometer operating at 79.43 MHz for ^{29}Si . Acquisition parameters were typically a 62.5 kHz sweep width with an offset of 0 ppm, a relaxation delay of 5 seconds and an acquisition time of 0.262 s. Under these conditions, 14,000 scans were collected at an average temperature of 21.4°C. Solvent was acetone- d_6 with added chromium (III) *tris*-acetylacetonate ($\text{Cr}(\text{acac})_3$) to a concentration of 0.25 M. $\text{Cr}(\text{acac})_3$ was used to allow for complete relaxation time recovery and quantitative spectra.

Mg-rich primer was prepared by mixing HOI binder and Ecka-Granules magnesium powder UF 20 Ultracoat, based on the target dry film volume fraction of Mg and binder of 60%. Aluminum panels were cleaned before coating using a four-step procedure described by Farrier and Szaruga.⁷ Mg-rich primer and Deft MIL-PRF85285D polyurethane topcoat were applied by spray using a DeVilbiss HVLP spray gun at an air pressure of 40 psi. The coatings were air dried at ambient temperature.

Electrochemical Impedance Spectroscopy (EIS) was collected on a Gamry PCI4-300 potentiostat coupled with Corrosion Measurement System CMS100 and CMS300 software. Detailed description of this electrochemical technique can be found elsewhere.^{8,9} Coatings were immersed in dilute Harrison's solution (0.35 wt% $(\text{NH}_4)_2\text{SO}_4$ and 0.05 wt% NaCl, pH=5.5) 30 minutes prior to the test. A removable glass cylinder (1" ID) was attached to the panel using a metal clamp and a rubber o-ring. A platinum mesh counter electrode and saturated calomel reference electrode (SCE) were utilized in a three-electrode configuration. The spectra were obtained in the frequency range from 10 mHz to 100 kHz at 5 mV imposed *ac* potential (vs. E_{oc}).

For full coating systems (primer + topcoat), standard criteria were used for evaluation of EIS results.¹⁰ Impedance values of above $1 \cdot 10^9 \Omega\text{cm}^2$ are indicative of coating systems affording excellent barrier protection. Coatings with modulus values below $1 \cdot 10^6 \Omega\text{cm}^2$ are considered poor, and $|Z|$ values between $1 \cdot 10^6$ and $1 \cdot 10^9 \Omega\text{cm}^2$ indicate a good coating.

Results & Discussion

Initial step in selecting binder compositions for use in Mg-rich primers involved four variables shown in the diagram in Figure 5. Three trifunctional methyl silicates (Variable 1) were reacted with colloidal silica at three different silane/silica ratios (Variable 2). Each silane/silica composition was processed via the sol-gel method with or without catalyst (TBAF, Variable 3) and allowed to proceed for either 2 or 24 hrs (Variable 4). Figure 6 shows the experimental matrix for primary binder screening based on one organosilane. The diagram represents only one-third of the thirty-six sol compositions generated in this high throughput approach.

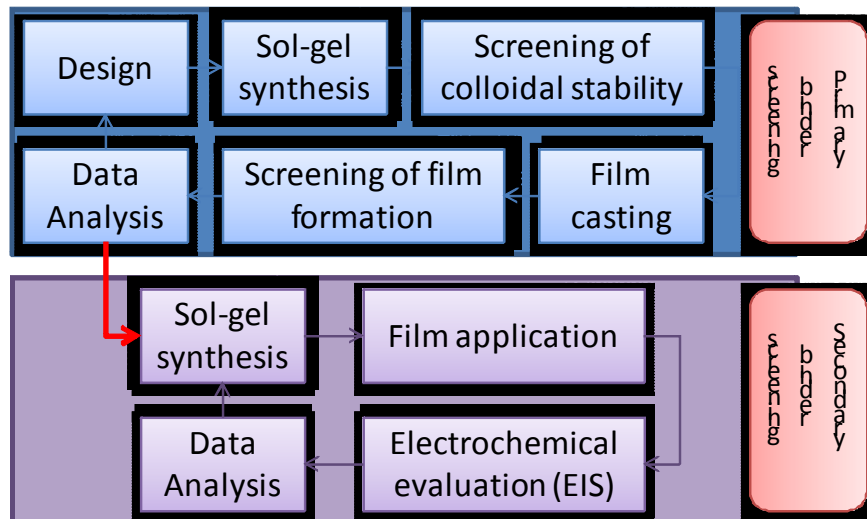


Figure 5. Combinatorial workflow for screening promising HOI binders for Mg-rich primers.

1	Organosilane: PhETMS, GPTMS, EchETMS											
2	0.00325 mol silane/grams silica				0.0065 mol silane/grams silica				0.013 mol silane/grams silica			
3	0 mol catalyst/grams silica		0.00003 mol catalyst/grams silica		0 mol catalyst/grams silica		0.00003 mol catalyst/grams silica		0 mol catalyst/grams silica		0.00003 mol catalyst/grams silica	
4	2 hrs	24 hrs	2 hrs	24 hrs	2 hrs	24 hrs	2 hrs	24 hrs	2 hrs	24 hrs	2 hrs	24 hrs

1 Variable 1 – organosilane
 2 Variable 2 – silane/silica ratio
 3 Variable 3 – amount of catalyst
 4 Variable 4 – reflux time

Figure 6. Experimental matrix for primary binder screening.

Initial screening results indicated that binder compositions containing PhETMS produced homogeneous and stable sols after evaporation and the resulting films were uniform and crack-free. These eight binder compositions were selected for secondary screening.

The second phase of binder optimization involved a scaled up experimental matrix shown in Figure 7. Because of the large amount of materials used in this step, only two silane/silica ratios were investigated. The alphanumeric codes given at the bottom of the diagram in Figure 7 will be used to identify film formulations based on the 4 variables: silane/silica ratio (Low and High), amount of catalyst (No catalyst and Catalyst: 30 μ mol/grams silica), and reflux time (2 hrs – 02, and 24 hrs – 24). The associated numeric codes are used for quick reference.

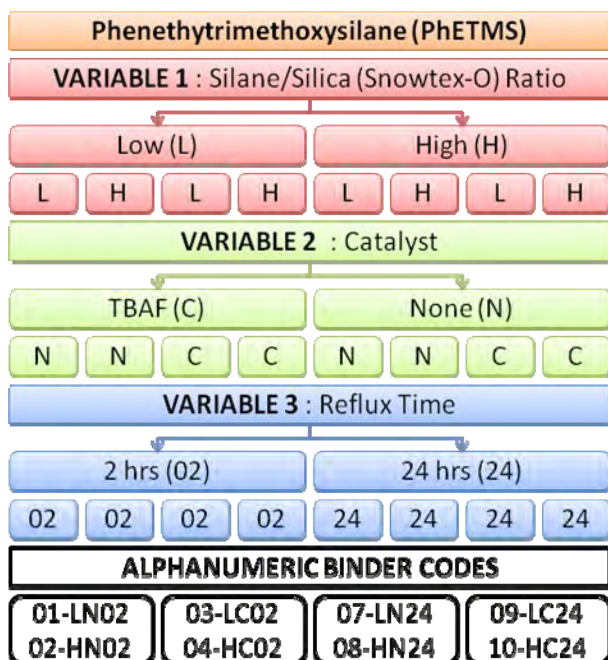


Figure 7. Experimental matrix for secondary binder screening.

All eight compositions produced stable, homogeneous sols after solvent removal. ^{29}Si NMR spectroscopy was used to estimate the extent of silanol condensation in solution during the functionalization process. Four groups of peaks can be observed for species derived from trifunctional organosilanes. These peaks are usually referred to as T peaks.¹¹ Species that have undergone 0, 1, 2, or 3 condensation reactions correspond to T_0 , T_1 , T_2 , and T_3 peaks, respectively. The chemical shifts associated with these peaks are typically in the range of -37 to -40 ppm for T_0 , -46 to -48 ppm for T_1 , -53 to -57 ppm for T_2 , and -37 to -39 ppm for T_3 .¹² A typical ^{29}Si NMR spectrum for colloidal silica functionalized with PhETMS and for unreacted PhETMS are displayed in Figure 8. ^{29}Si NMR spectra for all binder compositions show a broad peak at -95-120 ppm (Figure 8(b), right). This is the so-called Q region, and similar to the T peaks, the five Q_n peaks are associated with 0, 1, 2, 3, or 4 condensation reactions of a tetrafunctional silane. For colloidal silica, we observe a strong Q_4 peak at -110 ppm and a smaller peak at -100 associated with Q_3 . Therefore, as expected, colloidal silica particles represent a dense network of condensed siloxane bonds (Q_4) and some unreacted silanol groups (Q_3) on the exterior of the particles. The eight binder compositions produced ^{29}Si NMR spectra with almost identical Q regions due to the presence of colloidal silica.

For the purpose of this research, the T region is of particular interest to us. The ^{29}Si NMR spectra of PhETMS has a strong T_0 peak at -40 ppm indicative of the unreacted state of the silane. A smaller T_1 peak at -46 ppm and the absence of higher order peaks indicate that a small portion of the PhETMS molecules had undergone dimerization in the storage container or during NMR sample preparation.

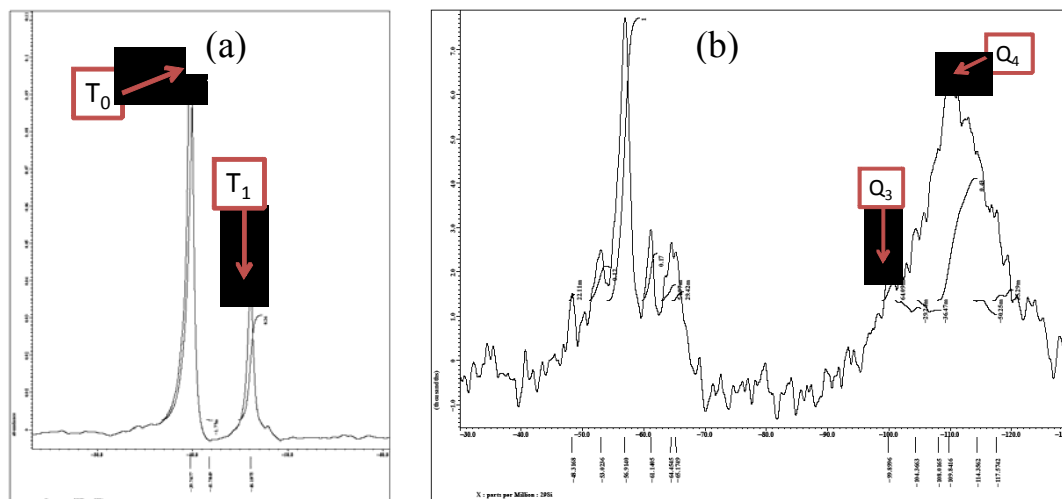


Figure 8. ^{29}Si NMR spectra of (a) phenethyl-TMS and (b) colloidal silica functionalized with phenethyl-TMS.

For the functionalized silica compositions, the T region consists of a large T_2 peak in the -54-57 ppm range, several much smaller peaks in the T_1 range, and medium to small T_3 peaks in the -60-64 ppm region (Figure 9). The absence of peaks in the T_0 region indicates that all PhETMS has entered the functionalization reaction with colloidal silica. The size of T_1 and T_3 peaks suggests that negligible amounts of PhETMS were expended in the dimerization reaction (T_1+T_1), some PhETMS reacted only once with colloidal silica (Q_3+T_1), and a measurable fraction of PhETMS formed siloxane bonds resulting in higher degree of condensation and possible formation of inorganic network (T_3). The chemical shifts and integration data for organically modified colloidal silica are listed in Table 1. The lack of peaks in the T_3 range for Binder 01-LN02 suggests that low concentration of silane and short reflux time without the benefit of the added catalyst result in the organosilane molecules primarily reacting with the silanols on the surface of colloidal silica particles.

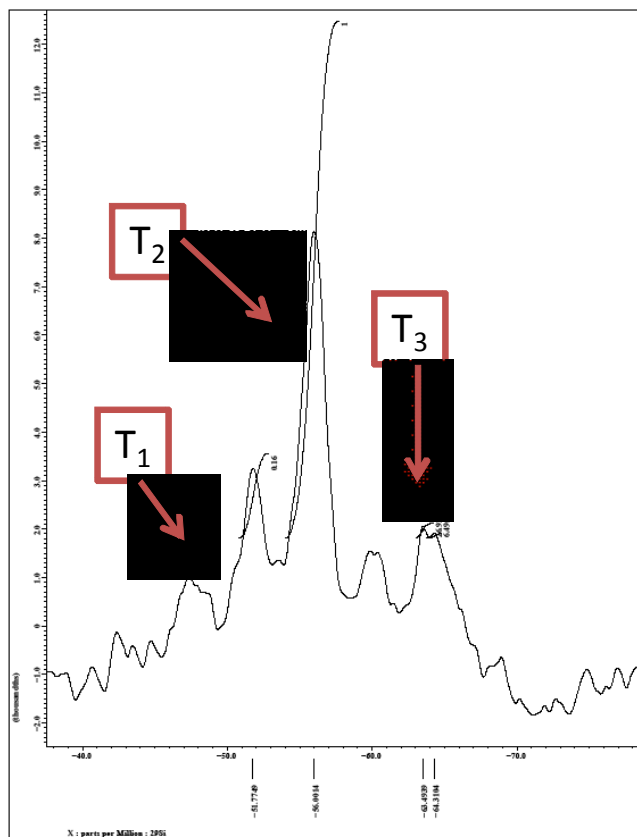


Figure 9. ^{29}Si NMR T region for colloidal silica functionalized with PhETMS.

Table 1. ^{29}Si NMR chemical shifts and peak ratios for colloidal silica functionalized with PhETMS.

Binder ID	Chemical Shift, ppm		T3/T2 peak ratio
	T2	T3	
01-LN02	-54.80		
02-HN02	-56.00	-60.28	3.3%
03-LC02	-55.85	-64.00	7.0%
04-HC02	-55.91	-64.00	7.5%
07-LN24	-56.00	-63.50	3.0%
08-HN24	-56.91	-61.14	17%
09-LC24	-59.96	-64.31	2.1%
10-HC24	-57.06	-61.19	12%

The addition of catalyst at low reflux times promotes condensation of the organosilane with colloidal silica, as evidenced by the higher T_3/T_2 peak ratio and the shift of T_3 peaks to the higher negative values. Overall, changing the reflux time and introducing catalyst in the reaction mixture does not seem to have a significant effect on T_2 (except for 09-LC24). This indicates that the organosilane-silica condensation is a relatively fast and reproducible process. Reactions involved in the formation of higher degrees of condensation, on the other hand, are highly dependent on the processing parameters. At longer reflux time without the catalyst, we observe that increasing the amount of the organosilane results in a higher ratio of species that have undergone three condensation reactions. However, with the addition of catalyst, at 24 hr reflux time Binder 09-LC24 appears to have decreased the formation of triply condensed species. This can be explained by the fact that compared to Binder 10-HC24, Binder 09-LC24 has a lower amount of trifunctional organosilane. In the case of Binder 09-LC24, the addition of catalyst and increased reaction time contribute to condensation reaction between colloidal silica particles and compete with the organosilane whose concentration is depleted in this case. The shift of T_2 and T_3 towards the highest values for this array of binders suggests that PhETMS is reacted with species with notably higher degree of condensation. Based on the analysis of the ^{29}Si NMR data, we could conclude that increasing the reaction time and the addition of catalyst promote further formation of inorganic network between organically modified colloidal silica particles. Moreover, Binder 09-LC24 is noted for the potentially highest degree of the inorganic network formation.

Electrochemical impedance spectroscopy (EIS) was initially performed on an uncoated Mg-rich primer 10-HC24 in order to compare its performance to the baseline electrochemical response of bare AA2024-T3. Figure 10 depicts the open circuit potential (E_{oc}) obtained from EIS and the low-frequency impedance modulus ($|Z_{lf}|$) for bare AA2024-T3 as a function of immersion time in dilute Harrison's solution. As expected, the E_{oc} exhibits an anodic shift with increased immersion time, while $|Z_{lf}|$ increases due to the formation of corrosion products on the surface of aluminum. The trend of increasing $|Z_{lf}|$ is observed in the case of Mg-rich primer based on Binder 10-HC24, shown in Figure 11, and is also due to the corrosion products giving rise to the overall impedance of the coated aluminum. However, the behavior of the E_{oc} follows a different trend. Upon immersion in corrosive electrolyte, Mg in the binder reacts with water and protects Al from corrosion by acting as a sacrificial anode. After 10 days of constant immersion, as the concentration of unreacted Mg in the being is being depleted, the E_{oc} approaches the value for bare Al. At the same time, corrosion products contribute to the increasing value of impedance modulus.

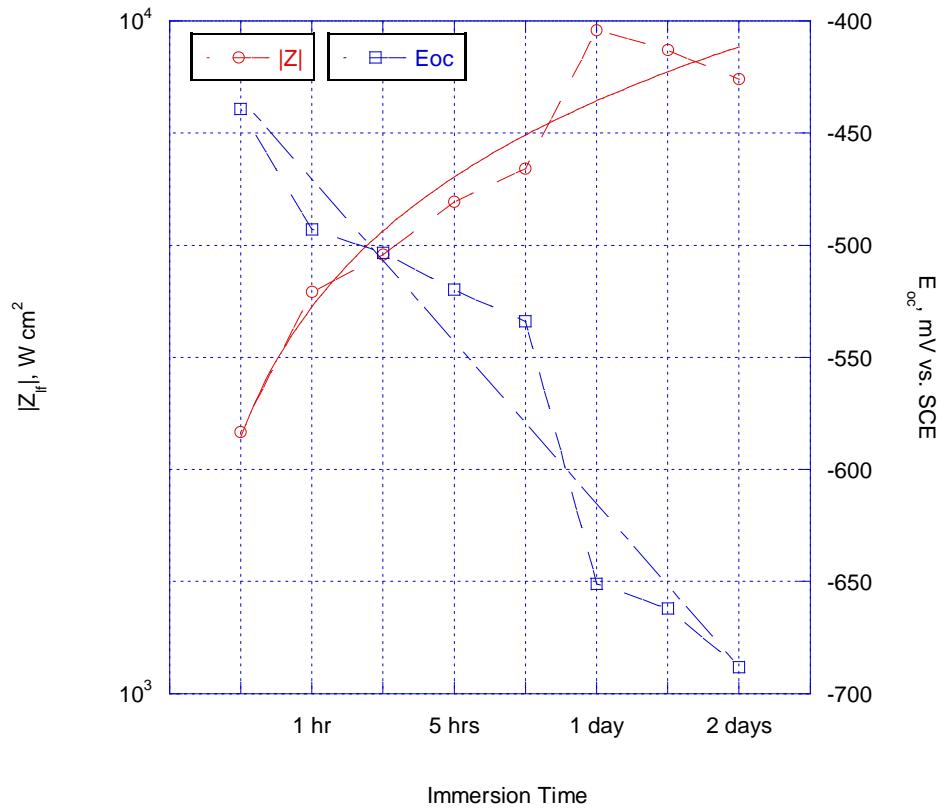


Figure 10. Open circuit potential and low-frequency impedance modulus for uncoated AA2024-T3 vs. immersion time.

In order to investigate the barrier properties of unpigmented HOI binders, constant immersion potentiostatic EIS was performed on all eight compositions. Figure 12 depicts the E_{oc} for the 8 binders as a function of time. As expected, the trends follow the “aluminum” pattern of decreasing E_{oc} upon increasing immersion time. However, the $|Z_{lf}|$ shown in Figure 13, decreases with time contrary to the behavior of the bare AA2024-T3. In a coated system, the current flowing through a small defect in the coating will significantly decrease the coating’s impedance. At the same time, due to the small size of the imperfection, not enough corrosion product is formed in the area of the defect to influence the overall impedance of the coated specimen. With time, as more and more defects are formed in the coating and as corrosion propagates over the entire surface exposed to electrolyte, the low-frequency impedance modulus of coated substrates will approach the value for the bare aluminum, which is what is observed in the case of HOI binders.

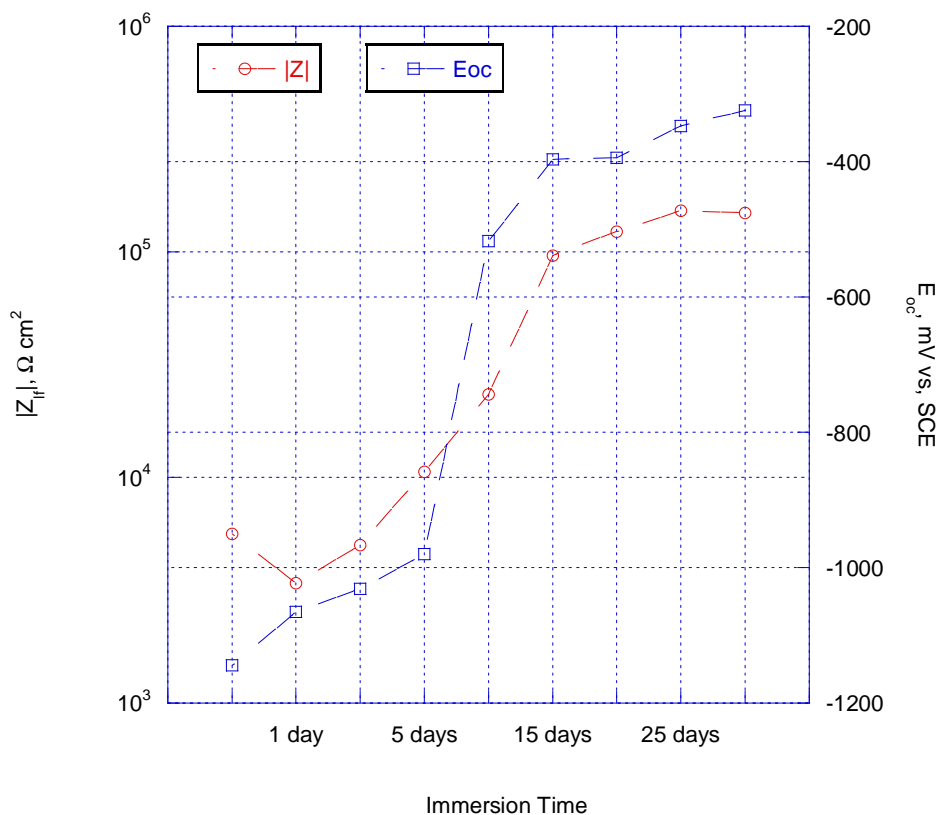


Figure 11. Open circuit potential and low-frequency impedance modulus for Mg-rich primer 10-HC24 (PVC60) vs. immersion time.

Binder 01-LN02 has the lowest initial $|Z|_{lf}$ and its open circuit potential approaches that for bare Al at the fastest rate. This finding is consistent with ^{29}Si NMR results, where Binder 01-LN02 possessed the lowest degree of condensation between colloidal silica particles. Based on the EIS results presented in Figures 11 and 12, the best performing unpigmented binders are 09-LC24 and 10-HC24.

In the next step, EIS was performed on full coating systems. Mg powder from Ecka-Granules was dispersed in Binders 09-LC24, 10-HC24, and 04-HC02 (for comparison purposes) and top-coated with Deft polyurethane topcoat. The open circuit potential and low-frequency impedance modulus for three full coating systems consisting of Mg-rich primer based on HOI binders and a polyurethane topcoat are shown in Figure 14. Here, the same alphanumeric sample IDs are used to denote full coatings systems based on a particular HOI binder.

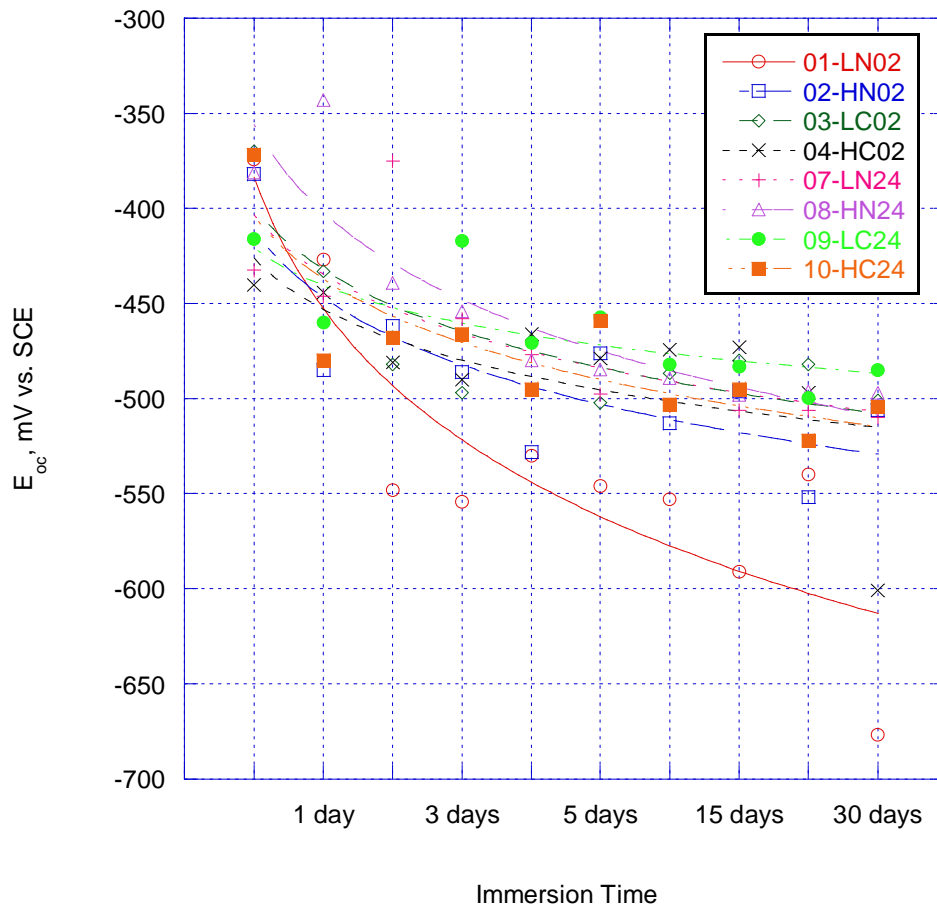


Figure 12. Open circuit potential for HOI binders vs. immersion time.

Due to time limitations at the time of writing, the immersion time in the case of binders 09-LC24 and 10-HC24 was reduced to 15 days (2 weeks), and in the case of 04-HC02 to 5 days. In the initial stage of immersion, Binder 09-LC24, due to its higher concentration of highly condensed silica exhibits a very high value of $|Z_{if}|$, on the order of $5 \times 10^8 \Omega \text{ cm}^2$. $|Z_{if}|$ of almost $1 \times 10^8 \Omega \text{ cm}^2$ is recorded for Binder 04-HC02. Binder 10-HC24 starts off with the $|Z_{if}|$ value slightly above $1 \times 10^7 \Omega \text{ cm}^2$. Upon further immersion, the impedance modulus values for Binders 04-HC02 and 09-LC24 decrease exponentially, while the value for Binder 10-HC24 remains almost constant.

The observed trend can also be detected in the case of the open circuit potential. Over the first 7 days of immersion, the E_{oc} for Binder 04-HC02 has been decreasing at an average rate of 30 mV/day, while the E_{oc} for Binder 09-LC24 has been dropping at a rate of almost 60 mV/day. At the same time, the E_{oc} for Binder 04-HC02 over the 5-day exposure has been decreasing at an average rate of only 15 mV/day. While Binder 04-HC02 may not have the highest initial value of impedance modulus and does not possess the most noble potential at the start of immersion test, it remains to see how these electrochemical parameters will be altered upon further exposure in dilute Harrison's solution.

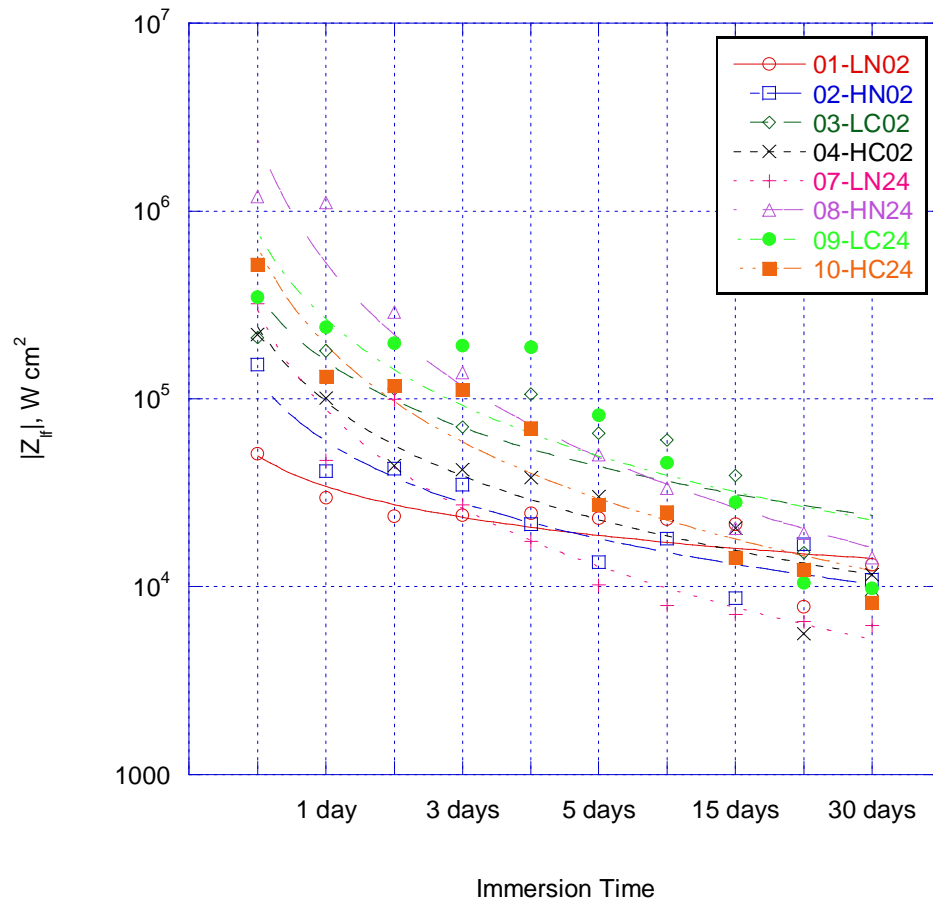


Figure 13. Low-frequency impedance modulus for HOI binders vs. immersion time.

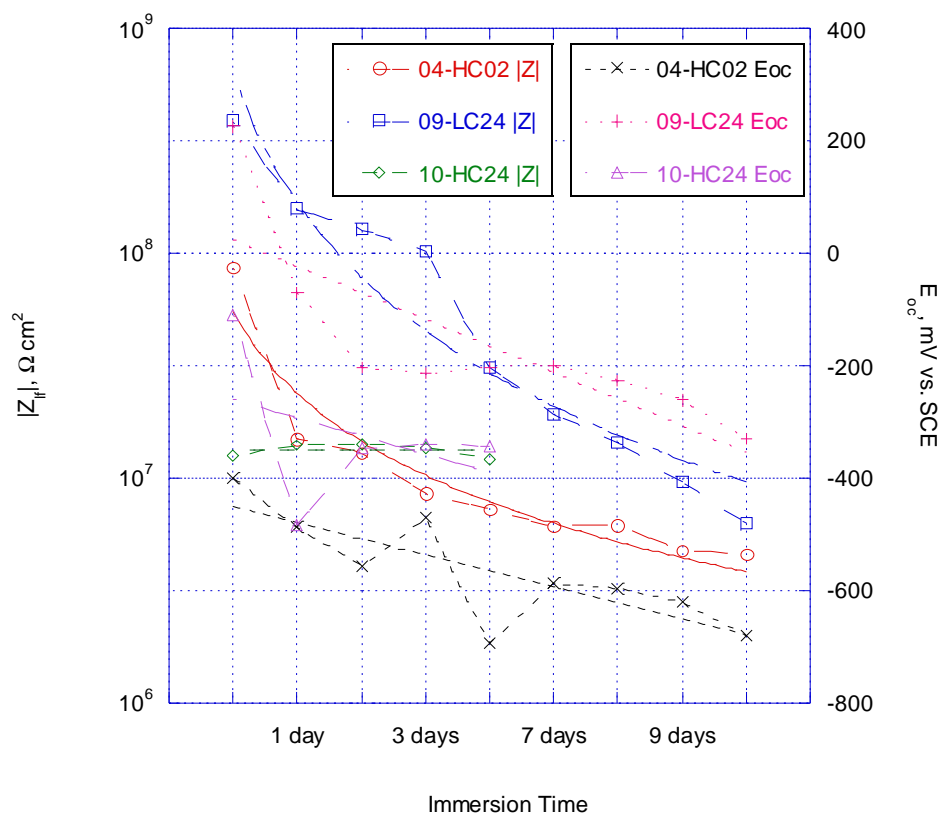


Figure 14. Open circuit potential and low-frequency impedance modulus for HOI binders + topcoat vs. immersion time.

Conclusions

Combinatorial/high throughput method was applied to the development of hybrid organic-inorganic binders for Mg-rich primers. The combinatorial workflow allowed rapid identification of 8 promising HOI compositions for binder formulations. ^{29}Si NMR of binder compositions and electrochemical impedance spectroscopy of unpigmented binder films immersed in dilute Harrison's solution for 1 month were utilized to further down select the remaining binder formulations for Mg-rich primer development. To date, only 10 days of constant immersion EIS have been completed on coated system based on Mg-rich primers and a polyurethane topcoat, and B117 corrosion salt spray test is currently underway.

Acknowledgment

The authors thank the Air Force Office of Scientific Research for funding through grants FA8650-04-1-5045 and RSC02050.

References

1. EPA Federal Register 12.4, 60, No. 170, 1995, 45947.
2. Nanna, M.E. and Bierwagen, G.P., *J. Coat. Technol. Res.*, 1, 2004, 69.
3. Battocchi, D., Simões, A.M., Tallman, D.E. and Bierwagen, G.P., *Corrosion Science* 48 (2006) 1292–1306.
4. Battocchi, D., Simões, A.M., Tallman, D.E. and Bierwagen, G.P. *Corrosion Science* 48 (2006) 2226–2240.
5. Brinker, C.J. and Scherer, G.W., *Sol Gel Science: The Physics and Chemistry of Sol-Gel Processing*, Academic Press, New York, NY, 1990.
6. Chisholm, Bret J.; Berry, Missy; Bahr, James; He, Jie; Li, Jun; Bonitz, Verena; Bierwagen, Gordon P., *The development of a combinatorial/high throughput workflow for hybrid organic-inorganic coating research*, *Polymer Preprints, ACS*, 48(1), 2007, 155-156.
7. Farrier, L. and Szaruga, S.L., *Mater. Charact.*, 55 (3) 2005, 179-189.
8. *Impedance Spectroscopy*, MacDonald, J.R., ed., Wiley-Interscience: New York, NY, p. 260-308, 1987.
9. *Principles and Prevention of Corrosion*, Jones, D.A., ed.; Macmillan Publ. Comp.: New York, NY, p. 122, 161, 1992.
10. Bacon, R.C., Smith, J.J., and Rugg, F.M., *Ind. Eng. Chem.*, 40, 1948, p. 161.
11. Chisholm, B. and Resue, J., *Paint and Coat. Ind.*, June 2003, 42-52.
12. Babonneau, F., Thorne, K. and Mckenzie, J.D., *Chem. Mater.*, 1 (5) 1989, 554.

The Use of Mg Alloys as Pigments in Mg-rich Primers For Protecting Al Alloys

Hong Xu¹ and Dante Battocchi^{1,2} and Gordon Bierwagen^{1,2}

¹*Coatings and Polymeric Materials Department*

²*Center for Surface Protection*

North Dakota State University

1735 NDSU Research Park drive, Fargo ND 58102

Abstract:

As an alternative to toxic Chromate coating, Mg-rich primer was designed to protect Al alloys (in particular Al 2024 T3) and developed in analogy to Zn-rich primers for steel substrate. The Mg pigments present in the primer can provide cathodic protection to Al substrate and show the promise to keep Al alloy away from corrosion when damage occurs¹.

In order to determine how much the pigment composition can be varied without scarifying corrosion protection, three different primers based on magnesium alloy powders as pigments were formulated with an epoxy-polyamide polymer binder at different PVCs. Their behaviours were studied after cyclic exposure in Prohesion Chamber via electrochemical methods.

Testing results from Electrochemical Impedance Spectroscopy (EIS) and Scanning Electron Microscopy (SEM) showed that the metal-rich primers with Mg alloys as pigments could provide certain cathodic protection, and the precipitate of Mg oxides/hydroxides from their oxidation might introduce some barrier protection. Furthermore, the investigation of the properties of the three alloy pigments gave a good understanding of the effects of particle shape, particle size, particle size distribution and chemical composition.

Introduction:

Aluminum alloys, especially AA2024 T3, are widely used in aerospace industry, because of their high strength and stiffness combined with low density. Although Al alloys are very sensitive to corrosion environments, Chromate coatings can increase their corrosion resistance². However, with increasing environmental concerns, toxic Chromate coatings need to be replaced from coating systems and stringent regulations are due to be enforced by the governments.

In analogy to the Zinc-rich primer coatings to keep steel from corrosion through cathodic protection, the Mg-rich primer coatings were designed, examined and developed by M.E.Nanna, D.Battocchi and G.Bierwagen at NDSU³⁻⁶. By using pure magnesium pigment, Mg-rich primers were formulated around the Critical Pigment Volume Concentration (CPVC). The AA2024 T3 panels coated by Mg-rich primer combined with topcoat passed 5000 hours of exposure in Prohesion cycle. It was proved that Mg-rich primer could provide good cathodic protection to AA 2024 T3 when damage occurred^{1, 7, 8}.

In this work, we want to evaluate how much we can vary the pigment composition from pure magnesium, as well as the effects of particle size and particle shape on the properties of the primer without losing the protective behaviours. Three different primers were formulated by using different magnesium alloys grains, AM60, AZ91B and LNR91 as the pigments in an epoxy-polyamide polymer matrix at different PVCs.

For these Magnesium alloy rich primers, an epoxy-polyamide organic coating system was used as the polymer binder, because it can provide good adhesion between primer and substrate, as well as certain barrier property and it has been used in Zn-rich primer for a number of years. The primers were formulated around CPVC in order to have good electrical conductivity within pigments and between pigments and metal substrate. Methanol ethanol ketone was used as solvent to give appropriate viscosity for spray application.

The particle size and Particle Size Distribution (PSD) of magnesium alloy pigments were measured by PSS.NICOMP Particle sizing system, and acetone was used as carrier. The shapes of pigments were investigated by Scanning Electron Microscopy (SEM) image.

Theoretical CPVCs were calculated from the Oil absorption and pigment density; experimental CPVCs

of magnesium alloy rich primers were determined by the method of Impedance at low frequency changing with pigment volume concentration (PVC). With increasing PVCs of coatings, the impedance of coatings decrease because of less polymer binder filling the pores existed in coatings and therefore lower barrier properties.

The electrochemical properties of the panels coated with different magnesium alloy primers (with and without topcoat) were tested by Electrochemical Impedance Spectroscopy (EIS), Electrochemical Noise Methods (ENM) during cyclic exposure in Prohesion Chamber; the surface roughness change with exposure time were evaluated by SEM; the composition of pigments in coating change with exposure time were measured by Energy Dispersive X-ray Spectroscopy (EDS).

Experimental procedure:

Measurements of Mg alloy pigments:

Particle size and PSD of pigments were measured by using Accusizer 780 optical particle sizer, which is a single particle optical sensing (SPOS) method. The magnesium alloy particle suspended by acetone passed through a “photozone” one by one, and the signal of detected pulse, which is related to the mean diameter of the particle, was recorded while pigment obscured a certain area in photozone. The particle size distribution was obtained by comparing the single signal strength with a standard calibration curve.

Oil absorption of pigments was tested according to ASTM D281 by using Spatula Rub-Out method. Linseed oil was added into certain quantity pigments drop by drop, pigments and Linseed oil were mixed thoroughly with the spatula. When the spatula could hold all pigments together, the end point was reached. Oil absorption was expressed as gram of oil per 100 gram of pigments.

The whole processes of experiments are presented in Figure 1.

Aluminum alloy panels’ pre-treatment and application of primers:

All the AA2024 T3 panels supplied by Q Panel Lab products (Cleveland OH) were polished by 220 grit and 600 grit sand paper to remove the oxide layer and finally rinsed by hexane. Magnesium alloy primer paints were formulated at different PVC and applied on the panel surfaces by air spray. Primer coatings were cured at

room temperature for two days and the thickness of dry primers was around 150 μm .

ENM measurement setup:

Two separate identical testing panels were clamped to glass cells with a 7.06 cm^2 exposure area, and both worked as working electrodes. A Saturated Calomel Reference Electrode (SCE) was in one cell body while the two cells were connected through a salt bridge. Dilute Harrison's Solution (DHS), which is an aqueous solution containing 0.35 % (wt) ammonium sulphate and 0.05% (wt) sodium chloride, was used as the electrolyte. All the ENM data were collected by using Gamry PCL4-300 with software of ZRA Mode Electrochemical Noise.

EIS measurement setup:

A testing panel was clamped to a glass cell with a 7.06 cm^2 exposure area and worked as the working electrode; a SCE was the Reference electrode; a Pt mesh worked as the counter Electrode; DHS was the electrolyte. All the EIS data were collected through frequency range from 10^5 Hz to 0.01Hz by using Gamry PCL4-300 in potentiostatic mode.

Results and discussions:

Properties of Magnesium alloy pigments:

The data of particle size, PSD, oil absorption, density and chemical composition for the three magnesium alloy pigments, AM60, AZ91B and LNR91 are listed in table 1.

We can see that the three magnesium alloy pigments have large particle size (above 60 μm); also they showed different shapes: AM60 has plate-like shape with smooth edge, AZ91B is chip-like shape and LNR91 has cubic-like shape with sharp edge. The oil absorption of LNR91 is the lowest, which indicates LNR91 pigments have smaller surface area or smoother surface. Although the mean particle size of LNR91 is smaller comparison with the other two pigments, its PSD exhibited much broader range. Furthermore, LNR91 has the highest Al composition within the three.

CPVC of magnesium alloy primers:

The theoretical CPVC for the three primers were calculated from the Oil absorption and pigment

density by using equation 1

$$CPVC = \frac{1}{1 + \frac{(OA)(\rho)}{93.5}} \quad (\text{Equation 1})$$

OA = oil absorption (gram of linseed oil / 100 gram of pigment)

ρ = density of Mg alloys

The theoretical CPVC of the three magnesium alloy pigments are listed on table 2.

The experimental CPVCs of magnesium alloy rich primers were determined by the method of Impedance at low frequency change with pigment volume concentration. With the increasing PVC of coating, the impedance of coating decreases, because there is less polymeric binder to fill the voids between pigment particles, therefore, a more porous coating. The plots of impedance at 0.01Hz change with PVC are shown in Figure 2. And the ranges of CPVCs of three different Mg alloy primers are listed on table 2.

It can be seen that the experimental CPVC are much lower than theoretical CPVC. A possible reason may relate to the pigment packing. First, all particle sizes of the three magnesium pigments are above 60 micron, and the thickness of primer coating films were around 150 micron. Thus, in comparison with the thickness of coating film, the sizes of all the three magnesium pigments were too big to obtain good packing efficiency. Second, from the SEM image of pigments, we can see that the shape of pigment particle and particle size are not well controlled, these may affect the pigments packing. Furthermore, problems in application processes, such as unsatisfied paint viscosity or non uniform film thickness, also can result in pigment packing issues.

Open Circuit Potentials (OCPs) change with exposure time (Mg alloy primers coated panels without topcoat):

Figure 3 shows the OCP plots of Mg alloy primer coated Al 2024 T3 panels (without topcoat) changing with exposure time. It can be seen that, the OCP of panels were increasing with exposure time, however, the measured OCP is located in a certain potential range being higher than OCP of pure Mg (about -1.60 V) and lower than that of bare AA2024 T3 substrate (-0.65V). Such mixed potential range indicated that Mg alloy pigments

could provide cathodic protection to Al alloy substrate.² Furthermore, at 0 hour exposure time, all the Mg alloy primer coated panels with different PVC had low OCP, between -1.50 V and -1.20 V, due to the high content of Mg in fresh primer films. With the increasing exposure time, the OCP increased indicating the consumption of the active pigments. When OCP of the panels reached to the OCP of the bare substrate, the primers no longer gave sacrificial protection to the Al alloy substrate, though still provided barrier protection through the corrosion products.¹

From the plots of OCP change with exposure time, it can be seen that all the three Mg alloy primers showed to provide cathodic protection to Al substrates. Among them, the OCP of AM60 primer coated panels exhibited the lowest increasing rate and was kept in low OCP range for longest time. It might be due to its highest Mg content and plate shape of pigments.

In addition, the OCP change also reflected the effects of PVC on primers. For LNR91 primer coated panels, the OCP of the lowest PVC (35%) primer increased much slowly; in contrast, the OCP of the highest PVC (50%) primer reached to -0.65V very fast. It might be due to the less barrier protection provided by polymer binder when PVC was higher than CPVC, and the electrolyte could easily penetrate into coating film and speeded up the corrosion of Mg pigments.

Mg alloy primers coated panels with topcoat (OCPs change with exposure time):

When the panels coated with Mg alloy primers were covered by a layer topcoat, the trends of OCPs change were very similar to ones without topcoat. At 0 hour exposure, the OCPs were very low; with the growing exposure time, the OCPs were slowly increasing.

However, for topcoated panels, the effects of PVC on OCP change were in contrast with the panels without topcoat. In Figure 6, it can be seen that the panels with higher PVC, such as AM60 at PVC 34% and AZ91B at PVC 38%, had lower OCPs combined with slower increase rates than AM60 at PVC 31% and AZ91B at PVC 36%, respectively. It might be due to that, the topcoat provided the barrier protection for the high porous primers and reduced the consumption of Mg pigments.

Mg alloy primers coated panels without topcoat (Impedances at 0.01Hz change with exposure time):

In EIS data, the impedance at low frequency is relative to the sum of Polarization Resistance (R_p), Pore Resistance (R_{pore}) and Solution Resistance (R_s).⁹ The plots of impedance at 0.01Hz for the panels coated with Mg alloy primers changing with exposure time were shown in Figure 4. We can see that, with exposure time increasing, the impedance at low frequency slowly decreased. It may due to the decrease of Pore Resistance and Polarization Resistance (Solution Resistance is normally very low and can be ignored comprising of R_p or R_{pore}). When the electrolytes penetrated the coating films through porous paths to reach the interface of coating and substrate, the value of Pore Resistance became smaller; in addition, with the existing electrolyte and electrochemical active species, the under-film corrosion was initiated and caused the decrease of Polarization Resistance.

Sometimes, an increase of impedance increased can be observed, especially during the first 24 hours. There are two possible reasons for this sharp increases at low frequency: the continuous curing of coating increased the T_g of system; the other is the formation of $\text{Mg}(\text{OH})_2$ or MgO precipitate improved the barrier protection. When Mg alloy primers were exposed to DHS solution, the Mg pigments on the top layer reacted with the electrolyte first and the less soluble corrosion products might fill the pores present in the film and increased the Pore Resistance. The Mg precipitates were observed by SEM (Figure 5), though the actual chemical composition of the precipitates still need more evidences to be confirmed. Thus, because of the low solubility of Mg precipitate, Mg alloy primer can provide certain barrier protection.

Again, from the plots of impedance at low frequency change with exposure time, we can see the dissimilar barrier protection of the three different Mg alloy primers. AM60 primer coated panels had the highest impedance, which may be a sign of AM60 primer having better barrier protection and LNR91 primer having poor barrier properties.

Mg alloy primers coated panels with topcoat (Impedances at 0.01Hz change with exposure time):

In Figure 7, when the Mg alloy primers coated panels were covered with a layer of topcoat, the impedances at low frequency increased by one order of magnitude, as expected because the topcoat can strengthen the

barrier protection. Furthermore, the change of impedances of topcoated panels with exposure time were much tender than ones without topcoat, the sharp increase of impedance in Figure 4 were no longer observed in Figure 7. It may be because topcoat contributed large scale impedance to coating systems and the little increase of Pore Resistance caused by Mg precipitates showed little effects.

Conclusions:

Similar to pure Magnesium pigment, Magnesium alloy pigments formulated in primer coatings could provide certain cathodic protection for Al alloys. EIS results showed that the metal-rich primers with the Mg alloys as pigments had mixed potentials between Mg alloys' and bare Al 2024 T3, which indicated Mg alloy pigment gave sacrificial protection to Al alloy substrates; the changes of impedances at low frequency with exposure time indicated that Mg oxides/hydroxides precipitates from their oxidation might contribute some barrier protection. Scanning Electron Microscopy (SEM) showed the existence of Mg precipitates. Furthermore, the investigation of the properties of the three alloys gave a good understanding of the effects of particle size, particle shape and chemical composition on particle packing in coating films, CPVC and electrochemical behaviours, which suggested that pigments with smaller particle size and better controlled shape would result in better primer systems.

References:

1. Battocchi, D.; Simoes, A. M.; Tallman, D. E.; Bierwagen, G. P., *Corrosion Science* **2006**, 48, 1292-1306.
2. Knudsen, O. O.; Steinsmo, U.; Bjordal, M., *Progress in Organic Coatings* **2005**, 54, 224-229.
3. Nanna, M. E.; Bierwagen, G. P., *JCT Research* **2004**, 1, 69-80.
4. Bierwagen, G. P.; Nanna, M. E.; Battocchi, D. Magnesium rich coatings and coating systems. 2004-US33089, 2005051551, 20041007., 2005.
5. Bierwagen, G.; Tallman, D.; Nanna, M.; Battocchi, D.; Stamness, A.; Gelling, V. J., *Polymer Preprints (American Chemical Society, Division of Polymer Chemistry)* **2004**, 45, 144-145.
6. Bierwagen, G.; Battocchi, D.; Simoes, A.; Stamness, A.; Tallman, D., *Progress in Organic Coatings* **2007**, 59, 172-178.
7. Battocchi, D.; Simoes, A. M.; Tallman, D. E.; Bierwagen, G. P., *Corrosion Science* **2006**, 48, 2226-2240.
8. Simoes, A. M.; Battocchi, D.; Tallman, D. E.; Bierwagen, G. P., *Corrosion Science* **2007**, 49, 3838-3849.
9. Loveday, D.; Peterson, P.; Rodgers, B., *JCT Coatings Tech* **2004**, October, 88-93.

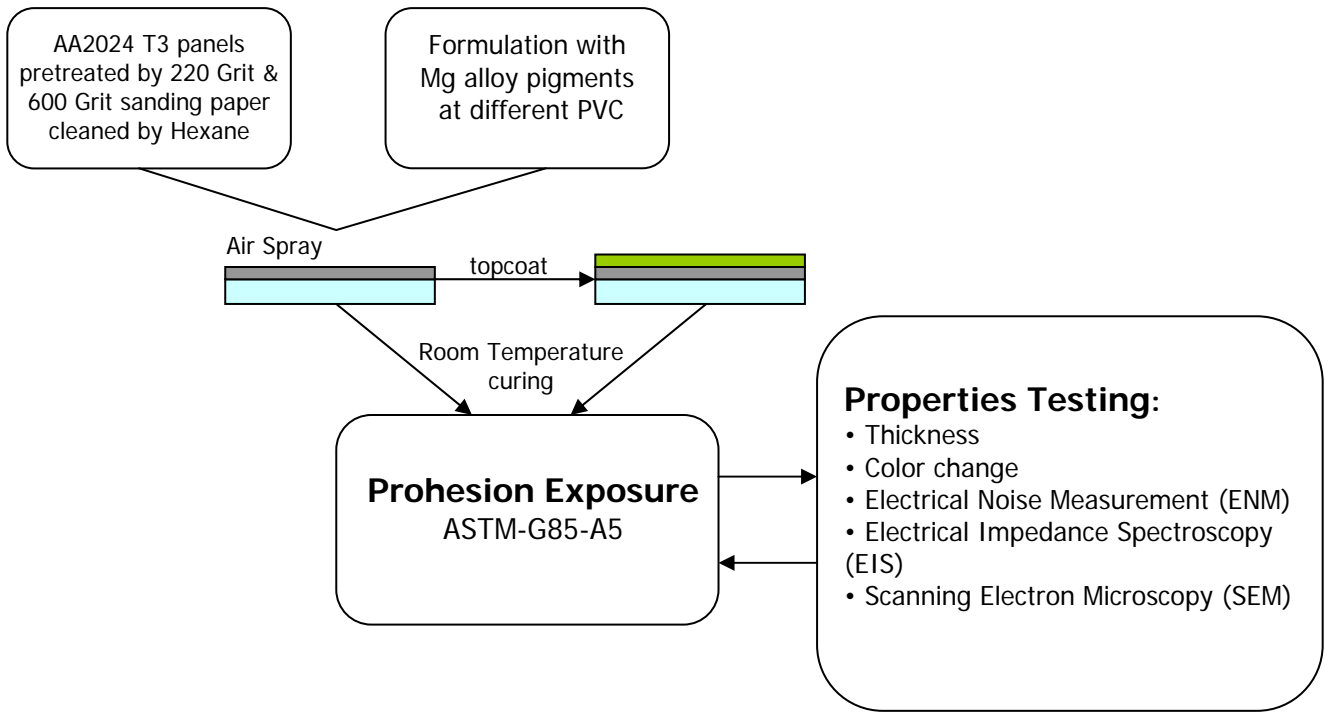


Figure1. Flow of Experiments

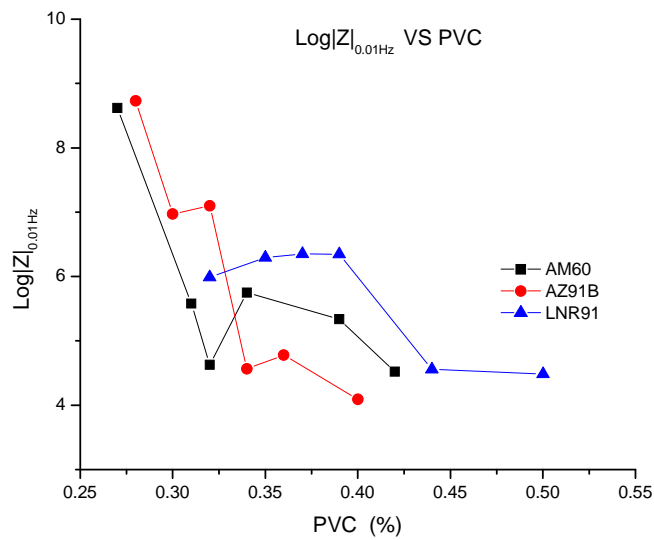


Figure 2. Impedances at 0.01Hz change with PVC of primers

Table 1: Properties of three magnesium alloy pigments

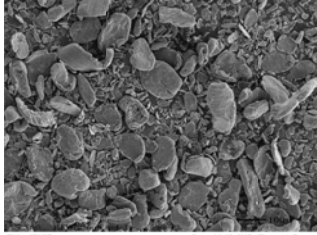
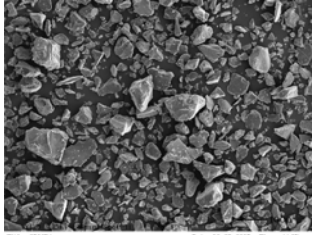
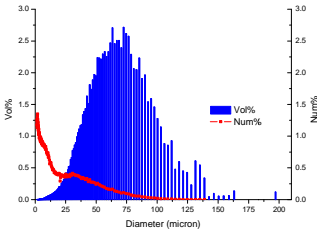
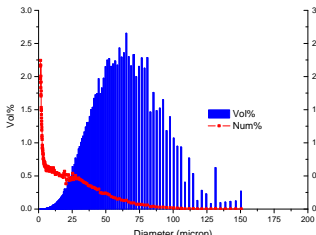
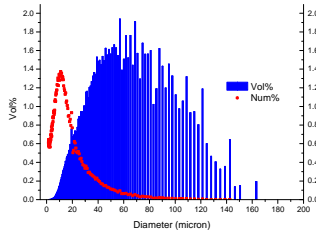
Mg Alloy Pigment	AM60		AZ91B		LNR91	
Particle Shape (SEM)						
Composition (wt%)	Al 5%, Mg 95%		Al 9.5%, Mg 90.5%		Al 50%, Mg 50%	
Oil absorption	61.53 g/100g pigment		68.30 g/100g pigment		33.45 g/100g pigment	
Density (g/cm ³)	1.80		1.81		2.22	
Particle Size Plot						
Particle Size	By Vol. (μm)	By Num. (μm)	By Vol. (μm)	By Num. (μm)	By Vol. (μm)	By Num. (μm)
Mean Diameter	63.00	10.66	58.96	10.36	56.21	11.23
Mode Diameter	63.46	1.95	74.61	1.66	87.72	11.59
Median Diameter	60.12	5.02	55.45	4.16	49.78	8.39

Table 2: Theoretic and experimental CPVCs of three Mg alloy pigments.

Mg Alloy Pigment	AM 60	AZ91B	LNR91
Theoretic CPVC	46%	43%	56%
Experimental CPVC	31%< CPVC <34%	31%<CPVC<34%	39%<CPVC < 44%

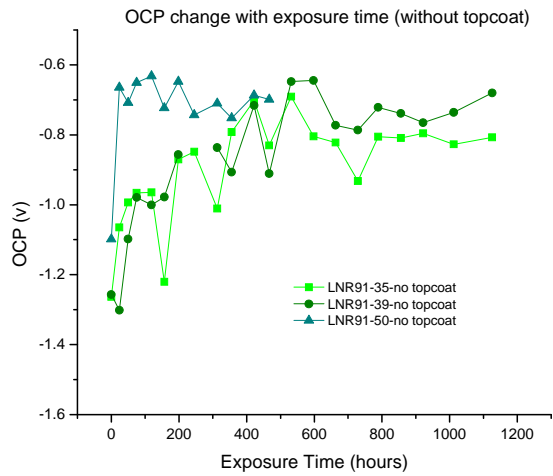
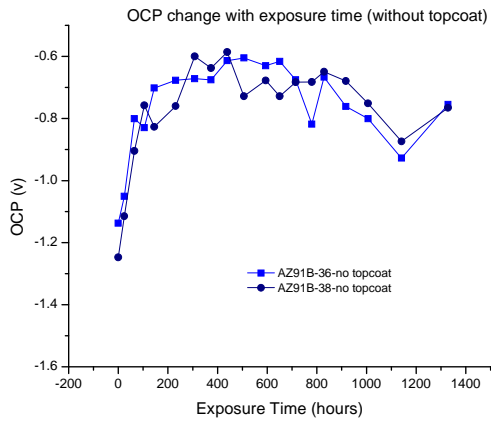
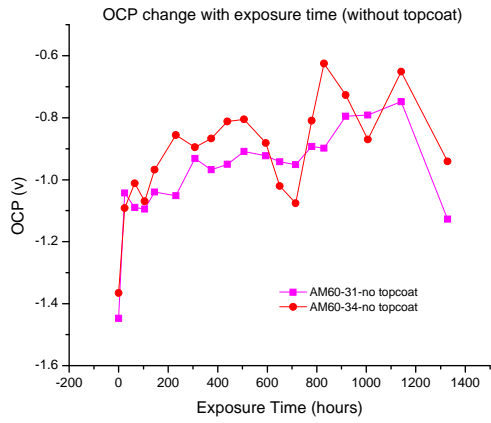


Figure 3: OCP of Mg alloy primers coated panels (without topcoat) change with exposure time

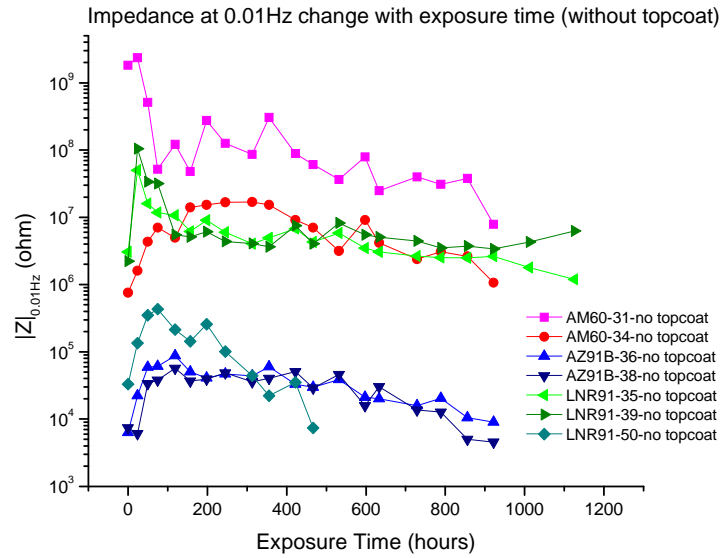


Figure 4: Impedances at low frequency of Mg alloy primers coated panels (without topcoat) change with exposure time

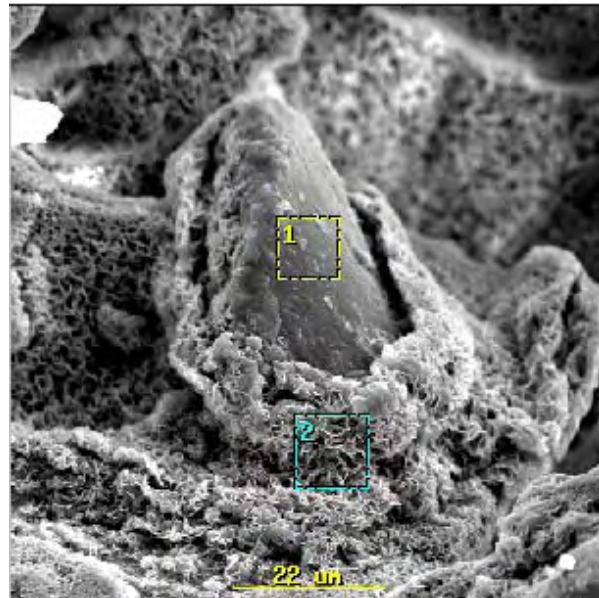


Figure 5: SEM surface image of AM60 primer coated panel (PVC = 34%, exposure time 715 hours)
Area 1) Mg alloy pigment; Area 2) Structure of Mg precipitate

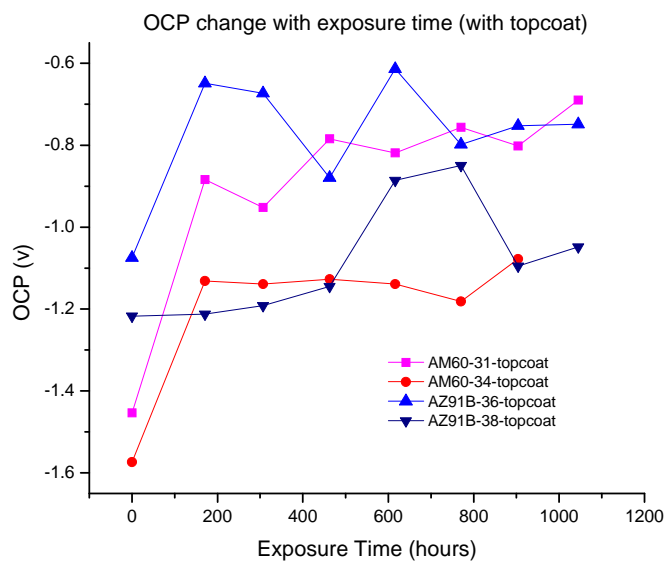


Figure 6: OCPs of Mg alloy primer coated panels (with topcoat) change with exposure time

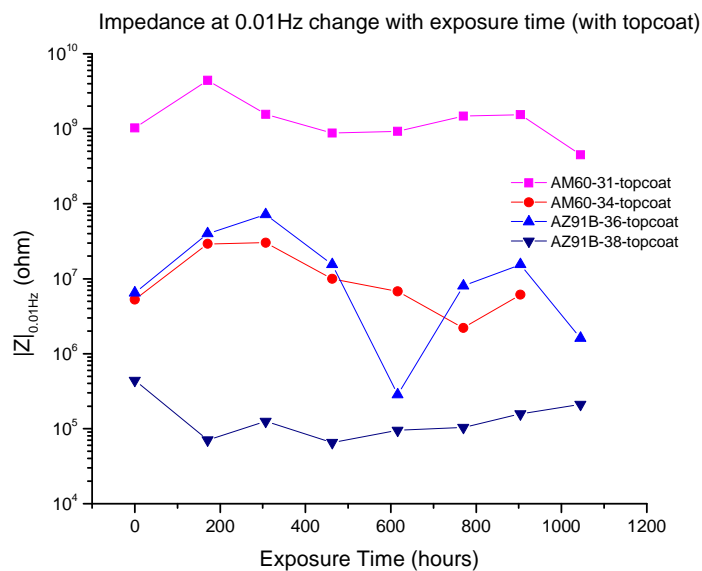


Figure 7: Impedances at 0.01Hz of Mg alloy primer coated panels (with topcoat) change with exposure time

Development of a High-Throughput Combinatorial Electrochemical Impedance Spectroscopy for Evaluating Corrosion Protective Coatings

Jie He, James Bahr, Jun Li, Bret Chisholm, Zhigang Chen, Séva Balbyshev, Missy Stafslie, Bret Mayo, Verena. Bonitz, and Gordon Bierwagen

Abstract

The objective of the present study is to develop a combinatorial high-throughput electrochemical impedance spectroscopy (HT-EIS) method for rapid and quantitative evaluation of corrosion protective coatings on metallic substrates. A 12-well (4 × 3 arrays) spatially addressable electrochemical platform was designed, fabricated, and validated. This platform was interfaced to a commercial EIS instrument through an automatic electronic switching unit. Using this setup, four parallel tests can be run simultaneously. The geometry of the cell configuration also allows 4 coating compositions to be measured in triplicate within a short time (typically 45 minutes). The performance of the electrochemical apparatus was validated by a Randle's cell circuit, an open lead experiment, an electrochemical reaction (Ti/K₄FeCN₆, K₃FeCN₆), and two forms of model film-coated AA2024-T3. The feasibility of the HT-EIS approach was further demonstrated through evaluating a variety of real organic coatings, including a form of polyurethane, a form of UV-curable epoxy, and a combinatorial array of four different coatings (chromated epoxy, polyurethane, our newly developed Mg-rich primer, and the primer with polyurethane topcoat) at Al alloy surface. It has been shown that the HT-EIS method described here can significantly reduce the characterization time and facilitate the screening process for coating evaluation.

1. Introduction

The corrosion of metal has been generating serious economic consequences for industry and our society in general. From a recent survey, the annual financial loss due to corrosion is about 3.1% of GDP, amounting to over 276 billion dollars^[1], in the US alone. Historically, the most economical and effective method for reducing the cost is through the use of corrosion protective polymer coatings. It has been reported that at least one-half of all anti-corrosion costs are spent on this method^[2]. Especially during the recent decades, a variety of high performance coatings of the past, such as lead, chromate, and tin containing coatings, have been or will be ruled out for future usage as a result of stricter environmental regulations and health concern. Therefore, a novel formulation of environmentally benign corrosion protective coating is critically needed. However, due to the complicate nature of coating compositions and metal-polymer interactions, the coating development process is usually quite arduous and time-consuming, particularly in the corrosion evaluation step. For example, a number of commonly used corrosion evaluation methods, including outdoor atmospheric exposure, salt spray exposure, Prohesion exposure, and QUV weathering, etc, require long exposure times and rely on the tester's subjective judgment, which cannot provide quantitative information to evaluate coating degradation and the progress of metal corrosion. This bottleneck limits their usage for reliable and accurate assessment of a coating's useful service lifetime.

As a dynamic electrochemical method, electrochemical impedance spectroscopy (EIS) has proven to be one of the most promising methods for evaluating the corrosion protection of coatings on various metal substrates. Compared to the traditional exposure tests, it offers a number of advantages. First, the EIS can provide quantitative data and detailed information about the metal corrosion and coating performance in a relatively short time. Second, the results obtained from EIS are independent of the operator's subjective judgment, which minimizes the involvement of human error and significantly improves the accuracy of the test. Additionally, the EIS test is a non-destructive method, so repeated tests can be used to follow the degradation of a coating as a function of exposure time.

However, even with the availability of high performance EIS methods, EIS can not be confined to a single measurement for coating evaluation because the complex nature of the coating composition usually makes the structure-property relationship of the system difficult to define. Thus, a considerable number of replicates have to be exposed to a corrosive environment and periodically connected to the EIS instrument and tested. Each test takes some time to set up and a significant amount of time to acquire and evaluate the data, making the evaluation process extremely time-consuming. This situation often happens in industrial research laboratories that need to evaluate hundreds and thousands of organic coatings per day using this technique. Consequently, a high-throughput EIS protocol that can overcome this difficulty is highly desirable.

In recent years, combinatorial methodologies, which were originally developed within the pharmaceutical industry, have been applied to coatings research in order to enhance sample throughput, reduce time to market, and lower the cost of development^[3-7]. These methods generally consist of several automatic experimental processes, including polymer synthesis, coating formulation, characterization, and subsequently screening for the desired physicochemical property. Besides the mere synthesis/formulation part, the success of the combinatorial methodologies strongly relies on the development of analytical instrumentations with high-throughput screening capability. These screening approaches basically require a reduced sample size, a miniaturization of the specimen arrays, and a fast characterization technique. Fortunately, these requirements have been made possible due to advancements in instrumentation, robotics, and computer software. Another outstanding feature of the combinatorial technique is the possibility of using parallel approaches to evaluate a great number of samples. Using this approach, the most time-consuming step in the workflow is arranged in parallel so that the characterization time can be significantly reduced.

In this context, we are introducing a high-throughput EIS (HT-EIS) approach based on the concept of parallel combinatorial methods. The main purpose of this work is to reduce labor requirements and solve the problem of time-consuming routine EIS measurements. A HT-EIS setup containing a 4 x 3 electrochemical cell

array was fabricated and an automatic switch system was applied to control the process of the measurement. The geometry of the cell configuration allows for 4 coating compositions to be measured with 3 replicate measurements per coating composition in a short time. The apparatus can also be used in conjunction with cyclic accelerated weathering tests to facilitate the screening process of corrosion protective coatings. To the best of our knowledge, the instrumentation of the HT-EIS has not been reported previously. It is anticipated that the apparatus will make a significant contribution in the area of coating development.

In the underlying work, we first present the fabrication of the HT-EIS apparatus. Then we validate the system using Randle's cell circuits, open lead experiments, electrochemical reactions on Ti surface (Ti/K₄FeCN₆, K₃FeCN₆), and two forms of model film-coated Aluminum alloy (A2024-T3) samples. Finally, we describe some applications of the HT-EIS setup in several real coating systems in order to characterize the feasibility of the instrument.

2. Experimental Section

Titanium electrode in K₄FeCN₆/K₃FeCN₆ solution was used to validate the 12-well HT-EIS setup. Titanium substrates (10 cm x 20 cm) from McMaster-Carr were first degreased in acetone, followed by rinsing with distilled water. Then the coupon was placed in an acid pickling solution (20 ml 70% HNO₃ and 2 ml of 50% HF/100 ml solution) for 1-3 minutes until the surface was uniformly white. Finally, the alloy was washed with distilled water 2-3 times and let dry in air^[8]. Equal molar concentration (5mM/5mM) of the redox couple K₄FeCN₆/K₃FeCN₆ in 0.5 M aqueous KClO₄ solution was used as electrolyte.

Two forms of polymer film, Tedlar® release film and 3M 471 tape, were involved in the validation of the HT-EIS apparatus. The Tedlar release film (polyvinylfluoride) with the thickness of 51 μm was obtained from Dupont®. The film's relative dielectric constant is 5-8 and the resistivity is 2.9 x 10¹⁴ Ωcm^[9]. Following the same procedure used in previous publication^[8], one side of the Tedlar film was coated uniformly with a thin layer of silver epoxy (Circuitworks® 7100), then the side with the silver film was pressed on AA2024-T3 substrate to make sure that a strong adhesion was established between the film and the metal. The 3M 471 tape is a transparent vinyl tape manufactured by 3M™. Since one side of 3M 471 tape was coated with rubber adhesive, the tape could be directly brought into contact with the AA2024-T3 substrate. Precaution was made to avoid the entrapment of air bubble between the film and the substrate during film application. The film thickness was measured to be 104.1±0.5 μm. For the experiments using the above two forms of model film-coated metal, the electrolyte used was 3% NaCl aqueous solution. The AA2024-T3 substrates were purchased from Q-panel Lab Products (Cleveland, OH). The panels were sandblasted to remove the oxide layer and then cleaned with hexane.

Several real coating samples were used to test the feasibility of the HT-EIS setup. Two-component chromate-based primer coating (MIL-PRF-23377J) and two-component polyurethane topcoat (MIL-PRF-85285D) were obtained from Deft, Inc (Irvine, CA). The Mg-rich primer coating (50% PVC) was prepared in our lab, and the detailed formulation is shown in Table 1. Briefly, two forms of Mg powders, Eckagranules™ PK31 and Eckagranules™ PK51 (Ecka GmbH), were mixed in a 52/48 vol./vol. ratio. Epon 1001-CX-75 is an epoxide containing 25 wt.% MIBK/xylene (vol. ratio 65/35) solvent mixture, and Epicure 3140 is a solventless polyamide curing agent. Both the Epon1001-CX-75 and the Epicure3140 were obtained from Resolution Performance Products®. Aerosil® R974 (Degussa, Inc.) was used as dispersing agent. MIBK and xylene were obtained from Sigma-Aldrich Company. These coatings were applied on AA2024-T3 panels and all primed specimens were allowed to cure for at least one week before applying the top coat. The average dry film thicknesses of the Mg-rich primer, chromate primer, and polyurethane coatings were about 50±10μm. The average film thickness of Mg-rich primer with polyurethane topcoat was about 100±10 μm.

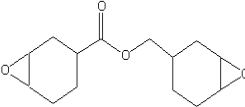
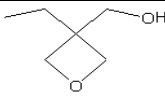
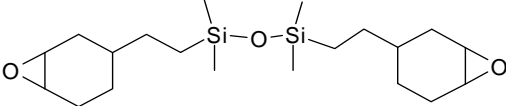
Table 1. Formulation of Mg-rich Primer Coating

Ingredients	Weight, g
Epon 1001-CX-75	67

Epicure 3140	9.5
Mg powder	95
Aerosil® R974	1
MIBK	45
Xylene	20

A set of UV-curable coatings, which were also used to test the applicability of the setup, is described in Table 2. The UV curable coating formulation was composed of 70% wt. UVR 6110, 15% wt. UVR 6000, 10% wt. SIB 1092 and 5% wt. UVI 6974. The above ingredients were mixed homogeneously, then the coating was applied onto the AA2024-T3 substrate by a draw-down method and UV cured in air at room temperature. The UV irradiation time was 60 seconds. The UV source was a Dymax 200 EC silver lamp (UV-A, 365 nm); light intensity was 35 mW/cm², measured by a NIST Traceable Radiometer (International Light model IL1400A). The measured film thickness was 80±10 μm.

Table 2. Description of the UV-curable coating

Trade Name	Abbreviation	Source	Structure and description
UVI 6974	PI	Dow	mixed triarylsulfonium hexafluoroantimonate salt in propylene carbonate
UVR 6110	ECC	Dow	
UVR 6000	OXT	Dow	
SIB 1092	EP-Si	Gelest Inc.	

3. Results and Discussion

Apparatus for the High Throughput Electrochemical Impedance Spectroscopy

An overview of the HT-EIS apparatus is shown in Figure 1. On the right side of the picture is a home-made Faraday cage containing an automatic electronic switch control unit and a 4 x 3 electrochemical cell array. A Gamry MultiEchem 8 workstation (black box in the middle of Figure 1) is connected through the electronic switch system to the 4 x 3 electrochemical cell setup. The custom-made Gamry workstation contains six femtostats (FAS-1) and two potentiostats (PCI4). In this HT-EIS setup, only four femtostats (channel 1 to 4) are interfaced to the 4 x 3 electrochemical cell array so that four measurements can be run simultaneously.

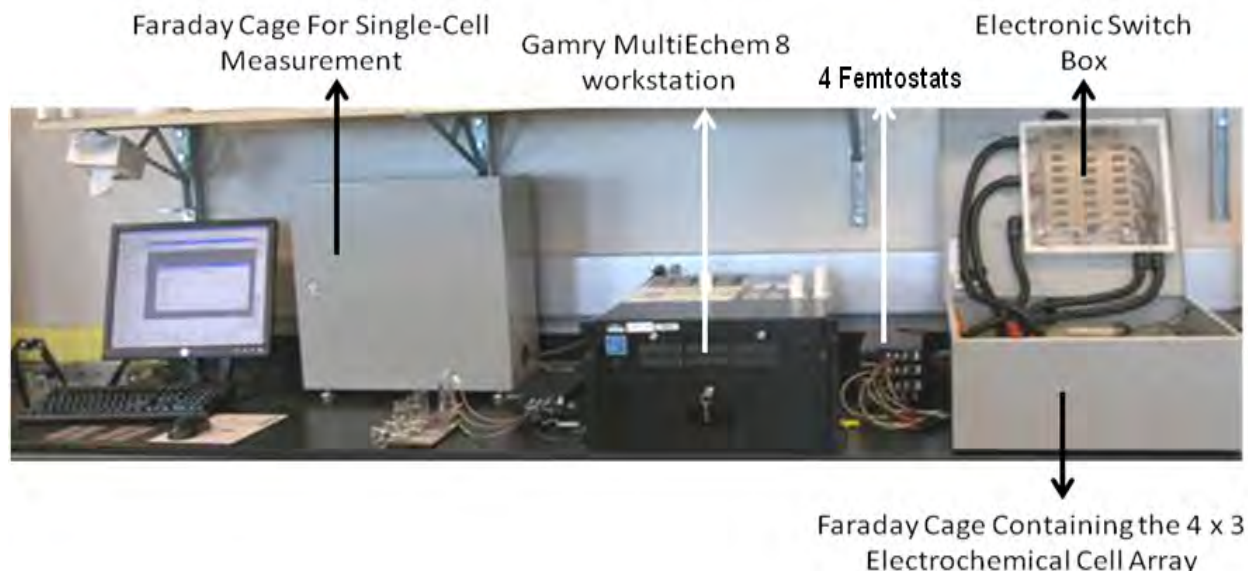


Figure 1. Apparatus of the HT-EIS system

The electrode array containing the 4 x 3 electrochemical cells is shown in Figure 2 and Figure 3. The assembly utilizes a 4-tab substrate bonded to a 4" x 8" black PVC backing plate by using a commercial fast cure epoxy (Marine Goop). After the substrate is securely adhered to the plate, the 4 tabs are electrically isolated from one another by saw cutting the top spine that holds them together.

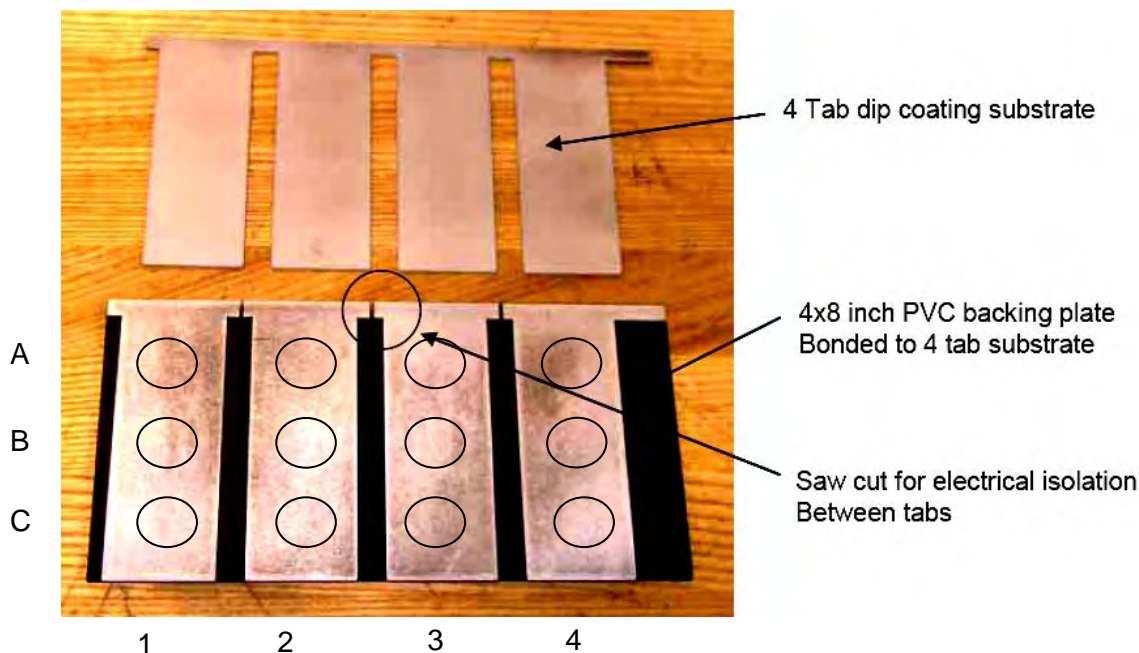


Figure 2. The 4 tab substrate for the HT-EIS

During the EIS experiment, the disconnected 4 tab substrates with the black PVC backing plate are placed onto a rectangle groove in a white plastic block (Figure 3 (1)), which is used as the bottom layer of the 4 x 3 electrochemical cell array assembly. The rectangle groove is designed to have exactly the same dimensions as the PVC backing plate so that the four tabs of the substrate (with or without coating) can be set in a designed position

(see Figure 3 (1)). Another plastic block is pressed tightly onto the top part of each tab by screwing down four metal screws until each screw is physically connected to the respective tab substrate. A digital voltmeter is used to make sure that a good electrical contact is established. The four metal screws are also used as connection posts for working electrode cables. A rubber gasket (dimension 4" x 8" x 0.25") with 12 circular holes (1 inch in diameter) is carefully positioned onto the four tabs so that each tab contains three circular holes (Figure 3 (2)). Subsequently, a 4 x 3 well template (Figure 3 (3)) made from nylon is placed on the gasket. The well diameters are maintained constant through the gasket. Three stainless steel toggle clamps are applied tightly to the template to prevent electrolyte from leaking. After filling the electrolyte into each cell, an electrode array assembly containing 12 pairs of saturated calomel reference electrodes (SCE)/Pt counter electrode (CE) is positioned on the top of the 12-well template (Figure 3(4)) so that each cell contain its respective SCE and CE. The whole set up can be loaded and prepared for the testing in less than 5 minutes.

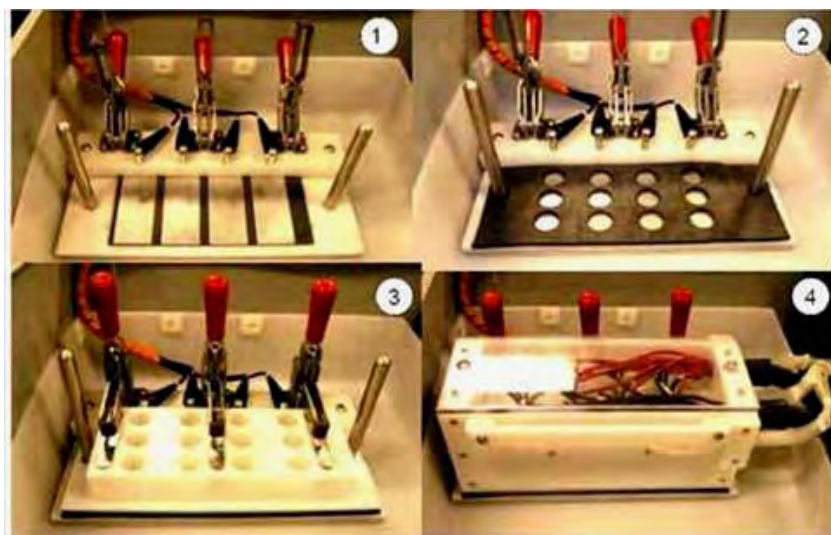


Figure 3. Photograph illustrating the new 12 well EIS assembly.

The geometry of the 12-well electrochemical cell configuration allows for 4 coating compositions to be measured with 3 replicates per coating composition. The top row (row A) of 4 cells (Figure 2), labeled A1 to A4 from left to right, will be measured simultaneously, followed by row B and then row C. For each cell configuration, as shown in Figure 4, a circular Pt mesh electrode (1.2 cm in diameter) is used as the counter electrode and is placed about 1.5 cm above the working electrode (tested sample) to form a parallel-planar arrangement with the working electrode. At the center of the Pt mesh counter electrode, a 5 mm hole is drilled in order to insert the tip of a small SCE reference electrode. The separation distance between working electrode and SCE is adjusted to about 1 cm.

One potential problem that the 12-well electrochemical cell setup may have is that the three cells, sharing the same tab of substrate, may generate different data output if they experience inconsistent exposure time in the electrolyte solution. This system error may change the EIS behavior of the coated sample and result in substantial error between the replicate EIS readings. To prevent this from occurring, we have integrated a series of fluid delivery and extraction tubes into each well of the 12 well assemblies (Figure 4). In one typical experiment, 10 mL of electrolyte was delivered to each cell of the same row simultaneously through respective fluid filling tube. The electrolyte was allowed to stabilize in the cells for five minutes and then the electrochemical measurements were set to run. After the measurement, the solution in the cells was sucked out and fresh electrolyte was injected into next row of four cells. The same or different electrochemical measurement would be continued in the next row. With this approach, only the row subjected to EIS testing is loaded with electrolyte while the others are evacuated.

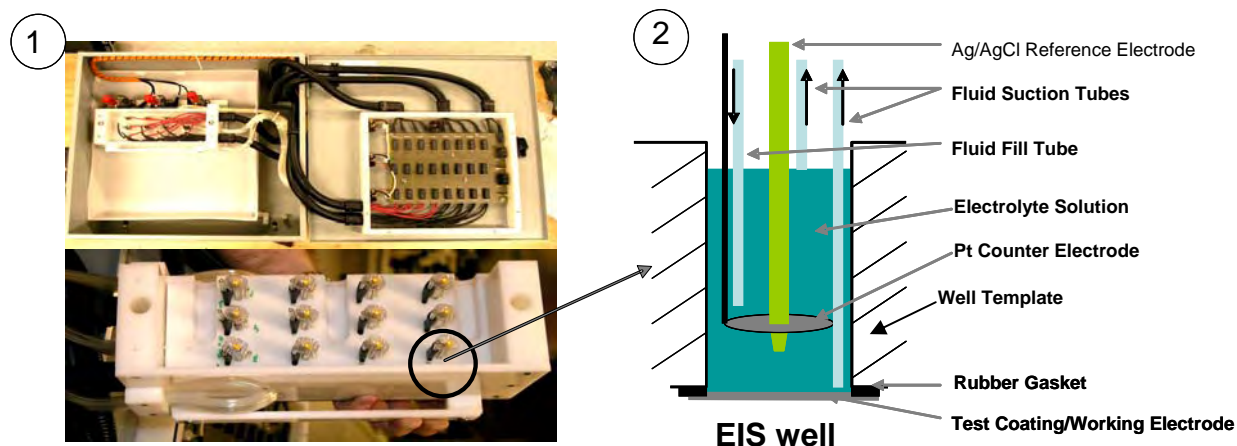


Figure 4. Detailed view of the 12-well HT-EIS assembly (1. Overall assembly with switch unit, 2. A typical cell in the setup).

An automatic electronic switch control unit was created to perform the required connection and disconnection of the electrodes when changing rows during a test (Figure 4). As previously mentioned, this circuit allowed for the 12 electrochemical cells to be measured sequentially in groups of four without operator intervention. The row selection was controlled through the control software using the two-channel TTL output available on the femtostat. A pair of four-pole mechanical relays was used to convert the two output channels to a fourstate binary coded decimal allowing for up to four measurement combinations. Two field effect transistors were used to match the impedance between the relay coils and the TTL outputs.

High quality shielded coaxial cable was used for all of the signal wiring and the entire unit was housed in an electro-magnetic interference (EMI) shielded cabinet. A form of high insulation reed relays (Coto Technology 9800 Series) are used for the on/off switching of reference electrodes and counter electrodes. No switching of the working electrodes was required since only one cell per tab was measured at a time. The working electrodes (tabs) were simply wired directly to the Femtostat input.

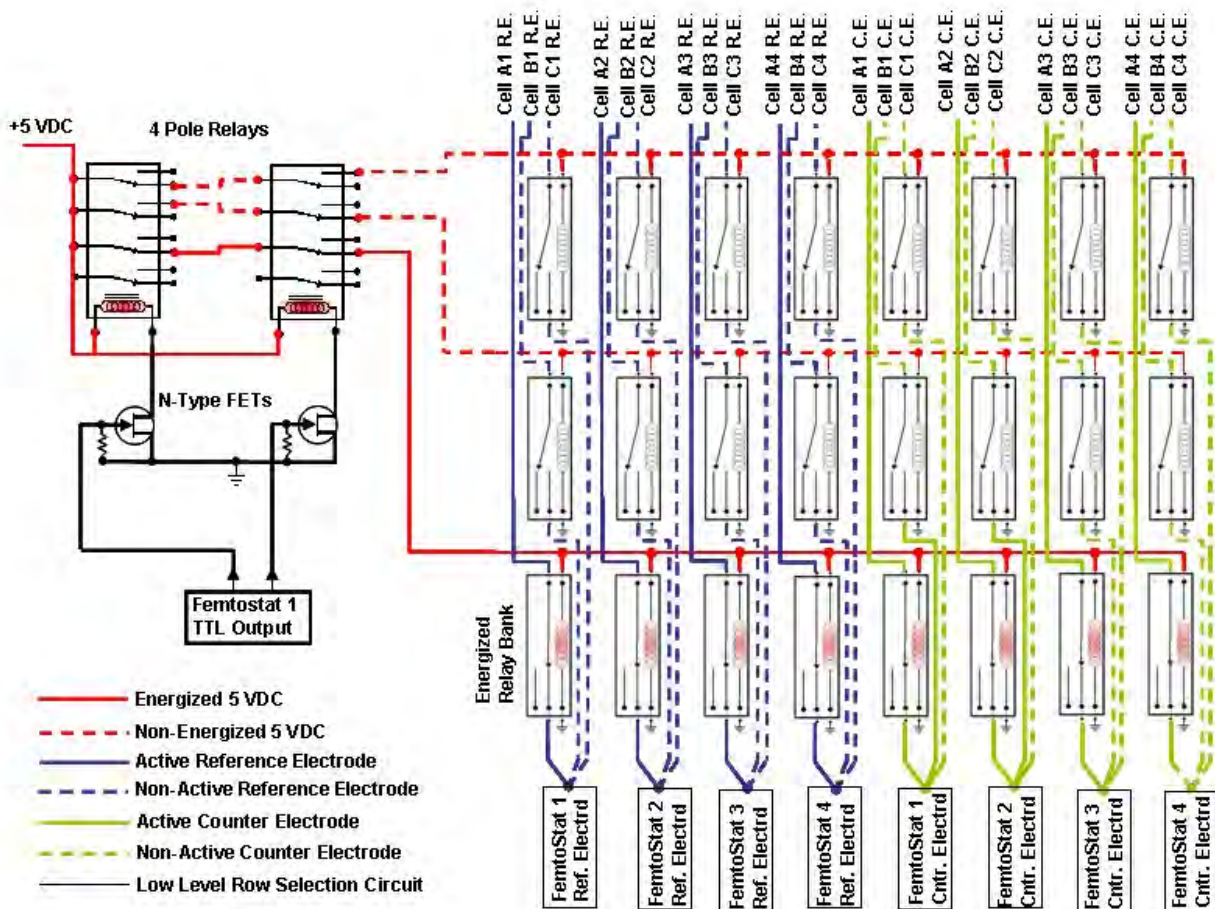


Figure 5. Schematic diagram of the switching system for the HT-EIS

Four femtostats (channel 1 to 4) of the Gamry MultiEchem 8 Electrochemical workstation were interfaced to the above electronic switch system. The EIS300 software was coupled to the system and the impedance spectra were acquired as a function of frequency with applied 10 mV R.M.S. voltages vs. open circuit potential. The resulting AC current (including phase shifts) was measured, and the impedance was derived (10 points/per decade). In this paper, all the HT-EIS validation work, including Randle's cell circuit calibration, open lead experiments, Ti/ K_4FeCN_6 , K_3FeCN_6 experiments, and model film calibration works, used the frequency range from 10 kHz to 10 mHz. For the HT-EIS measurement in real coating systems, the frequency range from 10 kHz to 0.1 Hz was applied in order to facilitate the measurement and analysis time. Bode plot was used as the impedance output format in this paper due to its well accepted nature in coating industry.

Validation of the Performance of the HT-EIS

In order to test the performance of the instrument, especially the compatibility of the electronic switch system with the commercial Gamry potentiostat, four identical Randle's circuits were used as a model system. Since the EIS spectrum generated from each circuit has a known response, any deviation from this response indicates the malfunction of the instrument. The Randle's circuits used are printed circuit boards made by Gamry (Figure 6). Each circuit was connected through its respective electronic switch to its respective cells in the same row of the 12-well setup, and EIS experiments were run simultaneously. As shown in Figure 7 (right), the 12 obtained Bode plots overlapped each other, showing a very reproducible result. Each obtained impedance spectrum was then simulated digitally with a Randle's cell model built through commercial software Zview (Scribner Associates). It was found that the accuracy of the measurement in the given frequency range was less

than 1.3% of error in the absolute impedance value and 1 degree of error in phase. A “single Randles cell measurement” was used as control for comparison, where the same Randle’s circuits were directly connected to the corresponding channel of the Gamry Femtostats and EIS experiments were run in series. A highly reproducible EIS result was observed for the single Randles cell measurement (Figure 7 (left)), the accuracy of which showed less than 1% of error in impedance modulus and 1 degree of error in phase for the given frequency range. Apparently, for these Randles cell experiments, no significant difference is observed in term of data accuracy and reproducibility between the parallel HT-EIS and the single cell measurement, suggesting that the HT-EIS setup is acceptable for measurement in the low impedance range (1-3000 Ω).

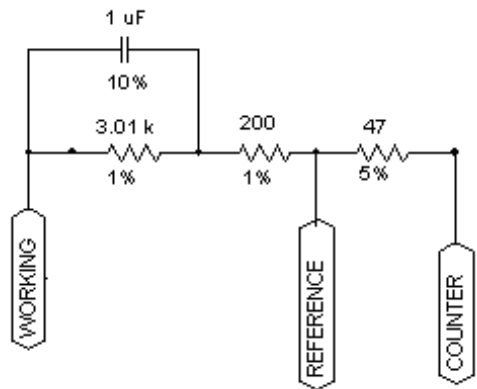


Figure 6. A Randle’s cell made from Gamry (Courtesy of Gamry)

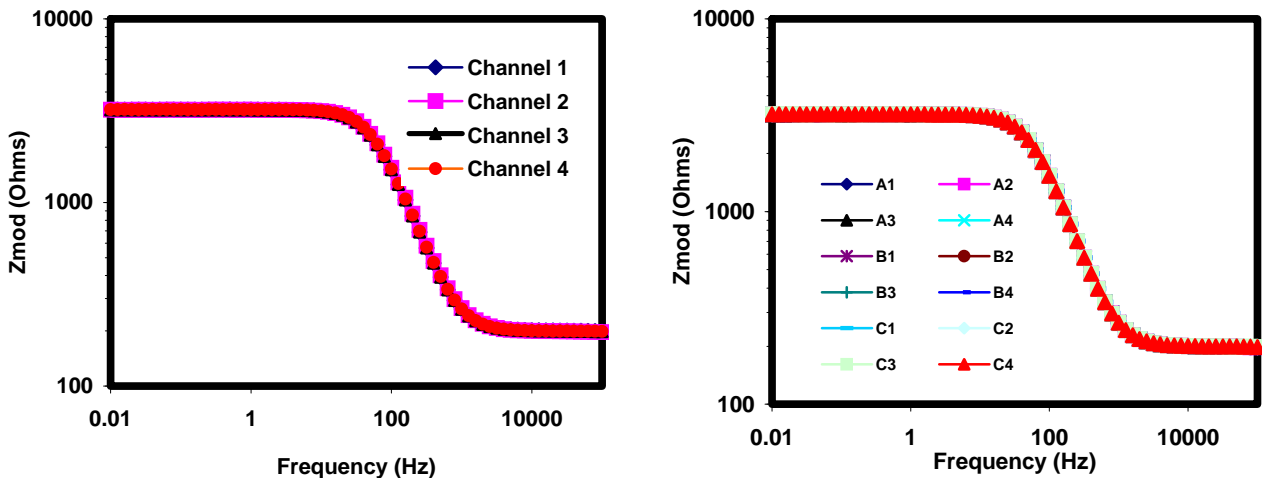


Figure 7. Bode plots of Gamry Randle’s cell from the single cell (left) and the HT-EIS setup (right)

In practice, corrosion protective coatings typically involve substantially higher impedances (i.e., in the range of $10^9 \Omega$ or higher) and rarely behave like ideal equivalent circuits of electronic component. Thus, the performance of the instrument needs to be further validated in the high impedance range in an actual cell setup. Recently, Bierwagen et al.^[9] proposed a method of using a commercial model film, the film thickness and composition of which have been well-defined, in order to calibrate or troubleshoot a potentiostat. The method is relatively simple, low-cost, and, more importantly, capable of giving highly reproducible results in the high impedance range. In this work, this method is re-examined and used to validate our HT-EIS apparatus. Two things need to be done before we used the method. One is to know the impedance limit (input impedance) of the instrument. The other is to make sure that each real electrochemical cell in the 4 x 3 electrode array generates the same data output at the same operating condition.

The open lead EIS experiments were conducted to evaluate the practical instrument limit of the HT-EIS apparatus. This is a conceptually simple experiment, but it provides us the information about the maximum measurable impedance and the lowest measurable capacitance of the instrument. For example, if the impedance of the test sample is beyond the range of the Open Lead Curve, then the EIS instrument cannot measure it. Following the procedures recommended by the Gamry operator manual^[10], the electrode cables for the four cells in the same row of the HT-EIS setup were first connected to respective Randle's circuits (Figure 6). Then the open circuit potential was measured to define the zero potential (0 ± 3 mV), which was used in the following open lead EIS experiment. Then, the experiment was paused manually and the four Randle's circuits were removed from the electrode cables. The working electrode cable in each cell was left dangling in the air. The cables for reference electrode and counter electrode were connected together to provide a feedback path for the femtostat. A separation between WE and RE/CE were set at least 5 cm apart. Since the experiment was done at the open lead condition which makes the setup prone to noise pickup (antenna effect), the EIS spectrum recorded is typically noisier than that recorded at the closed circuit condition, even if the measurement was done in a Faraday cage. Thus, the resulting open lead HT-EIS and 4 single cell open lead EIS spectra were numerically simulated using a parallel RC equivalent circuit. The fitted Bode plots were averaged, as shown in Figure 8. For the single cell EIS experiment, the maximum measurable impedance is on the order of $3 \times 10^{12} \Omega$ and the relative lowest measurable capacitance is about 3.0 ± 1 pF. In contrast, the maximum impedance (input impedance) recorded through HT-EIS is about $3 \times 10^{11} \Omega$, one order of magnitude lower than that obtained from single cell EIS. The corresponding lowest capacitance is 30 ± 1.2 pF, one order of magnitude higher than single cell EIS. The degradation of the performance of the HT-EIS may be due to the additional circuitry of the electronic switch system and cell cabling with the parallel multiplexer, making the DC background current much larger than AC signal. The test for the minimum impedance limit of the HT-EIS apparatus was not conducted because it cannot be encountered in coating research.

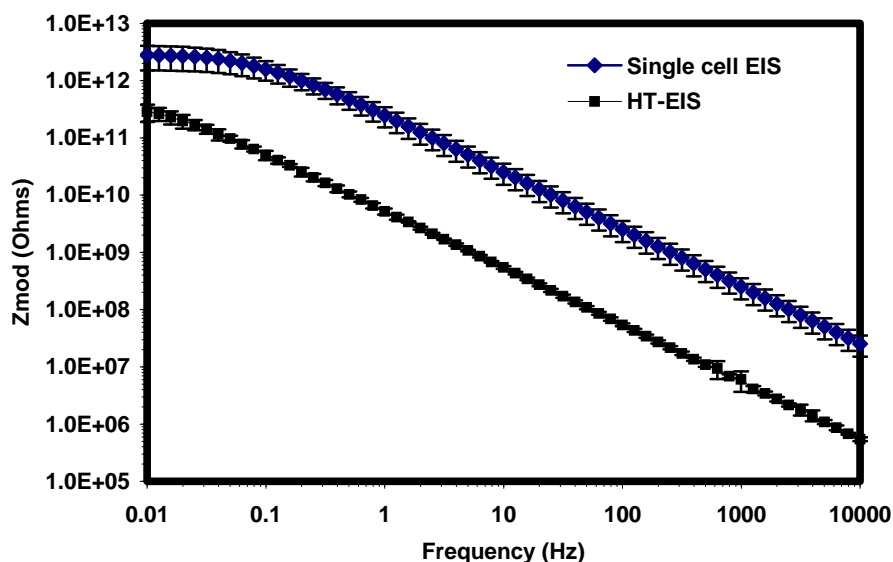


Figure 8. Open Lead Experiment for Single Cell EIS (left) and HT-EIS measurement (right)

Since it is not sufficient to validate the HT-EIS setup only using ideal equivalent circuits of electronic components (Figure 6), the instruments should be tested on actual electrochemical cells to make sure they are able to make the required measurements, and more importantly, generate the same signal throughput at the same operating condition. In the paper, titanium substrates in redox couple K_4FeCN_6/K_3FeCN_6 solution were used as

model systems to validate the performance of the 12-well electrochemical cell setup. There are several reasons in choosing this electrochemical model system. First, Ti generally exhibits strong chemical and electrochemical stability when immersed in electrolyte, which is due to the passive nature of this metal^[11]. Secondly, neither the K_4FeCN_6 nor K_3FeCN_6 shows significant adsorption at the Ti surface^[12], making this EIS experiment more reproducible. In contrast, K_4FeCN_6 and K_3FeCN_6 exhibited strong adsorption at Cu and Al surface^[13-15]. Thirdly, Ti is physically robust and is easy to handle in the HT-EIS setup. For example, indium tin oxide glass is also a potential candidate for this experiment. However, due to the fragile nature of the material, it is quite difficult to fit in our HT-EIS setup. Additionally, Ti is environmentally benign and relatively cheap. These properties eliminate the usage of mercury film electrode and Pt electrode in the experiment.

Four tabs of titanium substrates were set up in a format quite similar to Figure 2 and Figure 3. Since K_4FeCN_6/K_3FeCN_6 redox reaction is essentially a kinetically fast electron transfer process, when the passive titanium electrodes were switched to open circuit, the potentials for the entire tested cell can reach steady state in a few seconds, generating a relatively stable potential, at $0.22 \pm 0.02V$ vs. Ag/AgCl RE. The open circuit potentials (OCP) are similar to that for a platinum electrode in the same solution ($0.23 \pm 0.01V$ vs. SCE)^[12]. The OCPs for the four cells in the same row of the 12-well electrode assembly were recorded simultaneously and were observed to reach the same potential after 5 minutes of immersion, at which point four EIS experiments were initiated.

As shown in Figure 9 (left), EIS test for three rows (labeled A, B, and C) of the 12 electrochemical cells in the assembly provide highly reproducible results for the model system. Typically, at the highest ac frequencies ($f > 1000$ Hz), the amplitude of the impedance becomes frequency independent, suggesting the interfacial double layer and/or titanium oxide layer was shortened, and only the solution resistance was measured. At frequency below about 1 kHz, a parallel RC response was obtained, which was characterized by a straight line with a slope of about -1 in the mid-frequency range ($0.1 < f < 1000$ Hz) and a relatively flat region in the lowest frequency range ($0.01 < f < 0.05$ Hz). The parallel RC behavior of the EIS spectra indicates the interfacial Faradaic reaction occurring at the Ti surface. Since looking for the reaction kinetics of the model system is not the main goal of the study here, the subject will not further discussed in detail here.

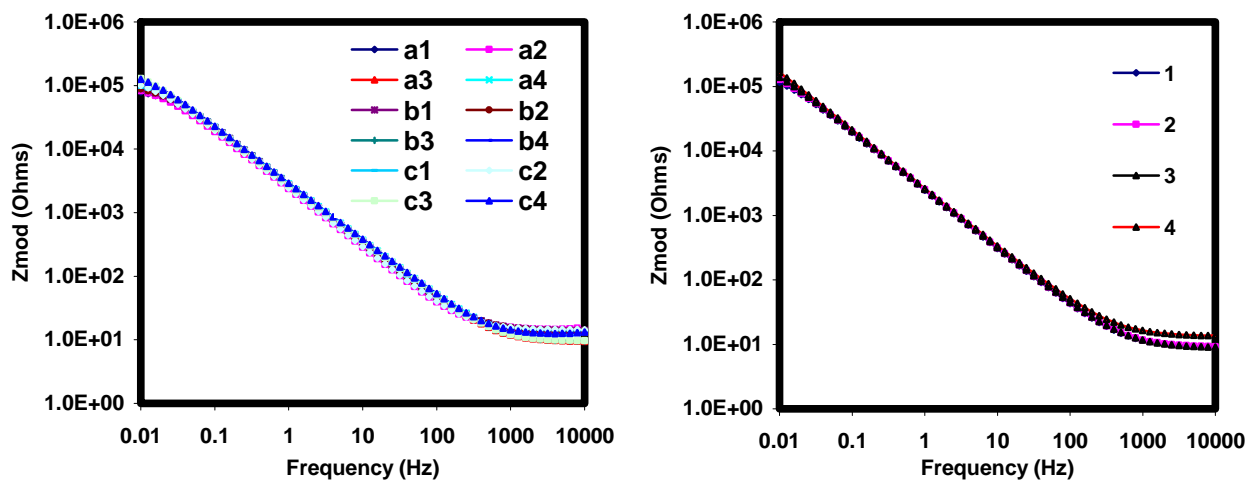


Figure 9. The HT-EIS (left) and the single cell (right) measurement of Titanium in solution containing K_4FeCN_6/K_3FeCN_6

In comparison with the results obtained from the above HT- EIS, single cell EIS measurements were also made as control for the same model system. For a typical single cell EIS setup, pieces of PVC tubes with the cross-section area equal to the exposed area of each cells in the HT-EIS setup (5 cm^2), were glued with a fast-cure epoxy (Marine Goop) onto the titanium substrate and the same amount of electrolyte (10 mL) was manually filled into each electrochemical cell. As previously discussed, the single cell was connected directly to the Gamry femtostat and the EIS was carried out in series. The geometry of the three-electrode setup in the single cell

experient was also trying to keep the same as the HT-EIS (Figure 4 (right)). As shown in Figure 9 (right), the Bode plots for the single cell EIS are quite similar to those obtained from the HT-EIS experiment (Figure 9 (left)). The raw EIS spectra for both experimental arrangements were fitted using an equivalent circuit model, shown below:



where R1, R2, and CPE represent solution resistance, charge transfer resistance, and constant phase element, respectively. The CPE is used to simulate a capacitor that compensates for any surface heterogeneity that occurred in this system. The impedance of CPE (Z_{CPE}) is given by Equation (1),

$$Z_{CPE} = \frac{1}{Y_0} (j\omega)^{-n} \quad (1)$$

where Y_0 is a parameter with the numerical value of the admittance ($1/|Z|_{CPE}$) at $\omega=1$ rad/s and n is a constant. The fitted results generally match the EIS spectra very well. The relative errors for the different parameters are shown in Table 3. We are not surprised to observe that the relative errors obtained in HT-EIS are to some extent higher (but acceptable) than those in single cell EIS measurement. This may be due to the parallel nature of the HT-EIS components, leading to a higher noise level and more difficulties obtaining accurate fitting models than the single cell experiment.

Table 3. Relative error of fitted parameters in single cell EIS and HT-EIS measurements in Ti/K₄FeCN₆, K₃FeCN₆ model system

	Relative Error for R1 (%)	Relative Error for R2 (%)	Relative Error for Y ₀ of CPE (%)	Relative Error for n of CPE (%)
Single cell EIS	0.68 - 0.90	3.0 – 10.2	0.42 - 0.62	0.11 - 0.17
HT-EIS	0.3 – 3.2	1.25 – 12.8	0.35 -1.8	0.06 -1.4

The calculated physical parameters based on the above equivalent circuit model are also shown in Table 4. No significant difference in the four parameters (R1, R2, Y₀ and n of CPE) was found between the single cell EIS and HT-EIS, suggesting the 12-well cell assembly was valid to generate the same quality of data output as the custom single cell EIS setup. It is worthy to note that the impedance spectra generated from both experimental arrangements (Figure 9) are also in good agreement with the previous publication^[15].

Table 4. The calculated physical parameters for single cell and HT-EIS measurement in model system Ti/K₄FeCN₆/K₃FeCN₆

	R1 (Ohm)	R2 (×10 ⁵ Ohm)	Y ₀ (× 10 ⁻⁶)	n of CPE
Single cell EIS	12.1±2.1	1.31±0.19	73.7±1.6	0.89±0.002
HT-EIS	11.8±3.8	1.04±0.18	78.5±2.79	0.92±0.001

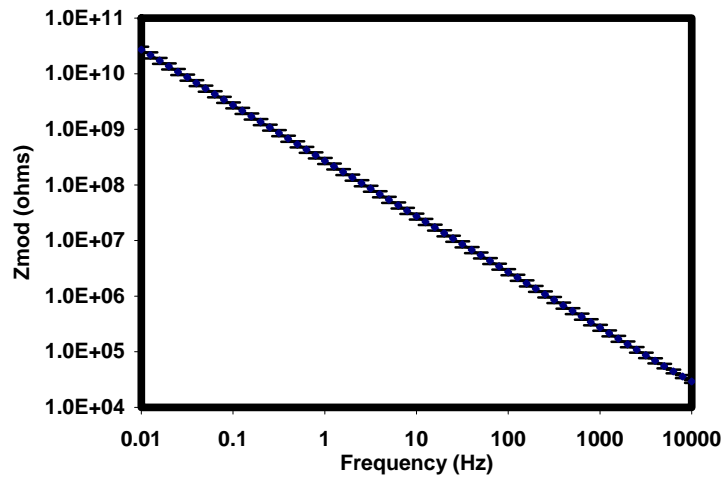
As previously mentioned, though the above Randle’s cell and the model system of Ti/K₄FeCN₆/K₃FeCN₆ validated the HT-EIS very well, they could not provide calibration for the setup in the higher impedance range that is usually associated with the real coating systems (typically 10⁹ Ω at low frequency). In the next part of our research effort, two forms of polymer model films with well-defined composition and film thickness are used for calibration in the high impedance range. The first model system is a Tedlar film (polyvinyl fluoride release films

from Dupont, film thickness 51 μm) coated on AA2024-T3. As shown in Figure 10 (top), the Bode plot obtained from the single cell experiment for this film was characteristic of a high performance coating with very low permeability. The film behaved like a capacitor, generating a straight line with a slope of about -1 and very high impedance (more than $10^{10} \Omega$) at low frequency. This result is in a good agreement with previous publication^[9]. Additionally, the impedance spectra of the Tedlar film remain the same for at least 2 days in 3% NaCl aqueous solution (figure not shown), suggesting that the barrier properties of the film were stable and no significant coating degradation was taking place under the test conditions. The good durability of the film guarantees the reliability of the measurement over the duration of the test period.

As shown in Figure 10 (bottom), the HT-EIS showed similar impedance spectra as the above single cell experiment, though the relative error of the measurement (12-19%) was somewhat higher than that obtained from the single cell EIS (7 -15%). Considering the speed of generating the data, losing a few percent of accuracy as a tradeoff is still acceptable for the HT-EIS, especially in such high impedance range. Alternatively, a CPE circuit model was used to simulate the results for both setups. Though the fitting errors for the CPE parameters (Y_0) in the HT-EIS are a few percents higher than those in the single cell experiment (Table 5), they are still within the error range of acceptability (about 5%). On the other hand, the parameters obtained from the two setups (Table 6) are quite similar, suggesting that the HT-EIS is capable of measuring the model film in such a high impedance range as the single cell experiment without significantly losing the quality of the data output. The relative dielectric constant (ϵ_r) of the model film is further calculated using Equation (2),

$$\epsilon_r = \frac{Y_0 \times d}{\epsilon_0 \times A} \tag{2}$$

where d is the thickness of the film (51 μm), A is the area of the working electrode being measured (5 cm^2), ϵ_0 is the dielectric constant of free space ($8.85 \times 10^{-12} \text{ F/m}$), and Y_0 is the parameter used to simulate the film capacitance. The calculated ϵ_r (about 7.3) is within the range of values given in the technical sheet (5-8) for the model film.



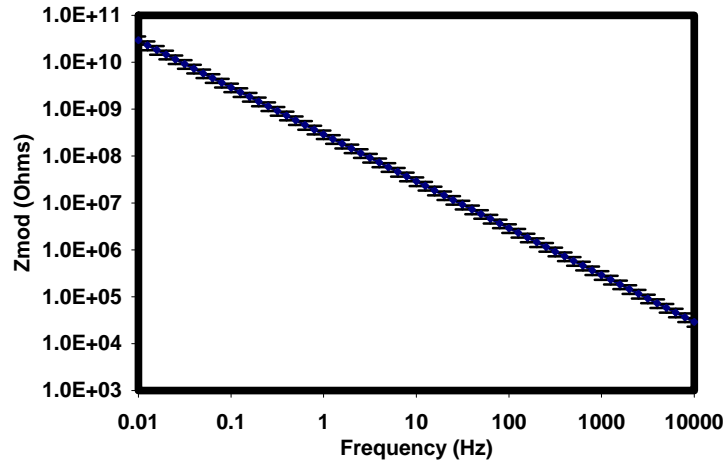


Figure 10. Single cell (top) and HT-EIS measurement (bottom) of Tedlar coating on Al 2024 in 3% NaCl

Table 5. Relative error of fitted parameters in single cell EIS and HT-EIS measurements for model film (Tedlar) on AA 2024

	Relative Error for Y_0 in CPE (%)	Relative Error for n of CPE (%)
Single cell EIS	0.53 – 1.52	0.7-1.2
HT-EIS	3.18 -5.27	1.5 - 3.2

Table 6. The calculated physical parameters for single cell and HT-EIS measurement measurements for model film (Tedlar) on AA 2024

	$Y_0 \times 10^{-9} (\Omega^{-1} \text{cm}^{-2} \text{s}^{-1})$	n of CPE
Single cell EIS	0.83 ± 0.13	0.96 ± 0.02
HT-EIS	0.64 ± 0.12	0.94 ± 0.02

AA2024 with 3M tape

The 3M-471 tape is a commercial product from 3M and is used for abrasion protection, sealing and surface masking. The reason for using this tape is mainly due to its relative uniform film thickness ($104.1 \pm 0.5 \mu\text{m}$) and the lower impedance value than the Tedlar coating. As shown in single cell EIS result (Figure 11 (left)), the film coated AA2024 showed excellent barrier properties in 3% NaCl aqueous solution. At frequencies lower than 0.1 Hz, the impedance spectra shows a frequency-independent plateau, where the magnitude of the impedance averagely reaches $8.7 \times 10^9 \Omega$. At frequencies above 0.1 Hz, the impedance decreases as frequency increases, indicating highly capacitive behavior of the coating. Comparatively, the impedance spectra for the HT-EIS showed largely similar results: the impedance at 10 mHz averages at $7.95 \times 10^9 \Omega$ and the average coating capacitance is 0.24 nF (Table 7).

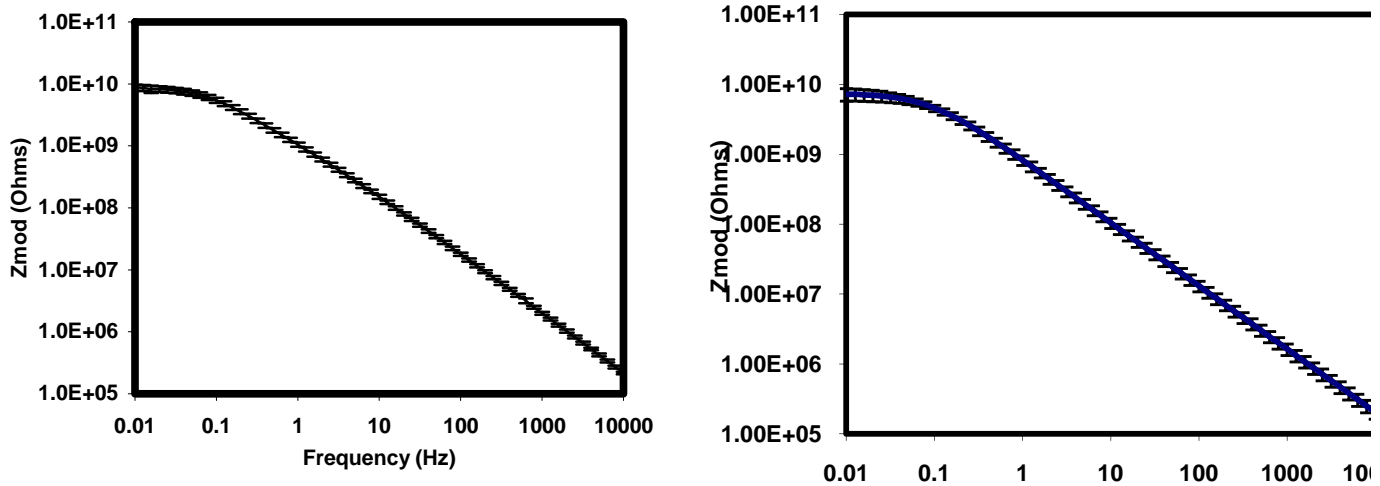


Figure 11. Single cell (left) and HT-EIS measurement (right) of 3M-471 coating on Al 2024 in 3% NaCl

The results for the single cell EIS and the HT-EIS of the 3M-471 coated samples have also been simulated by an equivalent circuit model, where a resistor R is in parallel with a CPE. Very good fitting results are obtained for the two setups, and the calculated parameters are shown in Table 7. No significant difference is observed for the three parameters (R , Y_0 and n of CPE) obtained from the two different setups. The replicate error of HT-EIS is slightly higher than the single cell experiment but still acceptable.

Table 7. The calculated physical parameters for single cell and HT-EIS measurement in model film 3M-471 coated AA2024

	R ($\times 10^9 \Omega$)	Y_0 ($\times 10^{-9}$) of CPE	n of CPE
Single cell EIS	8.76 ± 0.98	0.23 ± 0.02	0.89 ± 0.001
HT-EIS	7.95 ± 1.25	0.24 ± 0.02	0.91 ± 0.001

Application of the HT-EIS for organic polymer coated metal

In this paper, the feasibility of the 12-well HT-EIS is further examined using three real coating systems on metal substrate AA2024. The test electrolyte is dilute Harrison's solution (DHS, 0.35% $(\text{NH}_4)_2\text{SO}_4$ and 0.05% NaCl aqueous solution). The first application is to study the EIS response for a physical barrier coating with and without surface defects. As shown in Figure 12, a commercially available polyurethane coating was applied to four tabs of the AA2024 panel by the spray coating method. After the coating was fully cured, the "C" positions of the four tab substrates were carefully scratched so that the scribes were within the cell exposed area while the other areas ("A" and "B" position) remain un-scribed.

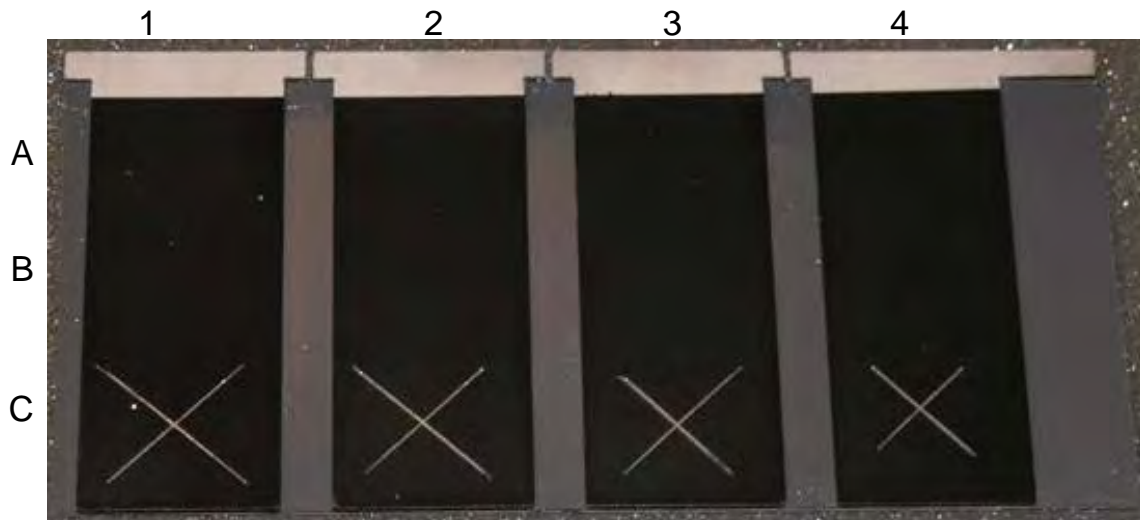


Figure 12. Polyurethane Coated AA2024, scribed and bonded to PVC backer.

As shown in Figure 13, the EIS spectra obtained from the eight non-scratched positions (position “A” and “B” of the four tabs) are similar: the impedance at low frequency (typically at 0.1 Hz) is on the same order of magnitude (10^6 to 10^7 ohm) and the coating capacitance is in the range between 5.28 nF and 21.6 nF. These parameters were obtained through fitting a parallel R(CPE) equivalent circuit model. These results are not as reproducible as those for the previously described model film coated samples because the commercial polyurethane coating may show more forms of heterogeneities in term of film thickness, surface composition, surface morphology and crosslink density. Compared with the non-scribed samples, the results for the scribed positions in row “C” show significantly different EIS response. Typically, the low frequency impedance values (at 0.1 Hz) for the four scratched position are about $10^5 \Omega$, which is two orders of magnitude lower than those for the non-scribed sample. In the high frequency range (above 1 kHz), the interfacial impedance is shorted and only solution resistance is measured. The EIS measurements on the four scratched positions produce similar, and in some cases overlapping spectra, although some variations do exist in terms of reproducibility, which may be due to the fact that the scribes made manually at the coated metal inflicted different extent of physical damage to the paint film and the underlying substrate. The whole measurement time for the 4×3 experiments typically took about 45 minutes, including experimental set up time (about 5 minutes), experiment running time (35 minutes), and electrolyte delivery/extraction time (about 3-5 minutes). In contrast, the 12 single cell EIS will take at least three hours, which is about four times slower than the HT-EIS.

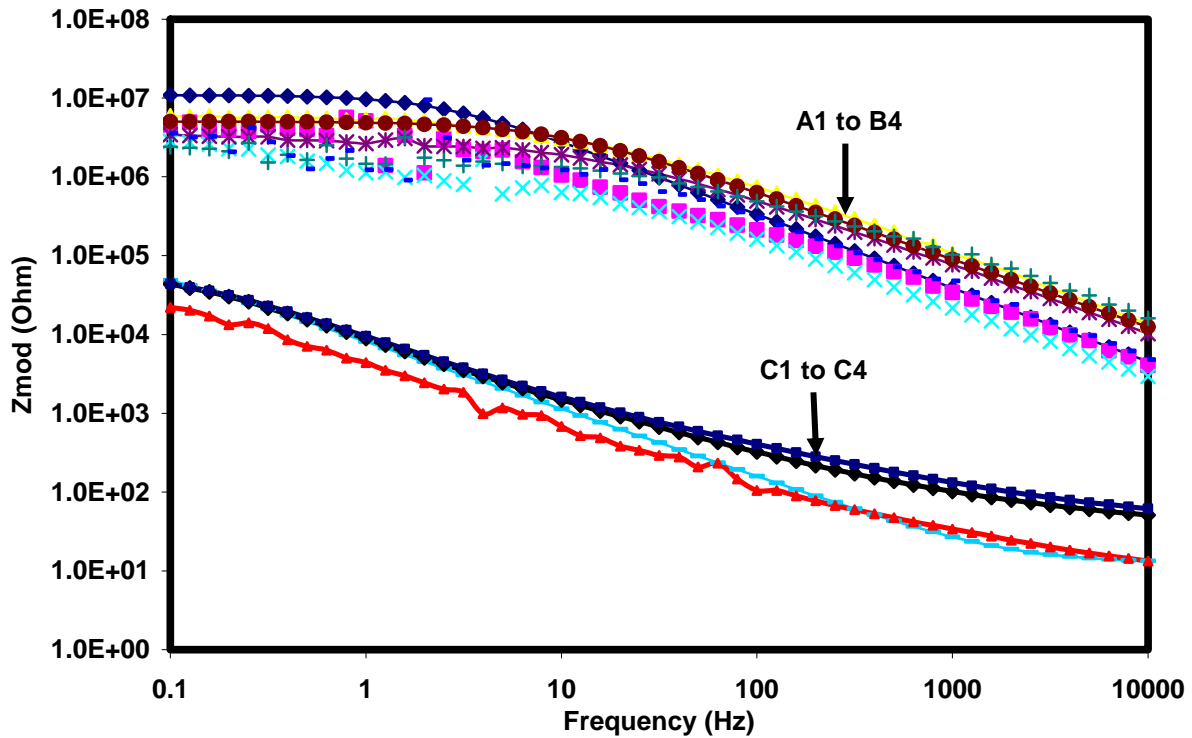


Figure 13. HT-EIS measurement of polyurethane coated Al 2024 in DHS

The second application of the HT-EIS is to test the feasibility of the system for fast evaluation of coatings' lifetime in terms of corrosion protection. In this experiment, a UV-curable epoxy coating was used as an example and EIS was performed as a function of constant immersion time in DHS. As illustrated in Figure 14, the results obtained from the 12-well setup are highly reproducible. Upon initial exposure to electrolyte, the low frequency impedances for the 12 replicates of measurements were all in the range of 10^8 to $10^9 \Omega$, indicating the coatings provided good barrier property at this stage. Then the coated samples with the PVC plate were taken out of the 12-well setup and placed in a separate assembly, which is specially made for the constant immersion study and shares the same basic design with the 12-well setup (figure not shown). After one week of immersion in DHS, the 4-tab sample was brought back into the HT-EIS setup and EIS was performed again. It was found that the impedances at low frequency were at least two orders of magnitude lower (typically $10^6 \Omega$) than measured one week ago, suggesting that the 12 replicates have experienced the same extent of degradation during this period of exposure. Following the rule of thumb proposed by Gray and Appleman^[16], low frequency impedance at 0.1 Hz was used as an indicator for coating evaluation. If the impedance modulus is above $10^7 \Omega \text{cm}^2$, it indicates that the coating is affording adequate corrosion protection to the metal surface. Below this impedance, the protection has failed. On this basis, the lifetime of the UV-curable coating in term of corrosion protection is established as 1 week, with the average value of normalized impedance of $5 \times 10^6 \Omega \text{cm}^2$ under these exposure conditions.

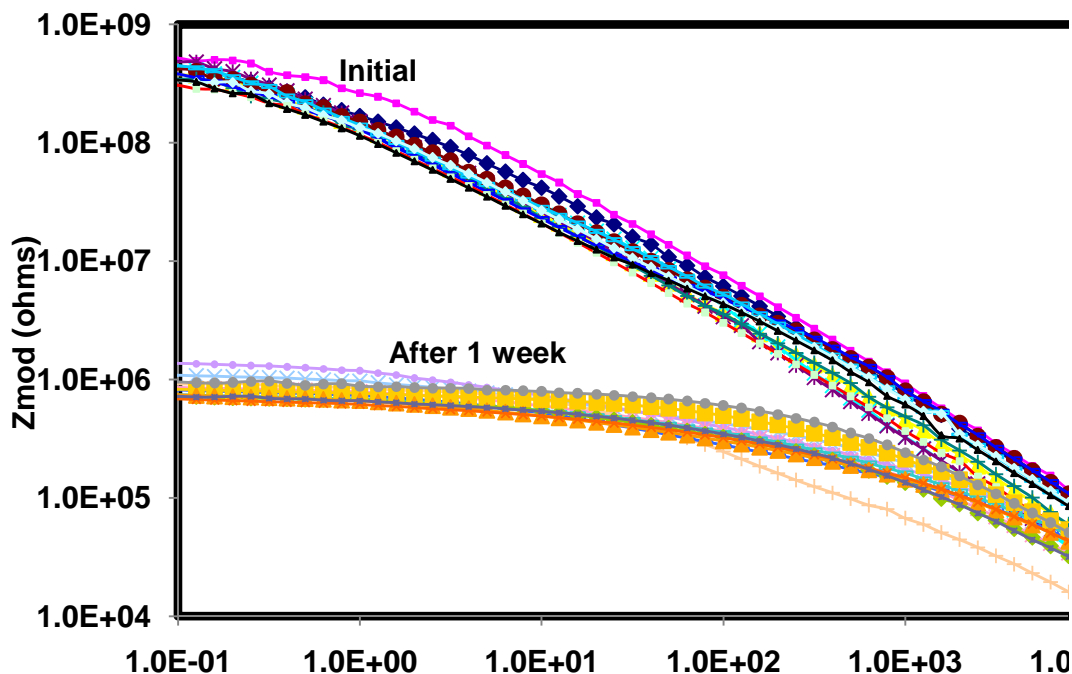


Figure 14. HT-EIS of UV-curable epoxy coated AA2024 as a function of exposure time in DHS.

The third application example is to test the feasibility of the HT-EIS for evaluating corrosion protection performance of four different forms of organic coating through different electrochemical techniques. As shown in Figure 15(a), four coating systems on AA2024-T3 were used to do the demonstration. They are respectively labeled as: (1) chromated epoxy primer; (2) Mg-rich epoxy primer; (3) Mg-rich epoxy primer with a polyurethane topcoat, (4) a polyurethane primer. In positions A of the four tabs, the EIS was performed to study the barrier properties of the four coatings. In positions B, the linear polarization technique was used to obtain such electrochemical parameters as corrosion rate, linear polarization resistance, and corrosion potential. In position C, a scratch was made at the respective tab, as shown in Figure 12, to study the metal-polymer interaction through the EIS technique.

The typical EIS results for the four different coating samples at row A are shown in Figure 15 (b). Of the four EIS spectra, the chromated epoxy coated sample (A1) exhibited the highest magnitude of impedance ($3 \times 10^7 \Omega$) at low frequency, which is due to the known inhibitive properties of chromate pigments by virtue of passivating the metal surface and enhancing or stabilizing the oxide layer at the metal surface. The impedance spectra obtained from the Mg-rich primer sample topcoated with polyurethane (A3) are quite similar to those obtained from the polyurethane-only sample (A4). Their impedances at low frequency are on the same order of magnitude (10^6 to $10^7 \Omega$), indicating that the electric conductivity of the 50% PVC Mg-rich coating is quite high, thus the impedance behavior of A3 is primarily dominated by the polyurethane coating. This hypothesis is further proved by the EIS measurement of the Mg-rich primer coated sample (A2), the low frequency impedance of which was at least three orders of magnitude lower than the rest of the samples.

As shown in Figure 15 (c), the linear polarization results obtained for position B qualitatively correlate with the EIS results for position A. Of the four different positions, the corrosion current measured from the chromated epoxy sample (B1) is the lowest (c.a. 10 nA), which correlates well with the highest impedance generated in the A1 position. The corrosion currents of B3 and B4 are quite similar and higher than that of B1, which were also in good agreement with the impedance results obtained from A3 and A4. The corrosion current of B2 was the highest (almost $100 \mu\text{A}/\text{cm}^2$), or at least three order of magnitude higher than the rest of the coatings. It is also shown that the open circuit potential of the Mg-rich coating (B2) was about -1.2 V vs. Ag/AgCl RE, indicating the unique coating protected the metal underneath through a cathodic, sacrificial protection mechanism.

The result is the same as that obtained from previous studies found in the literature^[17-19].

As is observed in Figure 15 (a), an artificial surface defect was made to the position C for each coating. The introduction of a surface defect is particularly relevant to the investigation of an “active” coating system, in which an “active” component, such as chromate and Mg pigments, are present. In contrast to the non-scratched sample area, the impedance for the four scratched coatings dropped significantly due to the physical addition of the surface defect (Figure 15 (d)). Of the four scratched coatings, the impedance of the chromated epoxy (C1) was still the highest, which may result from the healing effect established either by the inhibitive pigments leached from the coating^[20-25] or by a resistive corrosion product produced by the inhibitive pigments^[26, 27]. The low frequency impedance at positions C3 and C4 reached about $10^5 \Omega$, being two orders of magnitude lower than the results obtained at positions A3 and A4. For the C2 position, it is interesting to note that the impedance value at low frequency remains at the same order of magnitude as that obtained at A2, suggesting that the Mg-rich primer is highly electronically conductive and it protects the metal substrate through a mechanism different from common physical barrier protection. Since looking for corrosion protection mechanisms of these particular coating is not the main purpose of the study, the subject is not discussed in further detail here.

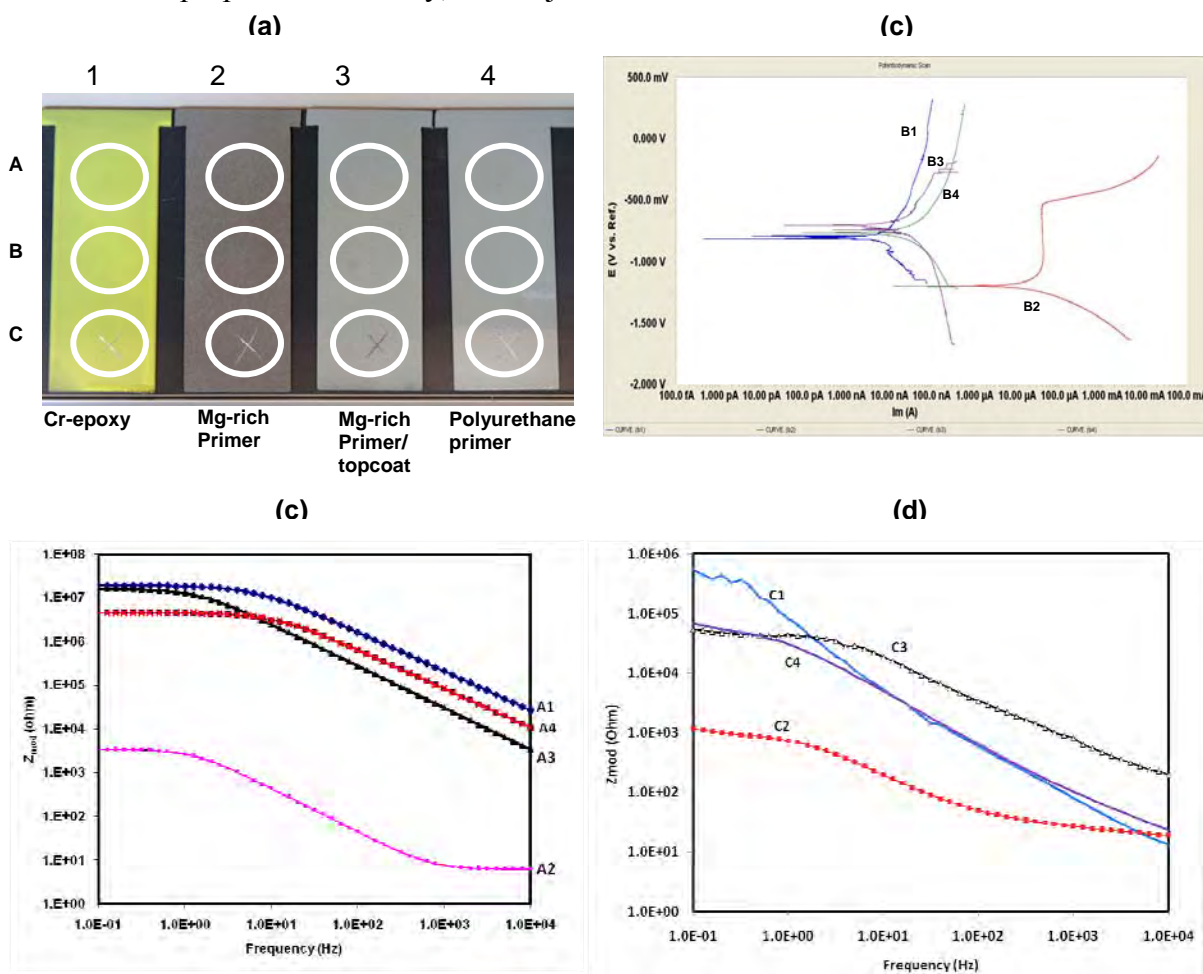


Figure 15. High throughput evaluation of four different coatings in the HT-EIS setup

4. Conclusions

In this paper, a high-throughput parallel EIS apparatus for rapid evaluation of corrosion protective coatings has been developed and validated. Using the assembly of 4 x 3 electrochemical cell arrays, most time-consuming steps in the measurement process are parallelized, thus significantly improving data throughput and providing significant time savings over conventional routine EIS methods. The maximum impedance and the lowest capacitance for the HT-EIS are respectively defined as about $3 \times 10^{11} \Omega$ and $30 \pm 1.2 \text{ pF}$. Within the operation limit, the validation results obtained from the Randle's circuit, Ti/ K_4FeCN_6 , K_3FeCN_6 electrochemical reaction, and two model film systems showed that the HT-EIS provided essentially the same quality of the data output as the single cell EIS experiment.

The HT-EIS protocol has also been successfully used to evaluate several types of scribed or non-scribed real coatings in term of corrosion protection. This HT-EIS apparatus allows for 4 coating compositions to be measured in triplicate. It is expected that this setup would significantly facilitate improvements to the coating evaluation process and enable the production and analysis of approximately 1000 coating samples per week.

Acknowledgements

The authors gratefully acknowledge support of the work by the US Air Force Office of Scientific Research under Grant FA8650-04-1-5045 with Major Jennifer Gresham as Program Manager.

5. References

- [1] CC Technologies Laboratories, Federal Highway Administration (FHWA), Office of Infrastructure Research and Development, **2001**.
- [2] G. Wranglen, *An Introduction to Corrosion and Protection of Metals*, Inst. for Metallogy, Stockholm, **1972**.
- [3] J. N. Cawse, D. Olson, B. J. Chisholm, M. Brennan, T. Sun, W. Flanagan, J. Akhave, A. Mehrabi, D. Saunders, *Progress in Organic Coatings* **2003**, *47*, 128.
- [4] B. Chisholm, R. Potyrailo, J. Cawse, R. Shaffer, M. Brennan, C. Molaison, D. Whisenhunt, B. Flanagan, D. Olson, J. Akhave, D. Saunders, A. Mehrabi, M. Licon, *Progress in Organic Coatings* **2002**, *45*, 313.
- [5] B. Chisholm, R. Potyrailo, R. Shaffer, J. Cawse, M. Brennan, C. Molaison, *Progress in Organic Coatings* **2003**, *48*, 219.
- [6] B. Chisholm, R. Potyrailo, R. Shaffer, J. Cawse, M. Brennan, C. Molaison, *Progress in Organic Coatings* **2003**, *47*, 112.
- [7] B. J. Chisholm, R. A. Potyrailo, J. N. Cawse, R. E. Shaffer, M. Brennan, C. A. Molaison, *Progress in Organic Coatings* **2003**, *47*, 120.
- [8] A. Khramov, UDRI method, **2006**.
- [9] V. S. Bonitz, B. R. Hinderliter, G. P. Bierwagen, *Electrochimica Acta* **2006**, *51*, 3558.
- [10] G. O. Manual, **2003**.
- [11] T. Hurlen, W. Wilhelmsen, *Electrochimica Acta* **1986**, *31*, 1139.
- [12] T. Hurlen, W. Wilhelmsen, *Electrochimica Acta* **1988**, *33*, 1729.
- [13] A. Bellomo, *Talanta* **1970**, *17*, 1109.
- [14] J. T. Bushey, D. A. Dzombak, *Journal of Colloid and Interface Science* **2004**, *272*, 46.
- [15] M. Kohn, *Analytica Chimica Acta* **1949**, *3*, 297.
- [16] L. Gray, B. Appleman, *Journal of Protective Coatings & Linings* **2003**, *20*, 66.
- [17] G. Bierwagen, D. Battocchi, A. Simoes, A. Stamness, D. Tallman, *Progress in Organic Coatings*

2007, 59, 172.

- [18] D. Battocchi, A. M. Simoes, D. E. Tallman, G. P. Bierwagen, *Corrosion Science* **2006**, 48, 1292.
- [19] M. E. Nanna, G. P. Bierwagen, *J. Coatings Technology Research* **2004**, 1.
- [20] Y. Lu, Y. Ren, H. Ying, J. Wu, P. Zhang, H. Meng, *Proc. Int. Conf. Surf. Sci. Eng.* **1995**, 205.
- [21] J. D. Ramsey, R. L. McCreery, *J. Electrochem. Soc.* **1999**, 146, 4076.
- [22] A. Suda, *Hyomen Kagaku* **2001**, 22, 136.
- [23] A. Suda, M. Asari, *Zairyo to Kankyo* **1997**, 46, 95.
- [24] J. Zhao, G. Frankel, R. L. McCreery, *J. Electrochem. Soc.* **1998**, 145, 2258.
- [25] J. Zhao, R. L. McCreery, G. S. Frankel, F. Allen, *Abstr. Pap. - Am. Chem. Soc.* **2000**, 220th, ANYL.
- [26] M. M. Lohrengel, *Materials Science & Engineering, R: Reports* **1993**, R11, 243.
- [27] G. Schmitt, J. W. Schultze, F. Fassbender, G. Buss, H. Luth, M. J. Schoning, *Electrochimica Acta* **1999**, 44, 3865.